Investigation of three-body forces from atomic mass data

Stamatina Alexandropoulou

Master of Science by Research in Physics

University of York

Physics

September 2021

Abstract

Although two-nucleon (NN) interactions successfully explain many aspects of nuclear structure, recent studies are pointing to the important role of three-body (3N) forces in the predictions of neutron-rich nuclei and in the evolution of shell structure [1], in particular from an ab-initio point of view.

The aim of this work is to investigate whether we can describe atomic masses using valence-shell corrections that include both NN and 3N forces in the mass formulae. The focus lies on pinpointing indications of NN and 3N forces in the residuals of the mass formulae fits from the standpoint of their dependence on the valence particles (or holes).

Starting from the Bethe–Weizsäcker formula, an investigation on the effects of NN and 3N forces by performing local fits to the experimental mass compilation AME2016 [2,3], was made. By introducing inert cores and a valence-configuration space, a search to identify hints of NN and 3N forces was conducted mainly around the traditional magic numbers 8, 20, 28, 50, 82 and 126 of neutrons and/(or) protons. Additionally, a modified Bethe–Weizsäcker mass formula was employed to estimate its ability to better fit the doubly magic nuclei.

The results show that the addition of the suggested terms of NN and 3N to the mass formulae are applicable to describe the trend observed around the doubly magic nuclei for some atomic mass regions. Although this is a fact, we cannot directly claim that these expressions correspond to the NN and 3N body forces.

Moreover, a shell correction [4] was employed to extend the Bethe–Weizsäcker mass formula. The results obtained from a fit using this modified formula show an agreement between the valence-shell corrections of the present investigation and the suggested ones, in the description of the parabolic-like behavior of the residuals between two doubly magic nuclei.

List of Contents

Abstract 2

List of Contents 3

List of Figures 5

List of Tables 9

List of Abbreviations 12

Acknowledgements 13

Author's Declaration 14

Chapter 1 15

Introduction 15

Chapter 2 21

Literature Review 21

2.1 Structural Evolution: 22

2.2 Nuclear masses and Binding energies: 25

2.3 The evaluation of nuclear masses: 30

2.4 Nuclear Models and Basic Theoretical Approaches: 31

2.4.1 The nuclear mass models: 31

2.4.2 The two LDM formulae: 34

2.5 The importance of 3N forces: 41

Chapter 3 44

Methodology 44

3.1 Research Strategy: 44

3.1.1 Research Approach: 44

3.1.2 Physical and Mathematical explanation of the suggested valence-shell corrections: 48

3.1.3 Regions of Interest: 55

3.1.4 Experimental Inputs: 59

3.2 Regression Analysis: 62

3.3 Uncertainties in the observables: 68

Chapter 4 70

Results 70

4.1 The BW Mass Formula Fits: 71

4.1.1 Weighted Least Squares Fit to binding energy data for the DM nuclei (A ≥16): 71

4.1.2 Unweighted Least Squares Fit to binding energy data for the DM nuclei (A ≥16): ...81

4.2 The LDM1 Formula Fit: 94

4.2.1 Fit to the traditional DM nuclei (A ≥16) binding energies and with the addition of the DM nucleus ^{24}O: 94

4.3 Comparison with Shell Corrections from the literature: 100

4.4 General Important Remarks that were detected during the analysis: 107

Chapter 5 113

Discussion and Conclusions 113

APPENDIX A 115

Input data and Results from the Fitting Procedure 115

APPENDIX B 129

Python Codes to Compute the Number of Valence Neutrons/Protons of Nuclides 129

1st Code: Calculation of Valence Neutrons, Valence Protons and Valence Nucleons: .. 129

2nd Code: Calculation of Valence Nucleons: 133

References 134

List of Figures

Chapter 1: Introduction

Figure 1.1: The three valence quarks of a proton and a neutron are presented. The nuclear force is mediated by virtual pion exchange. The RHS and LHS images adapted from the Refs. [13] and [14], respectively. 16

Chapter 2: Literature review

Figure 2.1: Deviations of the experimental binding energies from the predicted values of Bethe-Weizsäcker mass formula are shown as a function of neutron number N. Particularly, the ΔB quantity in y-axis is defined as the difference between the measured binding energy and its corresponding predicted value. Large discrepancies are prominent in specific locations across the nuclear landscape Adapted from Ref. [26]. 22
Figure 2.2: Splitting of nuclear levels due to the spin-orbit interaction. On the right side, partial and accumulated nucleon numbers are shown. The magic numbers (shown at the extreme right-hand side) are correctly reproduced, and the shell effect is evident. Adapted from Ref. [36]. 24
Figure 2.3: The scale example which illustrates that the mass of a nucleus is less than the sum of the masses of its constituent protons and neutrons. The energy, E, which is released to form the nucleus is also shown. Image by Author. 25
Figure 2.4: Chart of nuclides: The valley of stability, the N=Z line of stable light nuclides and the different types of radioactive decays are shown. Also, the magic (closed shell) numbers are illustrated in the ends of vertical and horizontal lines, while on the top left corner the beta decays are shown. In the grey area belong unknown nuclei which have been predicted but have not been yet experimentally found. Adapted from [41]. 27
Figure 2.5: Nuclear binding energy per nucleon (MeV) as a function of the mass number A. Nickel-62 (^{62}Ni) with the highest binding energy per nucleon is marked. In the left of the vertical dashed line lie nuclei in which fusion is common, while in the right fission dominates. Adapted from Ref. [43]. 28
Figure 2.6: Schematic explanation of the terms of the semi-empirical mass formula in the liquid drop model of the nucleus. Adapted from Ref. [24]. 35
Figure 2.7: Comparison of the residuals obtained from a linear least squares fit of the BW mass formula (Eq. (5)) and the LDM1 formula (Eq. (7)), for the oxygen isotopic chain. 39
Figure 2.8: Comparison of the residuals obtained from a linear least squares fit of the BW mass formula (Eq. (5)) and the LDM1 formula (Eq. (7)), for the beryllium isotopic chain. 39
Figure 2.9: Comparison of the residuals obtained from a linear least squares fit of the BW mass formula (Eq. (5)) and the LDM1 formula (Eq. (7)), for the lithium isotopic chain. 40

Figure 2.10: The location of the oxygen anomaly in the neutron drip line is presented. Some isotopes of the most neutron-rich nuclei are also highlighted as well as the location of the neutron drip line corresponds to the fluorine and neon isotopic chains. Adapted from Ref. [6]. 42

Chapter 3: Methodology

Figure 3.1: Schematic representation of the research steps followed in this work. 46
Figure 3.2: Expected parabola of residuals calculated using the BW baseline formula (Eq. (5)), between two DM numbers (DM1 and DM2), in a selected nuclide chain. 48
Figure 3.3: The contributions of NN, 3N and NN+3N. They were calculated using Eqs.(12) and (13) with B = D = 1 keV. 52
Figure 3.4: The contributions of NN, 3N and NN+3N terms. They were calculated using Eqs. (18) and (19) with B = D = 1 keV. 53
Figure 3.5: Graphical presentation of the five main regions of interest, depicted on the nuclear chart, used for testing the current theoretical framework. Image source [151]. 56
Figure 3.6: The magic chain Z=20 of the calcium isotopes. It is one of the regions of interest, where even-even nuclei included between the two DM nuclei, ^{40}Ca and ^{48}Ca, were used to apply the present theoretical framework. The arrows assist to understand the process of counting valence particles or holes starting from the nearest closed shell. Nuclear chart data were taken from Ref. [152]. 57
Figure 3.7: The magic chain Z=50 of the tin isotopes. It is one of the regions of interest, where even-even nuclei included between the two DM nuclei, ^{100}Sn and ^{132}Sn, were used to apply the present theoretical framework. The arrows are used as it was explained in Fig. 3.6. Nuclear chart data were taken from Ref. [152]. 57
Figure 3.8: The diagonal chain from the DM nucleus ^{40}Ca to DM nucleus ^{56}Ni. Region of interest, where even-even nuclei included between the two DM nuclei, were used to apply the present theoretical framework. Nuclear chart data were taken from Ref. [152]. 58
Figure 3.9: At the LHS: The isotonic magic chain N=28. Region of interest, where even-even nuclei included between the two DM nuclei, ^{48}Ca and ^{56}Ni, were used to apply the present theoretical framework. Nuclear chart data were taken from Ref. [152]. At the RHS: Presentation of the diagonal chain from the DM nucleus ^{16}O to the DM nucleus ^{40}Ca. Region of interest, where even-even nuclei included between the two DM nuclei, were used to apply the present theoretical framework. Nuclear chart were taken from Ref. [152]. 58
Figure 3.10: Extract from the atomic mass data compilation (AME2016) [125]. The decimal point was replaced by # for (non-experimental) estimated values. 60

Figure 4.1: Residuals of the weighted least squares fit of the BW mass formula to the binding energies of the DM nuclei when the pairing term is neglected. The estimated values of binding energies are noted as 'LDw/op'. 75
Figure 4.2: Residuals of the weighted least squares fit of the BW baseline formula to the DM nuclei binding energies, when a fixed value of 12 MeV was assigned to the pairing parameter. Also, the best values of the estimated parameters are presented. 77
Figure 4.3: Residuals of the weighted least squares fit of the BW baseline formula to the DM binding energies. The actual experimental uncertainties for the DM nuclei ^{100}Sn and ^{132}Sn were replaced with a small value (Test 1). 78
Figure 4.4: Residuals for the DM nuclei (A ≥16) obtained after the conduction of the Test 2 (the DM nucleus ^{100}Sn was excluded from the fitting procedure). The best values of parameters from the fit are also presented. 79
Figure 4.5: The residuals for the DM nuclei obtained from the weighted least squares fit of the BW baseline formula following the conditions of Test 3. 80
Figure 4.6: The residuals for the DM nuclei (A≥16) obtained from the unweighted least squares fit of the BW baseline formula, assigning the value of 12 MeV to the pairing term coefficient. 83
Figure 4.7: Residuals of the even-even nuclei between the two DM nuclei ^{40}Ca and ^{48}Ca. Three plots are shown for comparison purposes. The blue line color plot connects the BW_Residuals calculated using the parameters of Table 4.5, the green line corresponds to the residuals obtained after the fit of the Eq. (39) and the red color line shows the residuals' values when the NN contribution is only considered, Eq. (40). The best values of B and/(or) D parameters are also shown. 88
Figure 4.8: Residuals of the even-even nuclei between the DM nuclei ^{100}Sn and ^{132}Sn. Three plots are shown for comparison purposes. The blue color line plot connects the BW_Residuals calculated using the parameters of Table 4.5, the green line corresponds to the residuals obtained after the fit of the Eq. (39) and the red color line shows the residuals' values when the NN contribution is only considered, Eq. (40). The best values of B and/(or) D are also shown. 90
Figure 4.9: Residuals of the even-even nuclei between the DM nuclei ^{48}Ca and ^{56}Ni. Three plots are shown for comparison purposes. The blue line color plot connects the BW_Residuals calculated using the parameters of Table 4.5, the green line corresponds to the residuals obtained after the fit of the Eq. (39) and the red color line shows the residuals' values when the NN contribution is only considered in the fit, Eq.(40). The values of the best fit parameters are also shown. 92
Figure 4.10: The residual values for the DM nuclei (A ≥16) obtained from the unweighted least squares fit of the LDM1 formula plus the DM nucleus ^{24}O are shown. 95
Figure 4.11: Comparison of the residuals correspond to the even-even nuclei from the DM nucleus ^{40}Ca to ^{48}Ca. The blue color line connects the LDM1_Residuals calculated using the parameters of Table 4.10, the green color line the residuals after fitting the Eq.(42) and the red color plot the residuals after fitting the Eq. (43). 97
Figure 4.12: Comparison of the residuals correspond to the even-even nuclei from the DM nucleus ^{100}Sn to DM nucleus ^{132}Sn. The blue color line connects the LDM1_Residuals calculated

using the parameters of Table 4.10., the green color line, the residuals after fitting the Eq. (42) and the red color line the residuals after fitting the Eq. (43)..... 98
Figure 4.13: Comparison of the residuals correspond to the even-even nuclei from the DM nucleus ^{16}O to DM nucleus ^{24}O. The blue color line connects the LDM1_Residuals calculated using the parameters of Table 4.10, the green color line the residuals after fitting the Eq. (42) and the red color line plot the residuals after fitting the Eq. (43). 99
Figure 4.14: Comparison of the residuals for the even-even nuclei between the DM shell closures, ^{40}Ca and ^{48}Ca. The blue line color connects the BW_Residuals calculated using the parameters of Table 4.5 and the green color line connects the residuals obtained from a fit of Eq.(49). 103
Figure 4.15: Comparison of the residuals of the even-even nuclei between the DM shell closures, ^{100}Sn and ^{132}Sn. The blue line color connects the BW_Residuals calculated using the parameters of Table 4.5 and the green color line connects the residuals obtained from a fit of Eq. (49)..... 105
Figure 4.16: Comparison of the residuals of the even-even nuclei between the DM shell closures of the isotonic chain N=28, from the DM nucleus ^{48}Ca to DM nucleus ^{56}Ni. The blue line color connects the BW_Residuals calculated using the parameters of Table 4.5 and the green color line connects the residuals obtained from the fit of Eq. (49). 106
Figure 4.17: The residuals for the DM nuclei (A≥16) obtained from the unweighted least squares fit of the enriched BW baseline formula, Eq. (50). 110

Appendix A : Input Data and Results from the Fitting Procedure

Figure A.1: (a) Graphical representation of the uncertainties of the traditional DM nuclei for A ≥ 16 using a histogram. (b) Two boxplots are presented in the same plot. The LHS boxplot corresponds to the values of the residuals when a weighted least squares fit of the BW formula to the DM nuclei was performed (w_Exp.Un.) while the RHS boxplot corresponds to an unweighted least squares fitting procedure (w/oExp.Un.). (c) The box-and-whisker plot which is designed to present the distribution of a population, is shown. Available in Ref. [176]. . 117

List of Tables

Chapter 2: Literature Review

Table 2.1: Best fit results of the BW baseline formula (Eq. (5)) and the LDM1 mass formula (Eq.(7)) to the experimental binding energies data. 38

Chapter 3: Methodology

Table 3.1: Data for even-even nuclei extracted from Ref. [125]. After modifying the column of binding energy per particle in keV (BE/A(keV)) and its corresponding uncertainty (un(keV)), the columns which correspond to the total binding energy and its uncertainty, BE(MeV) and unT(MeV) are shown, respectively..... 62

Chapter 4: Results

Table 4.1: Best values of parameters from the weighted least squares fitting of the BW mass formula, Eq.(5), to the DM nuclei for A ≥ 16 , including the pairing contribution. 71
Table 4.2: Comparison of the best values of coefficients of the BW mass formula terms as obtained by different authors. The column 'Fit' contains the experimental values of the total binding energy (BE) in MeV to which the BW formula is fitted. 72
Table 4.3: Best values of parameters from the weighted least squares fit of the BW mass formula to the DM nuclei for A ≥16, without including the pairing term (ap) in the fitting procedure. 72
Table 4.4: The residuals from the weighted least squares fit of the BW formula to the DM nuclei binding energies which correspond to the edge of the regions of interest. The blue header columns contain the residuals of the doubly magic closed shells of the diagonal chain ^{16}O to ^{40}Ca, the burgundy red header columns the residuals of the DM nuclei of the diagonal chain ^{40}Ca to ^{56}Ni, the orange, purple and green header columns contain the residuals of the DM nuclei of the calcium, isotonic (N=28) and tin chains, respectively. 74
Table 4.5: Best values of parameters from the unweighted least squares fit of the BW mass formula to the DM nuclei for A ≥16, with 12 MeV assigned to the pairing term coefficient. 82
Table 4.6: The residuals from the unweighted least squares fit of the BW formula to the DM nuclei binding energies which correspond to the edge of the regions of interest. The blue header columns contain the residuals of the doubly magic closed shells of the diagonal chain ^{16}O to ^{40}Ca, the burgundy red header columns the residuals of the DM nuclei of the diagonal chain ^{40}Ca to ^{56}Ni, the orange, purple and green header columns contain the residuals of the DM nuclei of the calcium, isotonic and tin chains, respectively. 82
Table 4.7: The best fit parameters of Table 4.5 were applied to the even-even nuclei from ^{40}Ca to ^{48}Ca. In such a way, their theoretical binding energies in MeV (LD(MeV)) as well as the

residuals (BE(MeV)-LD(MeV)) were calculated. The column '(BEexp(^{A}Ca)-BEexp(^{40}Ca)) MeV' shows the results after the subtraction of the experimental binding energy of ^{40}Ca from the experimental binding energies of the rest of the magic nuclei. Similar calculations for the theoretical binding energies and are presented in column ' (BEtheor(^{A}Ca)-BEtheor(^{40}Ca)) (MeV)'. Finally, the new residuals relevant to the reference nucleus ^{40}Ca are shown in the last column, 'BW_Residuals'. 85
Table 4.8: The best fit parameters of Table 4.5 were applied to the even-even nuclei from ^{100}Sn to ^{132}Sn. The values of the residuals of the column 'BW_Residuals (MeV)' were derived taking into account the DM reference nucleus ^{100}Sn. 89
Table 4.9: Best fit parameters of Table 4.5 were applied to the even-even nuclei from the DM nuclei ^{48}Ca to ^{56}Ni. The values of the residuals of the column 'BW_Residuals (MeV)' were derived taking into account the DM reference nucleus ^{48}Ca. 91
Table 4.10: Best fit parameters obtained from the unweighted least squares fit of the LDM1 formula to the DM nuclei binding energies, for A ≥16, including the DM nucleus ^{24}O. 94
Table 4.11: The residuals from the unweighted least squares fit of the BW formula to the DM nuclei binding energies which correspond to the edge of the regions of interest. The blue header columns contain the residuals of the doubly magic closed shells of the diagonal chain ^{16}O to ^{40}Ca are presented, the burgundy red header columns the residuals of the DM nuclei of the diagonal chain ^{40}Ca to ^{56}Ni, the orange, purple and green header columns the residuals of the DM nuclei of the calcium, isotonic and tin chains, respectively. Also, the residuals for the DM nuclei of the oxygen isotopic chain are shown in red header color. 95
Table 4.12: The input data and the estimated theoretical and residual values correspond to the even-even nuclei of the calcium isotopic chain. 102
Table 4.13: The input data as well as the estimated theoretical and residuals' values of binding energies correspond to the even-even nuclei of the tin isotopic chain are presented. 104
Table 4.14: The input data and the estimated theoretical and residual values correspond to the even-even nuclei of the isotonic chain N=28, from the DM nucleus ^{48}Ca to ^{56}Ni are presented. 106
Table 4.15: Comparison of the best values of parameters obtained from fit of Eq.(50) and Eq.(5) to the traditional DM nuclei for A≥ 16. 109

Appendix A: Input Data and Results from the Fitting Procedure

Table A.1: Comparison of the results of the estimated best values of parameters between an analytical (or exact) and three numerical solutions for the weighted least squares fit of the BW baseline formula to the DM nuclei for A≥16. 115
Table A.2: An unweighted least squares fit of the BW formula was performed to the entire AME2016 mass table. The MINUIT automatic routine was used, and a value of 12 ± 0.5 MeV was assigned to the pairing coefficient. The latter was adapted as a fixed value associated with the pairing parameter in the present investigation. 116
Table A.3: A weighted least squares fit of the BW formula was performed to the DM nuclei (A ≥ 16) and the best fit coefficients are shown. The uncertainties of the experimental binding energies, that included in the fitting procedure, followed the conditions of the Test 1. 116

Table A.4: A weighted least squares fit of the BW formula was performed to the DM nuclei (A ≥ 16) and the best fit coefficients are shown. The uncertainties of the experimental binding energies that included in the fitting procedure followed the conditions of the Test 3. 117
Table A.5: Comparison of the results of the estimated best values of parameters between an analytical (or exact) and three numerical solutions for the unweighted least squares fit of the BW baseline formula to the DM nuclei for A ≥ 16, without considering the contribution of pairing term. 118
Table A.6: (I) Input data for the even-even nuclei lie between the DM nuclei: ^{40}Ca to ^{48}Ca 119
Table A.7: (II) Input and Output Data for the even-even nuclei lie between the two DM nuclei: ^{40}Ca to ^{48}Ca 119
Table A.8: (I) Input data for the even-even nuclei lie between the two DM nuclei: ^{100}Sn and ^{132}Sn 120
Table A.9: (II) Input and Output data for the even-even nuclei lie between the two DM nuclei: ^{100}Sn to ^{132}Sn 120
Table A.10: (I) Input data for the even-even nuclei lie between the two DM nuclei: ^{48}Ca to ^{56}Ni 121
Table A.11: (II) Input and Output data for the even-even nuclei between the two DM nuclei ^{40}Ca to ^{48}Ca 121
Table A.12: (I) Output data for the even-even nuclei lie between the two DM nuclei: ^{40}Ca to ^{48}Ca 122
Table A.13: (II) Input and Output data for the even-even nuclei lie between the two DM nuclei: ^{40}Ca to ^{48}Ca 122
Table A.14: (I) Output data for the even-even nuclei lie between the two DM nuclei: ^{100}Sn and ^{132}Sn 123
Table A.15: (II) Input and Output data for the even-even nuclei lie between the two DM nuclei: ^{100}Sn and ^{132}Sn 123
Table A.16: (I) Input data for the even-even nuclei lie between the two DM nuclei from ^{16}O to ^{24}O..... 124
Table A.17: (II) Output data for the even-even nuclei lie between the two DM nuclei from ^{16}O to ^{24}O 124
Table A.18: Unweighted least squares fit of the BW formula to the BW formula to the DM nuclei for A ≥ 16:..... 125
Table A.19: Weighted least squares fit of the BW formula to the DM nuclei for A ≥ 16:.... 126
Table A.20: Best fit parameters for the unweighted least squares fit of the BW formula, Eq. (5), to the DM nuclei for A ≥16. (Fit BE/A (MeV))..... 127
Table A.21: Best fit parameters for the unweighted least squares fit of the BW formula, Eq. (5), to the DM nuclei for A ≥ 16 (Fit BE(MeV)). 127
Table A.22: Best fit parameters for the weighted least squares fit of the BW formula to the DM nuclei for A ≥ 16 (Fit BE/A(MeV)) 127
Table A.23: Best fit parameters for the weighted least squares fit of the BW formula, Eq.(5), to the DM nuclei for A ≥ 16.(Fit BE(MeV))..... 128

List of Abbreviations

BW	Bethe- Weizsäcker
LDM	Liquid Drop Model
DM	Doubly Magic
BWM	Bethe–Weizsäcker Modified

Acknowledgements

First and foremost, I cannot thank enough my supervisor, Dr Marina Petri, for her valuable support, guidance, and patience throughout the conduction of the present research. She is an excellent supervisor and a very kind person who always helping, encouraging, and challenging me to reach my full potential and further improve my research skills and nuclear physics knowledge. I am deeply grateful to her as she provided me with the opportunity to conduct my Master by Research degree under her supervision and in an excellent academic group and environment.

Also, I would like to really thank her for assisting and supporting my application for the Atomic Energy Agency (IAEA) Marie Sklodowska-Curie Fellowship Programme (MSCFP) as well as my PhD application in Imperial College London, UK, for the upcoming academic year.

Additionally, I very much thank the collaborators Dr Augusto O. Macchiavelli from Nuclear Science Division, Lawrence Berkeley National Laboratory, Berkeley, USA, and Dr Stefanos Paschalis, from the Physics Department of University of York, UK, for their significant contribution in the present research.

Moreover, I would like to thank very much Dr Alessandro Pastore, from the Physics Department of University of York, UK, who was always so much willing to help me and answer any of my questions in computational tools and statistical analysis. His initial codes related to the liquid-drop model, included in the graduate module ''Statistical methods and Data Analysis'', paved the way for a solid start of the present research.

I also thank IAEA which selected me for the scholarship and provided me with the financial support which I was so much needed. It was a huge help for me during the conduction of my master's studies.

Finally, I would like to thank my wonderful parents.

This project was supported by IAEA Marie Sklodowska-Curie Fellowship programme

Author's Declaration

I declare that this thesis is a presentation of original work, and I am the sole author. This work has not previously been presented for an award at this, or any other, University. All sources are acknowledged as References.

Chapter 1

Introduction

One of the long-sought goals of nuclear physics is to understand the strong nuclear force. The structure of the nucleus and the fundamental interactions between quarks and gluons are expanding frontiers in science [5]. Although, considerable progress has been made toward exploring the nuclear force acting among the nucleons, there are only phenomenological expressions to describe NN interactions.

Also, addressing questions such as where the limits of stability are and what combinations of neutrons and protons can form a bound nucleus, are major issues in nuclear structure physics that seek solutions [6]. Mapping the position of the neutron drip line is necessary on models of nucleon-nucleon interactions and many-body correlations [7]. Measuring phenomena away from the valley of stability, in the limits of nuclear existence, could shed light to the mechanism responsible for new and at the same time unique nuclear structure phenomena that are evident in several recent studies and seems to have a crucial impact to the understanding of nuclear interactions. To this end, there is evidence that properties of exotic nuclei are sensitive to nuclear forces [8]. Entering this exciting new era of opportunities, a direct understanding of the element production in the universe can be achieved.

The forces between two nucleons, the NN forces, are the forces between pairs of protons and neutrons within the nucleons. Two-body forces are mostly responsible for nuclear properties. However, to explain nuclear properties further, the three-nucleon forces were introduced as interactions between three particles: three neutrons, three protons, or two of one and one of the other. Also, it was observed [9] that 3N forces play a significant role and should be included in physical implications and extensions of theoretical models [10]. Although the consideration of three-nucleon potentials provides new keys to understanding the nuclear stability at neutron-rich conditions, calculations in many body systems are difficult and require advanced computational techniques [11]. Particularly, the computational effort increases exponentially with the mass number, while when the calculations are performed considering the three-body forces, the computational challenge is particularly enormous [12].

The atomic nucleus is composed of a certain number of neutrons N and protons Z and the force which is responsible for holding them together is the nuclear strong force, also named as strong force or strong interaction. It is a complex arrangement which mathematically could be described as a ‘many-body’ problem. When a given nucleon of an atomic nucleus interacts with the rest of the particles, this interaction can be approximated by an averaged energy term, the so-called ‘’mean-field potential''. A nucleon experiences an average (or mean) attractive energy which is due to the strong interaction with its neighbors. The strong nuclear interaction appears among all the nucleons, p-p, p-n, n-n where n is the neutron and p is the proton. In quantum mechanics, the nature and source of the strong force are investigated by the quantum chromodynamics (QCD) theory. The strong force is mediated by virtual pion exchange, Fig. 1.1. The nuclear force binds the nucleons together and it prevents the nucleus

from disintegrating. The nuclear strong force is a short-range force. At short distances the nature of the nuclear interaction is attractive. Hence, when two protons are far apart the Coulomb electromagnetic force dominates, and the one nucleon repels one other.

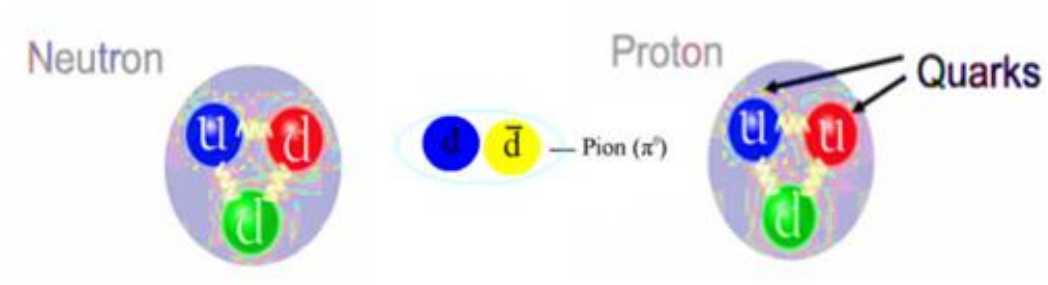

Figure 1.1: *The three valence quarks of a proton and a neutron are presented. The nuclear force is mediated by virtual pion exchange. The RHS and LHS images adapted from the Refs. [13] and [14], respectively.*

Similar to electrons in atoms, neutrons and protons exist inside the nuclei in certain energy states which correspond to different arrangements of the nucleons in their allowed states. Details on the nuclear shell model will be given in an upcoming section (2.1). Mass measurements have a significant and unique role in the establishment of the shell model also known as the independent particle model. To this end, studies of nuclear masses give us important insights in mapping the structural formation for a certain number of protons and neutrons inside the nucleus, revealing information about more energetically favorable configurations [15]. These energetically stable configurations form large gaps between the energy states of the nucleus which are caused by fully completed particle's shells.

Closed shell configurations correspond to specific numbers of protons or (and) neutrons across the nuclear landscape and have an important role because they produce additional stability to nuclei. Nuclear closed shells of protons or neutrons are the so-called magic numbers, N and Z = 8, 20, 28, 50, 82 and the magic number 126 which has so far only been observed for neutrons [16]. Nuclei that correspond to such magic numbers of protons or (and) neutrons have exceptional stability as they are more tightly bound compared with nuclei that have simply one more proton or neutron [17]. A nucleus with both magic numbers of protons and neutrons is called a ''doubly magic nucleus''.

The existence of magic numbers has been called into question due to recent studies conducted far from the region of stability and show that the magic nature of these nuclei are not all that robust and can significantly change with proton and neutron number. There are several experimental proofs that point out to the lack of the magic character of some of these rather exotic nuclei and the existence of new magic numbers [18].

Moreover, the most challenging experiments are those that measure nuclei far from the stability line where there is a large excess of neutrons or protons. In nuclear physics, the boundaries for particle-stability are referred to as drip lines. In such extreme conditions, a combination of protons and neutrons does not necessarily yield a bound nucleus and lead to the formation of resonances that decay via particle emission.

Nuclei far from the valley of stability, with extreme numbers of either protons or neutrons, are also of great importance for the understanding of nucleosynthesis of the elements. Tracing the location of driplines accurately constraints the path for the process of nucleosynthesis and other astrophysical phenomena [19]. Hence, a combination of accurate nuclear physics with precision astronomy is essential to understand astrophysical scenarios.

The various production mechanisms that are used at the radioactive-beam facilities provide access to drip line nuclei. However, future developments in the experimental techniques for the spectroscopic measurements of these nuclei as well as the adoption of powerful theoretical tools for the interpretation of the data are critical components for the success of the future scientific programs in these facilities [20,21]. Particularly, theoretical models, employed in nuclear astrophysics related studies, strongly relied on an accurate determination of the reaction energies as well as the reaction rates.

Although there are some well-developed theoretical models available, there is not yet a complete theory which fully reflects the structure and behavior of these complex nuclear systems and can consider some of the complicated correlations that characterise complex nuclei [22]. Indeed, over the last few years, nuclear physics has made significant advances in the description of nuclear masses; this will lead in the future to a better description of properties of exotic nuclei lying in unexplored nuclear-mass regions.

The aim of the present thesis is to propose certain valence-shell corrections to theoretical models, so to reproduce the data between two doubly magic nuclei. Towards this end, it is important to clarify two critical points:

1) The proposed valence-shell correction terms have been assumed to be due to the effects of NN and 3N forces, respectively. However, it is crucial to be stressed that this is only a hypothesis, and it cannot be readily claimed that these terms are a manifestation of NN and 3N nucleon forces. Initially the purpose is to prove (or not) that the observed trend of the data can (or not) be explained using the expressions of the proposed terms.

2) Modern nuclear mass models are able to significantly improve the agreement between the experimental and theoretical atomic mass data. The theoretical approach and formulation adapted in the present analysis, does not aim to describe nuclear masses as accurately as possible, based on the root mean square (RMS) of discrepancies between the observables and predictions. The scope of the present work is initially to identify if the inclusion of the extra terms are able to reproduce the data. To this end, the calculation of the residuals is only used to evaluate how good the minimum is in terms of reproducing the investigated trend.

To this end, it is the purpose of the next chapters to discuss some intriguing subjects that are at the frontiers of nuclear structure investigations focusing on the important role of nuclear masses and binding energies for the understanding of two-nucleon forces and the effective interactions between nucleons in nuclei, by combining macroscopic and microscopic theoretical approaches especially from an independent particle structural point of view.

This thesis contains chapters which are divided into sections and subsections and is organized as follows:

Chapter 2: Literature Review:

In this chapter, an extended description of the research questions that were pointed out in the introduction will be given. First, the basic underline physics theory which underpins the present research work is presented. The information here aims at providing an overall description of the developments which have been adapted or are currently underway to address major nuclear structure questions, directly connected to this research work.

- **Section 2.1: Structural Evolution:**

  In this section, a short history in the theory of the liquid drop model of the nucleus as well as in the establishment of the nuclear shell model is presented. A brief description of the observations which led to a microscopic theory for the structural formation of the nucleons inside the nucleus will be given.

- **Section 2.2: Nuclear masses and Binding Energies:**

  This section starts with the definition of nuclear masses and binding energies. Then, it briefly discusses some challenges in measuring nuclides at and towards the drip lines which are of great importance for addressing questions in nuclear structure theory and other branches of physics.

- **Section 2.3: The evaluation of nuclear masses:**

  This section is focused on the important role of the Atomic Mass Evaluation for providing reliable information related to the atomic mass measurements. The different experimental methods of acquiring such measurements and their required evaluation before entering the atomic mass database will be also commented.

- **Section 2.4: Nuclear models and theoretical approaches:**

  In this section, a basic classification of nuclear models will be presented. Also, a short literature review of the most notable nuclear mass models which are available up to date will be given. Particularly, the focus lies in the understanding of the theoretical

models that will be used to reproduce the experimental observables of the present research work. To this end, the liquid drop model theoretically described by the Bethe–Weizsäcker' Semi Empirical Mass Formula will be included in the subsection (2.4.2). Moreover, an alternative mass formula will be presented in the same subsection, which later was used to test its ability to reproduce the observed parabolic shape around doubly magic nuclei.

- **Section 2.5: The importance of 3N forces:**

  In this section, an introduction to the three-nucleon forces theory and its importance in nuclear physics and astrophysics will be discussed. Also, a focus on the role of three-nucleon forces to explain the oxygen anomaly and why the ^{24}O is the heaviest bound oxygen isotope will be included, since it motivated the present research work.

After the introduction of the theoretical basis of the current research, the key chapters of this thesis follow:

Chapter 3: Methodology:

- **Section 3.1: Research strategy:**

  This section aims at presenting the research design and discussing the case study approach, based on the phenomenological description that was adapted. The information is divided into subsections. First, the research approach and the mathematical and physical interpretation of the suggested NN and 3N terms are extensively discussed. The nuclear chart regions and subsets of atomic mass data that were employed to evaluate the efficacy of our theory will be included. Ending this section, the experimental inputs that were used to derive the unknown parameters of the mass formula and the adopted modified theory, will be also presented.

- **Section 3.2: Regression analysis:**

  Developing theories and determining the fitting parameters properly, require a good knowledge of regression analysis techniques. The most important application to this approach is in data fitting. The linear least-squares regression methods, which were utilised in the present research analysis, for the determination of the nuclear model parameters, will be presented. Remarks will also be given to the derivation of the uncertainties of the estimated parameters.

- **<u>Section 3.3</u>: Uncertainties in the observables:**

  The purpose of this section is to highlight the role of the experimental uncertainties in the fitting procedure. The inaccuracy of the Bethe–Weizsäcker' Semi Empirical Mass Formula due to missing underlying physics was pointed out and analysed in parallel with the case of including the weights in the regression analysis.

<u>Chapter 4</u>: Results:

This chapter aims at discussing and analyzing the results obtained after fitting binding energies according to the adapted phenomenological approach. Following the estimation of the parameters obtained by the fit, theoretical binding energies and thus the residuals will be presented through plots in order to evaluate the strength of our theory. An improvement of the obtained by the modified theoretical formula, which includes the valence-shell corrections of NN and 3N terms will indicate the validity of our proposed theory. Also, minor modifications to the theoretical baseline formula of Bethe–Weizsäcker will be taking into consideration with the inclusion of an alternative version of the nuclear mass model. Moreover, suggested terms from the relevant literature were adapted to introduce a simple shell correction to the Bethe–Weizsäcker mass formula and a comparison of these terms with the ones proposed by the current investigation will be presented. The results' chapter will close with some important remarks on findings acquired during the conduction of the present research.

<u>Chapter 5:</u> Discussion and Conclusions:

Important points are discussed and conclusions extracted from the present investigation are of great importance for identifying the efficacy of the present phenomenological approach as well as for presenting suggestions for further investigation.

The thesis is completed with a remark on references to the literature. In addition, an Appendix A which includes parameters of the fits and relevant input and output data are added as well as an Appendix B containing two python codes for the calculation of valence particles of nuclides.

Chapter 2

Literature Review

This chapter will focus on the past literature, summarizing some of the most important concepts of nuclear physics theory which will help us to build a proper understanding of the investigated topic. Particularly, the following sections will provide explanations in basic theoretical aspects of nuclear structure theory, pointing out basic features of the nucleus and cornerstones of theoretical approaches that has been developed across the years for an understanding of the fundamental nature of matter.

To this end, it is highlighted the paramount importance of the nuclear mass, through its binding energy, as well as its first theoretical determination back in 1935, when Bethe and von Weizsäcker, released the well-known liquid-drop model for the calculation of nuclear masses. Following this establishment, a number of experimental facts provided a clear evidence of shell model structure. The magic numbers are also underlined as a significant component of the shell structure theory and the shell model potential which predicts higher magic numbers is also illustrated.

Additionally, the vital role of mass measurements and current challenges towards this direction are given, including a presentation of the comprehensive assessment of all the currently available atomic mass data, the so-called 'Atomic Mass Evaluation'.

Nuclear models that are necessary to derive nuclear properties and make reliable predictions for unknown nuclei, are also presented. At the same time, understanding the underlying forces between the nucleons is key objective in nuclear structure theory. The important role of the three-nucleon forces towards this justification are discussed.

At this point, it should be also stressed that although some basic principles and concepts of nuclear physics are presented herein, a detailed theoretical treatment is beyond the scope of this thesis and only topics considered to be relevant for the current research are included. For a more detailed account, one can access the bibliographical reference section.

2.1 Structural Evolution:

In 1935, von Weizsäcker and Bethe suggested a semi-empirical mass formula which considers the atomic nucleus as a drop of a uniform liquid fluid, a theory based on the liquid drop model first introduced by George Gamow and then developed by Niers Bohr and John Archibald Wheeler [23,24]. Although it successfully explains some of the macroscopic aspects of the nucleus, this formula did not take into account specific details of the structure of the nuclei related to microscopic effects. Thus, this phenomenological model does not provide solutions to several important questions related to nuclear structure and the forces acting between the nucleons inside the nucleus [25]. A detailed view of this model is given in an upcoming section (2.4.2). It is used as a baseline formula and although several refinements have been made to its structure over the years, it remains a guideline for producing modern mass formulas.

As a greater understanding of the nuclear structure and other nuclear properties came into existence, clear discrepancies in the residuals plot of the nucleus' binding energies, notified the research community for additional microscopic effects that had not been yet considered and had to be included in the modeling. The following figure, Fig. 2.1, shows indications of shell structure which are presented in the deviations of the measured binding energies from the semi-empirical mass formula of Bethe and von Weizsäcker.

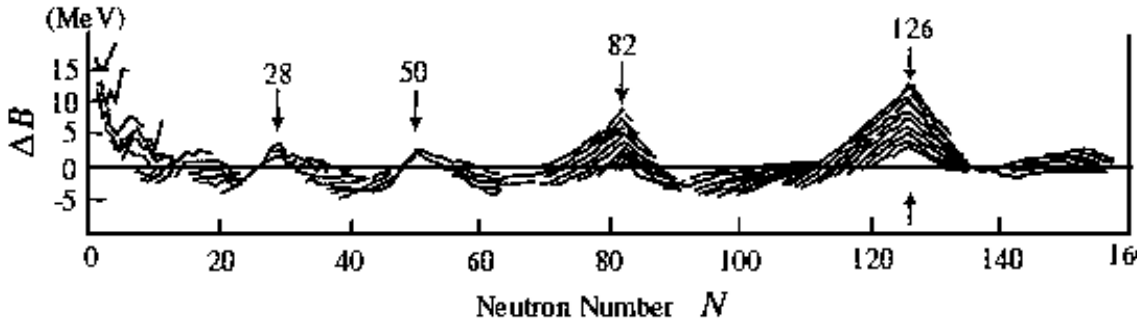

Figure 2.1: *Deviations of the experimental binding energies from the predicted values of Bethe-Weizsäcker mass formula are shown as a function of neutron number N. Particularly, the ΔB quantity in y-axis is defined as the difference between the measured binding energy and its corresponding predicted value. Large discrepancies are prominent in specific locations across the nuclear landscape Adapted from Ref. [26].*

Some other evidence of discontinuous behavior of nuclear properties occurred at the same numbers of neutrons and protons, verifying the above observations in the residual's plot of the binding energies. As an example, breaks of the two-neutron separation energies for isotopic sequences at neutron numbers 82 and 126 are also important pieces of evidence that nuclei have shell structure. Additionally, the relative abundancies of even-even nuclei, the neutron capture cross sections close to shell closures, the densities of excited states are further signs which notify the discontinuities in specific numbers of protons and neutrons.

These experimental observations led to the justification that an atomic nucleus exhibits shell structure. This structure become more evident in specific regions of the nuclear chart and more specifically, close or at the so called ''magic numbers''. Combining all the evidence, we can summarize the relevant magic numbers for nuclei as: 2,8,28,50,82,126 (as mentioned before 126 applies to neutrons only) [27]. The presence of magic numbers is analogous to noble gases in atomic physics. Nuclei with magic numbers of both neutrons and protons are the so-called ''doubly magic nuclei''.

Indeed, all the aforementioned evidence established the nuclear shell model theory which considers that there is a specific structure inside the nucleus which is governed by certain rules. In these arrangements, the nucleons fill orbits and complete shells with increasing energy levels within the nuclear potential [25,28]. For magic numbers of neutrons or protons, extra stability is observed, compared to their neighbors and it manifests itself in the mass and related binding energy for these nuclei. Nucleons fill shells inside the nucleus in a manner which is consistent with Pauli exclusion principle [29]. Completed shells of protons and/or neutrons manifest themselves in several other nuclear properties related to electric quadrupole moments, nuclear charge radii, particle separation energies and so on [29].

Additionally, in order to reproduce the magic numbers, the inclusion of a spin-orbit potential is necessary. The upcoming Fig. 2.2, presents the spin-orbit potential and the proper splitting of the subshells which reproduced the observed magic numbers exactly [10].

However, it is worth noting that today's experimental advances and relevant studies have revealed modifications to some of the classic magic numbers, and the appearance of new ones. Understanding of quenching or disappearance of the magic character for nuclei lying far from the valley of stability is important, especially in nuclear astrophysics because it is directly related to the production and abundance of the heavy elements [30]. The discussion is extended in section (2.5) where experimental proof for unexpected shell closure at N=16 suggests that oxygen-24 (^{24}O) might be a doubly magic nucleus, contrary to what would be expected from stable nuclei. Also, the doubly magic character of nickel-68 (^{68}Ni) (Z=28 and N=40) has been examined in several investigations and put into question how strong its magic character really is [28,31].

The nuclear shell model gives an understanding of the magic numbers that are observed in an atomic nucleus [32] and it is very important in approximations which consider these closed shell configurations as closed shell cores plus the valence nucleons in the valence space [28,33]. Indeed, one can considers that some of the nuclei behave in a manner where most of the nucleons form an inert core and the rest of the nucleons occupy orbitals in a valence configuration space. Therefore, these nucleons are considered as active and are subject to nucleonic interactions [34]. Residual interactions among valence nucleons are of a great importance for nuclear models by functioning as input data.

In ab-initio theory, the underlying interactions among nucleons are crucial determinants of nuclear structure. Hence, identifying key issues in ab-initio nuclear theory is critical for understanding nuclear properties. The fundamental approach of the valence-space formulation is widely used to solve the many body problem incorporating the two- and three-nucleon forces [35].

As will be further discussed in section (2.4), there is not yet a complete theoretical formulation which is capable to describe the structure as well as the complex way of nucleonic interactions in a many body environment based only on the underlying forces among the nucleons. Despite the significant progress that has been made in the recent years in the development of nuclear models, identifying such interactions and solving the exact problem is extremely demanding especially when the three-body forces are involved in the problem. A derivation of nuclear interactions from fundamental interactions between quarks, is challenging and a fully successfully description has not yet been achieved [5].

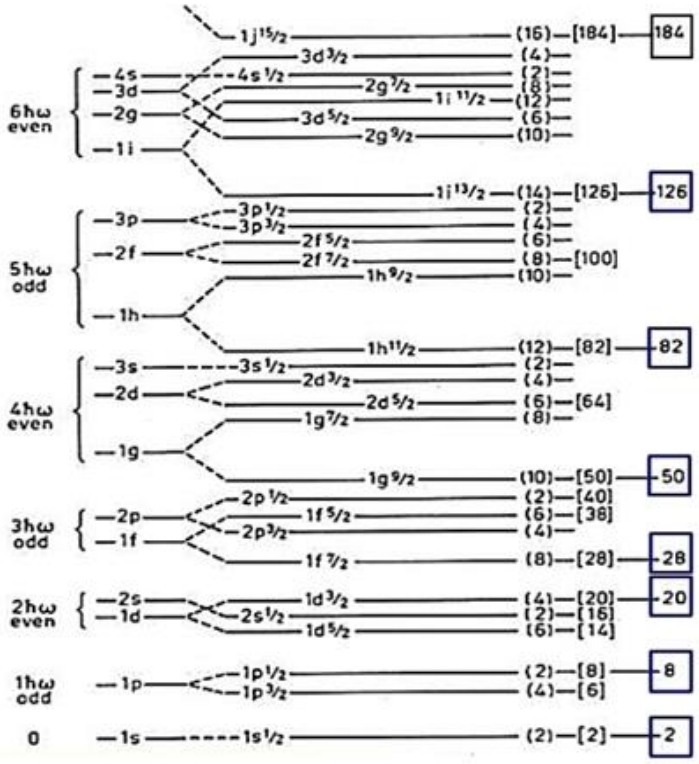

Figure 2.2: *Splitting of nuclear levels due to the spin-orbit interaction. On the right side, partial and accumulated nucleon numbers are shown. The magic numbers (shown at the extreme right-hand side) are correctly reproduced, and the shell effect is evident. Adapted from Ref. [36].*

2.2 Nuclear masses and Binding energies:

Nuclear masses have been of great interest to nuclear physics. The mass of the nucleus should be regarded as one of its main characteristics reflecting the role of the strong nuclear interaction on nuclear binding energies [37]. The binding energy is defined as the difference between the sum of the masses of the nucleons which constitutes a nucleus and its nuclear mass [38]. As an example, by observing the simplest nuclear system that exist, the deuterium nucleus ($^{2}_{1}H_{1}$), it is easy to identify that when a neutron and proton bind together to form a deuteron, a part of their rest mass energy is released [39].

Therefore, the mass of an atomic nucleus composed by N neutrons and Z protons and A=Z+N nucleons, where A is the mass number, is given by:

$$M(Z,N) = Z * m_p + N * m_n - \frac{1}{c^2} BE(Z,N) \quad (1)$$

Using the Einstein's mass energy equivalence, the mass defect Δm is equal to ΔE = Δm*c^2 [29]. The quantity ΔE or BE(Z,N) presents the nuclear binding energy.

Indeed, given the nuclear masses one can easily extract the nuclear binding energy which is expressed by:

$$BE(Z,N) = (Z * m_p + \mathrm{N}*m_n - \mathrm{M(Z,N)}) * c^2 \quad (2)$$

where m_p and m_n are the rest mass of a proton and a neutron respectively, M(Z,N) is the total nuclear mass and BE(Z,N) is the nuclear binding energy. A schematic representation of the last statement is shown in the following Fig. 2.3:

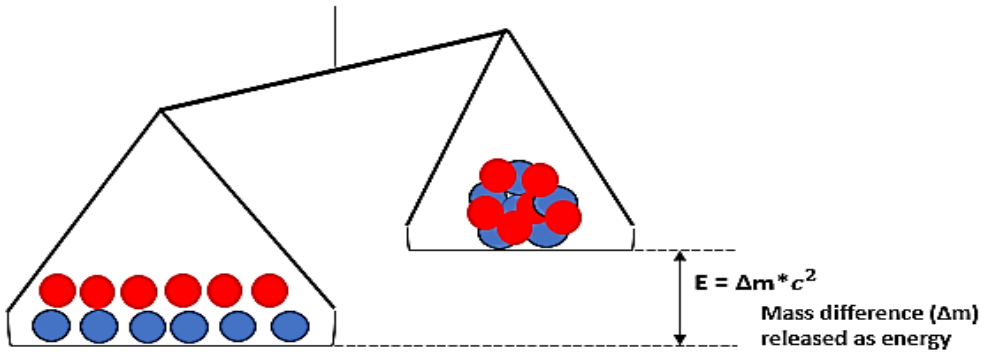

Figure 2.3: *The scale example which illustrates that the mass of a nucleus is less than the sum of the masses of its constituent protons and neutrons. The energy, E, which is released to form the nucleus is also shown. Image by Author.*

The Eqs. (1) and (2) correspond to the mass, and hence the binding energy, for a nucleus with mass number A. If one wants to determine the atomic mass of the same nucleus, then the aforementioned Eqs. (1) and (2) should be modified to account for the mass of the atoms of ^{1}H (hydrogen atom), M(^{1}H). Those modifications are given by the Eqs. (3) and (4). In general, as it is also highlighted in the upcoming section (2.3), it is considered easier to use atomic masses rather than nuclear masses. Atomic masses instead of nuclear masses are also adapted for the calculations of the present investigation.

$$M(Z,N) = Z * m_p + N * m_n + Z * m_e - \frac{1}{c^2} BE(Z,N) \quad (3)$$

or

$$BE(Z,N) = (Z * m_p + \mathrm{N}^{*}m_n + \mathrm{Z}^{*}m_e - \mathrm{M(Z,N)}) * c^2 = (\mathrm{Z}^{*}\mathrm{M}(^{1}\mathrm{H}) + \mathrm{N}^{*}m_n - \mathrm{M(Z,N)}) * c^2 \quad (4)$$

where m_e is the total electron mass which one can also ignore its contribution as it is not considered so significant compared to the range of the nuclear mass [40].

The nuclear binding energy indicates which nuclei are stable and which undergo radioactive decay and therefore gives an explanation of the chart of nuclides, Fig. 2.4. An imbalance in neutron to proton ratio initiates that there is an excess of either neutrons or protons and the nucleus must change a neutron into a proton and vice versa, through the process of beta decay (beta minus or plus decay).

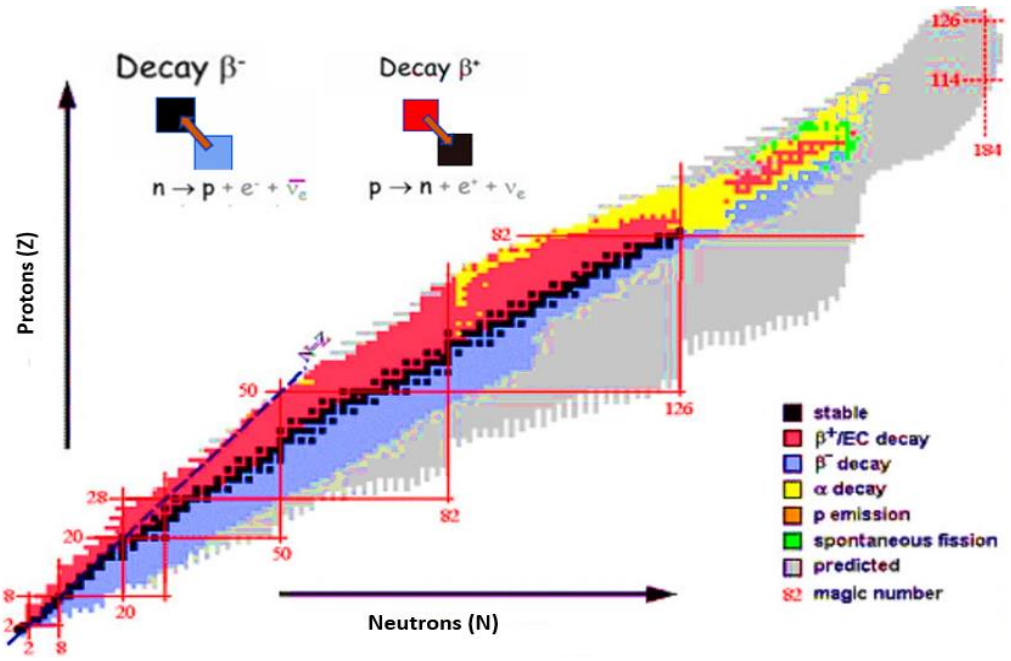

Figure 2.4: *Chart of nuclides: The valley of stability, the N=Z line of stable light nuclides and the different types of radioactive decays are shown. Also, the magic (closed shell) numbers are illustrated in the ends of vertical and horizontal lines, while on the top left corner the beta decays are shown. In the grey area belong unknown nuclei which have been predicted but have not been yet experimentally found. Adapted from [41].*

The binding energy BE(Z,N) of a nucleus is the energy required to separate all the nucleons of a nucleus, or equivalently, the energy released when a nucleus is formed by its component's nucleons. These properties explain nuclear fission and fusion, correspondingly, and are described by the plot of experimental binding energies per nucleon shown in the following Fig. 2.5 [29,42]. Hence, this curve is of extremely importance in nuclear physics as indicates the nature of the force that composes the nucleus as well as α and cluster decays.

This plot also explains the region of stability including the most tightly bound nuclides which are around the mass number A ≈ 62. At this point the curve reaches a maximum of approximately 8.7945 MeV/A (according to the data of AME2016 [2,3]) and after that decreases gradually.

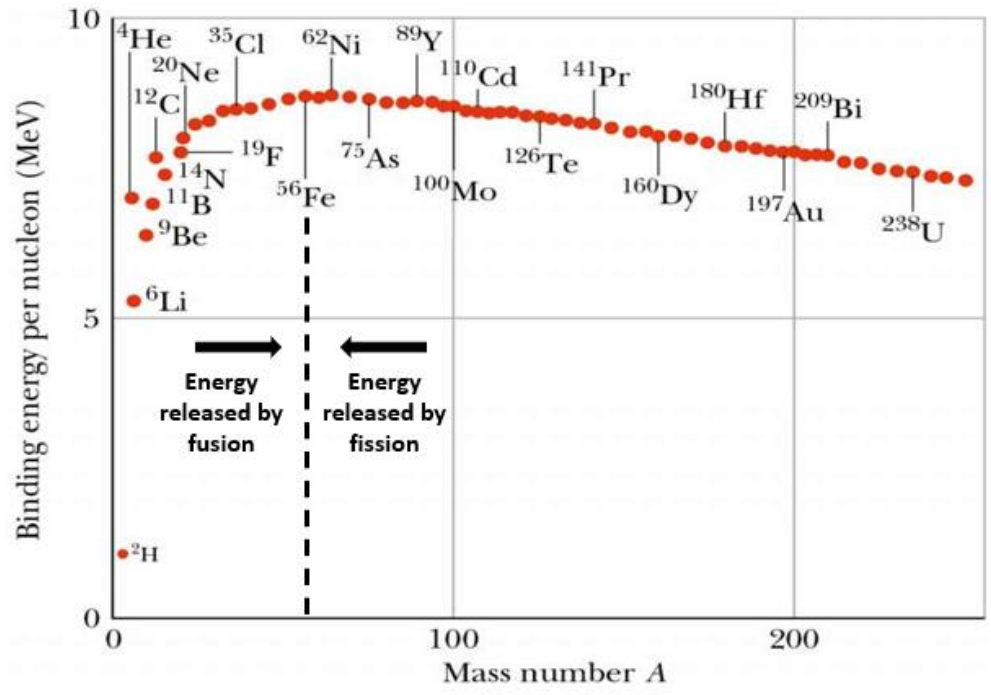

Figure 2.5: *Nuclear binding energy per nucleon (MeV) as a function of the mass number A. Nickel-62 (^{62}Ni) with the highest binding energy per nucleon is marked. In the left of the vertical dashed line lie nuclei in which fusion is common, while in the right fission dominates. Adapted from Ref. [43].*

Nowadays, experimentally measured nuclear masses count more than 2400 and have been obtained with a very high degree of accuracy [44]. The increase of the number of the measured nuclides' masses, is of paramount importance for the completeness of our knowledge of nuclear structure, as nuclear masses can provide crucial inputs and answer questions in several unanswered and challenging topics of nuclear physics.

Especially, in nuclear physics, nuclear mass data are of great importance in describing global properties [45] and extracting nuclear symmetry energy [46,47,48] which is closely connected with the dynamic process of nuclear reactions as well as the structure of the nuclei [47]. Moreover, for the understanding of the properties of the three-nucleon forces experimental mass data are mandatory [11].

Also, the mass of a nucleus and its binding energy, is an important ingredient for various aspects of studies in nuclear structure and reactions and also in nuclear astrophysics, contributing to the understanding of the origin of the elements in the universe [45] or the determination of the chemical composition of the crust of a neutron star [49].

Recent developments of experimental techniques at rare-isotopes-beam facilities have led to the measurement of the masses of many exotic nuclei. These nuclei play a key role in the study of astrophysical nucleosynthesis, for example r-process, the formation and evolution of

nuclear magic numbers far from the well-studied valley of stability, at neutron-rich side. It is worth mentioning that studies of exotic nuclei paved the way to the understanding of the island of inversion, where standard magic numbers break down (disappearance of N=20 neutron magic number) [35].

Despite the recent advances in the experimental facilities and modern mass measurements, many of these masses remain still unknown (gray area of Fig. 2.4), especially for nuclei of super-heavy element region as well as for those at extreme neutron and proton rich regions of nuclear chart [50]. To this end, there is an increased need on precise nuclear mass measurements of experimental masses as well as reliable theoretical models which are capable to predict unknown nuclear mass data by extrapolating from the measured nuclei. Therefore, a sufficient accuracy in the predictions of the exotic nuclei can be achieved [50]. However, even though theoretical models have been given an impressive level of accuracy and sophistication [51], differences that are still present in the predictions of unknown masses between different theoretical models, uncover serious weaknesses in the calculations and sometimes put under question the predictive power of the models.

2.3 The evaluation of nuclear masses:

As discussed in the last section, nuclear masses and binding energies provide one of the major and fundamental tools that are employed to map the structural evolution across the nuclear landscape. Although there is a large number of known experimental mass data that have been measured and are available up to date, new, and still better measured nuclear mass measurements are necessary to contribute to our understanding of nuclear structure.

Also, improvements or validation of some of the already measured atomic masses are needed to be performed due to the enormous quantity of information that is available and has been obtained by different studies and experimental techniques. The process of the evaluation involves comparison, combination, or derivation of an average adopted value of the measured results [52]. Therefore, the interest of nuclear physicists lies in finding an appropriate and consistent method to execute and report these experimental mass values. To this end, the Atomic Mass Evaluation, which is often referred as AME or the 'mass table', is a comprehensive atomic mass database including experimental as well as extrapolated atomic mass results.

Atomic masses can be determined with several experimental methods. The first technique is based on the differences resulting from the Q value when a radioactive decay or nuclear reaction occurs (indirect methods). The Q value is defined as the energy absorbed or released following a nuclear reaction. Although this method can achieve accurate measurements, it should be treated with a special care in the determination of the ground states to prevent cumulative errors. The second method that is widely used and tends to generate small errors, is mass 33 spectrometry measurements, where atomic mass data are determined through time-of-flight or frequency measurements (direct methods). However, several other types of mass spectroscopy can be used, providing valuable experimental results. Also, determination of atomic masses can be achieved by conducting measurements with respect to a well-known reference nucleus [53].

Physicists, who are involved in these calculations, should make readjustments to the measured values creating a coordinated network which is applicable to check the validity of the new mass values. To this end, experimental mass measurements, most of the times, are accepted after appropriate treatment and then follow a mass adjustment procedure. Regardless of the adapted process, the mass values are not considered as absolute mass measurements [54].

However, taking into consideration the error accompanying each technique, it always requires a critical evaluation and judgment over the new mass measurements before entering the database. With this way, precise measurements can turn into accurate ones [53]. Particularly, in reference [55], it is highlighted that there are mass values that are not taken into consideration due to the large values of uncertainties. Other reasons could reflect a wrong mass measurement caused by a possible mistake in the estimation of the final decay energy level or the decay energy associated with an isomer rather than to a ground state or the mass number assigned to a decay was wrong.

Additionally, it is significant to be stressed that mass tables of Atomic Mass Evaluations record atomic mass values and not nuclear mass values due to the technique of estimation of the majority of nuclei involved in the database. Thus, most of the existing mass data have been obtained using indirect methods, which deal with mass differences between atomic nuclei rather than nuclei or by mass spectrometry. However, experimental mass measurements obtained by the in-flight separation production mode can lead to nuclear mass measurements [53].

The Atomic Mass Evaluation, which is issued every few years, provides a complete assessment of all the currently available atomic mass data. Recently, the most up to date atomic mass evaluation was published and it is known as AME2020 [55,56]. The data analysis presented in the current report, is exclusively derived by using the Atomic Mass Evaluation published in 2016, known as AME2016. However, a comparison between a specific subset of experimental atomic masses of AME2016 and their corresponded values obtained from AME2020 was occurred and any relevant outcomes are commented in the chapter of results, if necessary.

The results included in the AME2020 have been obtained using mass-spectrometry methods, Penning traps, as well as energy measurements [55]. Reference should be made to the use of Penning traps as a mass spectroscopy tool which generates the most accurate input data for stable or long-lived nuclides [55]. In AME2016, the mass-spectrometry results were taken from measurements using cyclotron frequencies of ions in Penning traps [2].

2.4 Nuclear Models and Basic Theoretical Approaches:

2.4.1 The nuclear mass models:

In order to answer fundamental questions in nuclear physics, as those presented in chapter 1, it is essential to successfully construct an accurate theoretical formulation for a description of the nuclear properties of nuclei (such as binding energy, shape, nuclear size etc.) across the nuclear landscape. The theoretical efforts towards this investigation is crucial for understanding several physical phenomena not only in nuclear physics but also in nuclear astrophysics.

There are several methods and approaches for prediction of experimentally inaccessible nuclear masses and all of them include fitting to known mass data to a larger or smaller extent in an attempt to uncover the physics of these elusive mass regions [17,57]. Hence, nuclear models are semiempirical in the sense that include a number of free parameters, associated with specific physical terms, that are fitted to nuclear data [58].

Theoretical nuclear models are mainly distinguished into global and local approximations. The philosophy of these two approaches differs. The global models make use of all the currently available experimental measured nuclear masses, while the local approaches use techniques for the prediction of nuclear masses in a limited region. Although, global nuclear mass formulae cannot capture ‘‘higher resolution structures’’ which are important for an

accurate prediction [53,59], are able to explain some general characteristics and the main properties of the mass surface and N-Z plane. On the contrary, local approaches are able to perform more accurate nuclear mass predictions compared to global techniques, but only for the mass region around to the experimentally known nucleus [59].

It is also essential to further categorised the nuclear mass formulae, usually starting from the simplest case of the liquid-drop model, which is expanded with additional corrections to its initial form. Particularly, nuclear mass models can be classified into three main categories based on the adapted theoretical approach and physical terms involved in the calculations. Macroscopic mass formulae as well as macroscopic-microscopic (macro-micro) approaches or purely microscopic mass formulae have been developed over the past decades [4,53] aiming to reproduce the already measured atomic mass data as well as to provide reliable extrapolations, especially for nuclei in the highly neutron rich part of nuclear chart.

The term 'macroscopic mass formula' is used to describe the sum of the energy terms which are generally given by the liquid-drop model [60]. Macroscopic mass formulae are applicable to reproduce the gross nuclear features while they are unable to consider deviations which are caused due to the presence of quantum shell effects. When shell and pairing corrections are also added to the macroscopic part of the theoretical formula, the coexistence between macroscopic and microscopic effects composes the aforementioned 'macroscopic-microscopic' (macro-micro) approach [60], which so far provides a valuable and highly functional tool in the description of the systematics of nuclear properties. Also, purely 'microscopic' theories have been developed for the description of the atomic nucleus from the base of nucleonic interactions via realistic two- and three-body forces [61].

Therefore, one can find and assess nuclear models of various kinds available in the literature. In the introduction section of Ref. [50], a short review on the different nature of nuclear models is presented. Some of the nuclear models which fall into the category of the macroscopic-microscopic approach are the improved Bethe–Weizsäcker liquid drop model, modified to account for surface and volume contributions as well as Wigner effects [38], the finite-range droplet model (FRD) [62,63,64], the Thomas-Fermi Model [65], the Thomas-Fermi with the addition of the Strutinsky integral model (ETFSI) [66], the relativistic Hartree (RH) or mean field theory (RMF) [67], which it is considered as a successful theory in describing several nuclear phenomena [68,69,70], with lots of applications in nuclear astrophysics field [71-76], the Wigner-Kirkwood mass formula [51,77,78,79], the Garvey-Kelson model (GK) [80-83], the Liran-Zeldes model (LZ) [84], the Koura et al., Koura– Tachibana–Uno– Yamada mass model (KTUY) [85,86], the nuclear Lublin-Strasbourg Drop (LSD) model [87,88], an infinite nuclear matter (INM) model [89,90], the Weizsäcker-Skyrme model [45,47,91,92,93,94,95], the Duflo-Zuker mass formula [96-99]. Among the aforementioned nuclear mass models, some characteristic examples of global mass models, are the finite-range droplet model, the Duflo-Zuker mass model, while the Garvey-Kelson model (GK) [37,47] is an example of local approximation.

At this point, special reference should also be made to the Duflo-Zuker (DZ) mass model which is capable to describe measured nuclear masses with a standard deviation of approximately 500 keV, if only 10 parameters are included in the fitting procedure, while the Duflo-Zuker mass model (DZ33) with 33 parameters achieves the best fit with a standard deviation of about 400 keV [49,100]. Also, the Thomas-Fermi statistical model with a well-chosen effective-interaction [95,101] is used for accurate calculations of nuclear masses.

Additionally, the rapid expansion of computational techniques have opened an exciting new era of capabilities in the nuclear structure theory and particularly, in microscopic theoretical approaches of nuclear models. To this end, several microscopic nuclear mass equations have been suggested based on the Hartree-Fock-Bogoliubov (HFD) mean field models with the BSk21 Skyrme interaction (HFB21) [102] (global method [37,50]) or alternative with the D1M Gogny forces (GHFB) [103]. Also, the Density-functional theory is considered a significant microscopic approach which has also attracted attention since it can successfully describe data of known nuclei using relativistic and Skyrme interactions. Moreover, neural networks have been recently used for nuclear mass predictions and their error's estimation [104,105].

A detailed description of the above nuclear mass models as well as their key ingredients and physical interpretation can be found in the references accompanied each of the theoretical model. However, a special reference should be made to studies related with an accurate determination and predictive power of nuclear mass equations across the years. These models were tested and compared both for their ability to precisely predict as-yet-unknown masses as well as in producing the lower standard deviations (rms) in the selected atomic mass regions. A study relevant to the above process was conducted in Ref. [106], where ten frequently applied nuclear models of different features were tested and compared in different atomic mass regions of nuclear chart. This paper should also be viewed as a valuable guidance for future investigations related to the present theoretical framework. The proposed nuclear models can be tested incorporating theoretical framework of this work. Correspondingly, similar studies can be found in Refs. [38,53,107,108,109,110].

Significant modifications as well as extensions of the Bethe–Weizsäcker mass formula has been devoted in the macroscopic parts of some of the aforementioned mass models in order to improve its formalism. Some of these modified macroscopic parts were also tested in terms of the current investigated topic. In Refs. [4,30,48,53,58,111,112,113,114,115,116], modified liquid drop mass formulas, mainly based on the Bethe–Weizsäcker formalism, are tested for their ability to describe nuclear masses as well as to predict unknown nuclei. As it will also be pointed out in the section of methodology, only the most notable models (among the tested ones) for this study, are presented to some extent. An analytical reference of such an approach is analyzed in the upcoming chapter 3 of this thesis. However, the theoretical formalism of the latter models will also be presented in the upcoming subsection (2.4.2).

In addition, a reference should be made to the study [117], where the semi-empirical mass formula of Bethe–Weizsäcker is extended with the addition of terms to account for macroscopic and shell corrections. The correlations between the terms are examined as well as mutual influences that it is possible to be revealed between them. The nuclear models, suggested in this paper, were also tested for their efficacy to reproduce the parabolic trend of the residuals between doubly magic nuclei which is investigated in the present research.

2.4.2 The two LDM formulae:

At this point, two Liquid Drop Mass (LDM) formulas will be presented, as their formalism will be employed in the fitting procedure to the experimentally available atomic mass data.

Indeed, this subsection shall focus to the demonstration of the general expression of the following mass formulas as well as in the physical interpretation of their constituent terms:

1) The BW-mass formula:

One of the first nuclear models, the BW-mass formula considers the nucleus as a droplet of uncompressed fluid which resembles in some ways a classical liquid drop. Based on the Liquid Drop Model, the semi-empirical mass formula (SEMF) was derived and estimates fairly accurately the systematic behavior of the nucleon binding energy with the mass number [34], assessing how much energy is available for consumption [24]. It gives a general description of masses and related stability of nuclei [5] and incorporates the essential macroscopic physics [37,118].

In the liquid-drop model, the binding energy is expressed by a sum of terms which are individually functions of the neutron number N, proton number Z, and the mass number A=N+Z [119]. Specifically, this formula consists of five terms which are the volume, surface, coulomb, asymmetry, and pairing terms. Although refinements to these terms have been followed over the years aiming to add additional corrections to existing terms or capture more effects, the general baseline expression of the formula is the same today. Modifications to the Coulomb and pairing terms expressions have also been proposed by different authors [120,121]. Several of these terms were tested and compared for the purposes of the present research study to conclude which are the most appropriate for our analysis.

The nuclear binding energy BE(N,Z) is expressed by the SEMF:

$$BE(N,Z) = a_v * A - a_s * A^{\frac{2}{3}} - a_c * \frac{Z*(Z-1)}{A^{\frac{1}{3}}} - a_a \frac{(N-Z)^2}{A} + a_p \delta(N,Z) \qquad (5)$$

where δ(N,Z) is:

$$\delta_{N,Z} = \begin{cases} \frac{1}{A^{1/2}}, & \text{N is even and Z is even} \\ -\frac{1}{A^{1/2}}, & \text{N is odd and Z is odd} \\ 0, & \text{N is even and Z is odd} \\ 0, & \text{N is odd and Z is even} \end{cases} \qquad (6)$$

The delta function δ(N,Z) relates to the superconductivity properties of atomic nuclei. Since nuclei are systems that are normally at zero temperature, they form cooper pairs that are the basic blocks of the electronic superconductivity and thus they are superconductors. Hence, the delta function is important to be considered in the mass formula of Eq. (5) [122].

Each of the terms in the SEMF (Eq. (5)) has a physical meaning which is based on general nuclear properties and forces:

- **Volume energy term (a_v):** The volume energy term depends on the strong nuclear interaction between neutrons and protons when they are near each other. Thus, a positive, linear term which accounts for the number of nucleons in a nucleus should be added in the calculation of the total binding energy.
- **Surface energy term (a_s):** The surface term is a correction to the volume term which accounts for the smaller contributions of the surface nucleons. The surface nucleons have only a few nearest neighbors and do not interact with as many nucleons as those inside the nucleus [123].
- **Coulomb energy term (a_c):** This term is derived from the Coulomb interaction among protons and shows that protons repel each other through the repulsive electromagnetic Coulomb force. A nucleus with many protons is forced to a large Coulomb repulsion and thus has lower binding energy [123].
- **Asymmetry energy term (a_a):** This term accounts for the protons and neutrons occupying independent quantum states and it is related to the Pauli principle. The imbalance caused by the difference in the number of protons and neutrons of the asymmetric nuclei, provides higher energies to the nucleons which are occupied by higher energy quantum states creating a more unstable nucleus [123].
- **Pairing energy term (a_p):** The final term indicates that nucleons in nuclei tend to form pairs. This is physical evidence which is given by the Eq. (6) and shows that when N and Z are even, the binding energy is greater, while it is decreased in the case of N and Z are odd numbers [123]. Also, for even-odd configurations, the pairing term is neglected and there is no physical influence depending on it.

The coefficients of the terms in Eq.(5), a_v, a_s, a_c, a_a, a_p , which have a clear physical interpretation, as explained above, are presented in the following Fig. 2.6:

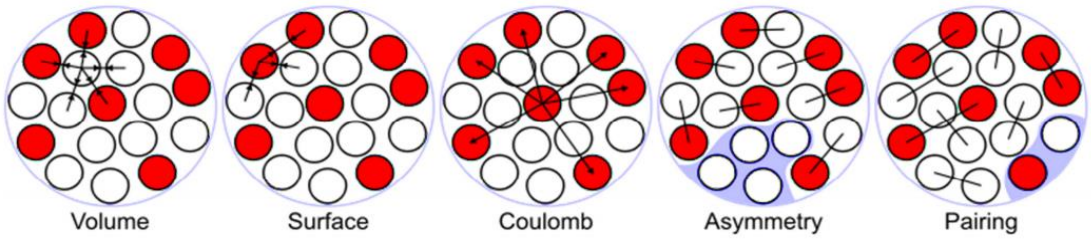

Figure 2.6: *Schematic explanation of the terms of the semi-empirical mass formula in the liquid drop model of the nucleus. Adapted from Ref. [24].*

Moreover, it is worth mentioning that, in Ref. [112], the results show an independence in the contribution of the pairing term in the vicinity of closed shell nuclei. The contribution of the pairing term to the fitting procedure of doubly magic nuclei has also been investigated in the present research work and is analyzed in the methodology and results section.

From now on, the mass formula presented by the Eq. (5) will be referred as 'BW' and/or baseline formula. This is the standard-baseline formula which does the groundwork of the current investigated topic.

2) A LDM formula which is a modified expression of the Bethe-Weizsäcker one, first introduced in Refs. [30,124]:

As previously mentioned, the origin of the traditional magic numbers 2, 8, 20, 28, 50, 82, and 126, can be explained by the shell model. The original expression of the Bethe-Weizsäcker mass formula, Eq. (5), is inadequate to describe the shell closures related to the magic numbers and their signature is clearly observed by the large deviations in the residual plot of binding energies as a function of the neutron or proton number. Although, modern mass formulae, as those presented in the subsection (2.4.1), successfully account for such nuclei, light nuclei, especially close to the neutron driplines are also subject to investigation. The standard BW mass formula gives an overall description for nuclei of medium and heavy mass regions while it is incapable to predict the mass of light nuclei especially for those approaching the drip lines.

Additionally, the BW mass formula cannot predict new magic numbers and the disappearance of some traditional ones. As an example, the unexpected shell closure at neutron number N=16 has experimentally been confirmed, making the ^{24}O the heaviest last bound oxygen isotope found in nature, ad doubly magic nuclei [16].

These observations notify for necessary modifications that need to be applied to the standard BW formula in order to alleviate the above problems. Hence, the interest lies in designing a modified version of the BW mass formula which accounts for light nuclei, identifying the new magicity or its loss and setting better boundaries in the prediction of the neutron drip line.

Taking into consideration all the above, a newly modified formula was introduced by Samanta and Adhikari [30], from an easy phenomenological form:

$$\mathrm{BE(A,Z)} = \mathrm{a_v} * \mathrm{A} - \mathrm{a_s} * \mathrm{A}^{\frac{2}{3}} - \mathrm{a_c} * \frac{\mathrm{Z}*(\mathrm{Z}-1)}{\mathrm{A}^{\frac{1}{3}}} - \mathrm{a_a} * \frac{(\mathrm{A}-2\mathrm{Z})^2}{1+e^{-\frac{A}{k}}} * \mathrm{A} + a_p * \delta_{new} \qquad (7)$$

where the constant k is set to 17 (k=17) and associated with the modifications applied to the asymmetry term.

Also, a new delta quantity δ_{new} is added in the pairing term, including a constant value given by c = 30, while $\delta = \delta(\mathrm{N}, \mathrm{Z})$ is the old pairing expression as described by:

$$\delta_{\mathrm{new}} = \left(1 - \mathrm{e}^{-\mathrm{A/c}}\right) * \delta \tag{8}$$

This mass equation, Eq. (7), includes modifications to the asymmetry and pairing terms and accounts well for light nuclei as well as reveals extra stability associated with particular positions of neutron and proton numbers in the light mass region. In this way, the existence of new magic numbers was supported or suggested by the above modified formula. In the present work, the modified formula presented by the Eq. (7) is referred as 'LDM1'.

Also, it should be stressed that similarly, to the BW baseline formula, the newly updated mass equation, Eq. (7), does not incorporate shell effects, and therefore, large discrepancies between the theoretical estimations and experimental exist when trying to justify the extra stability near the magic numbers [30].

Particularly, at this point it is interesting to compare the optimal parameters obtained from a fit of the present generalized BW formula, given by the Eq. (7), with the parameters of the BW baseline formula of Eq. (5). To this end, two linear least square fits were performed to all the experimentally known binding energies data included in the AME2016 [2,3] text file [125]. The best parameters of each fit are displayed with their accompanied uncertainties in the following Table 2.1 and the calculation of the goodness of the fit is also considered useful. This calculation was conducted using the well-known quantity root-mean-square (rms) deviation of the measured binding energies from the estimated values described by:

$$rms = \sqrt{\frac{\sum_i (M_i - P_i)^2}{N}} \tag{9}$$

where i is the index of each data point, M_i is the experimental binding energy, P_i is the predicted value of binding energy from the fit and N is the number of data points involved in the fitting procedure, i.e., N is equal to 2494 for the AME2016 tabulation [125].

Linear Least-Squares Fit to the entire AME2016 mass table		
(MeV)	BW formula, Eq.(5) rms: 3.61 MeV	LDM1, Eq. (7) rms: 2.99 MeV
a_v	15.27 ± 0.02	15.84 ± 0.02
a_s	16.42 ± 0.07	18.25 ± 0.06
a_c	0.685 ± 0.002	0.721 ± 0.001
a_a	22.17 ± 0.06	23.55 ± 0.05
a_p	10.77 ± 0.88	14.31 ± 0.96

Table 2.1: *Best fit results of the BW baseline formula (Eq. (5)) and the LDM1 mass formula (Eq.(7)) to the experimental binding energies data.*

By inspecting the results of the fit coefficients as well as the calculated rms deviations between the experimental and estimated binding energies, for the nuclides presented in the entire AME2016 mass table, it is concluded that there is a difference between the results of the two fits. Particularly, it can be seen that the incorporation of only two parameters to the BW baseline formula leads to a reduction in the rms deviation from 3.61 MeV to 2.99 MeV, for the 2494 experimental binding energies of the AME2016 evaluation. The interest also lies in particular identifying the role of the LDM1 formula in better describing the light nuclei away from the valley of stability, compared to the BW baseline mass formula. To this end, the residuals obtained from a fit of the BW baseline formula and the modified LDM1 formula were compared for the three isotopic chains of oxygen, beryllium and lithium and are presented in the following Figs. 2.7, 2.8 and 2.9, respectively. In each graph ΔE denotes the difference between the experimental and the corresponding calculated binding energy values.

By the inspection of the residuals of the BW baseline formula and the LDM1 formula, it can be seen that the additional parameters which have been added to the LDM1 formula contribute significantly to the description of the light nuclei in the neutron rich side of the N-Z plane. Although the modified mass formula lacks shell corrections, its ability is notable to describe nuclei further than the stability line, by introducing only two modifications to already well-known parameters of the standard BW mass formula.

However, is should be noted that the modified mass equation, Eq. (7), has the same behavior as the BW mass formula when it comes to the description of heavy nuclei. Large deviations in the heavy mass region are also considered evidence for shell closures.

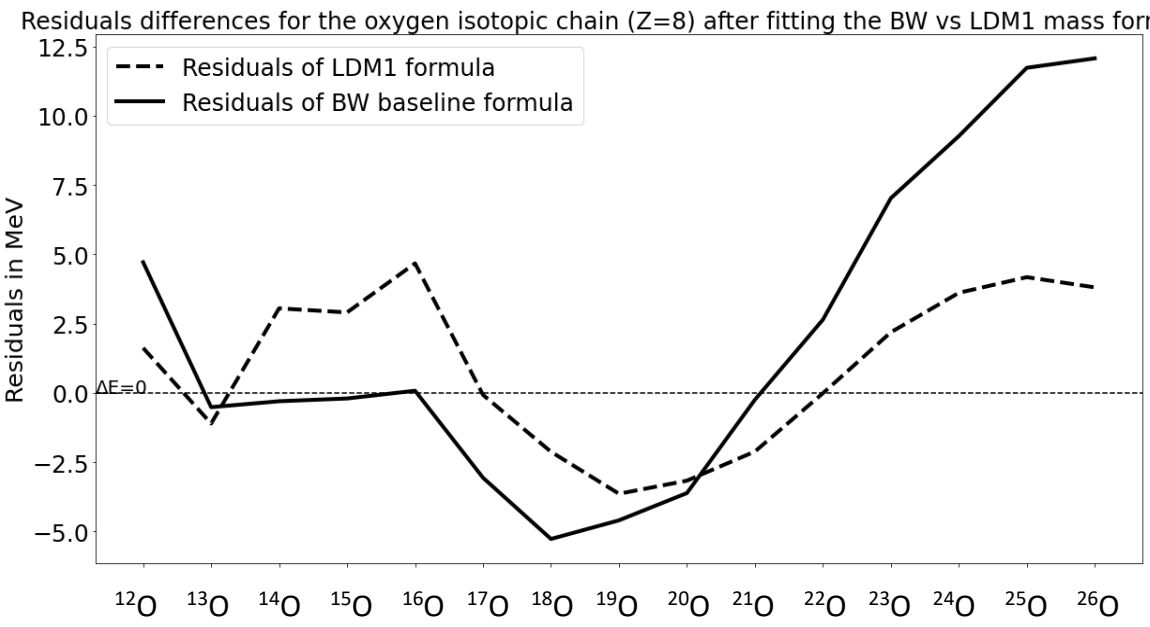

Figure 2.7: *Comparison of the residuals obtained from a linear least squares fit of the BW mass formula (Eq. (5)) and the LDM1 formula (Eq. (7)), for the oxygen isotopic chain.*

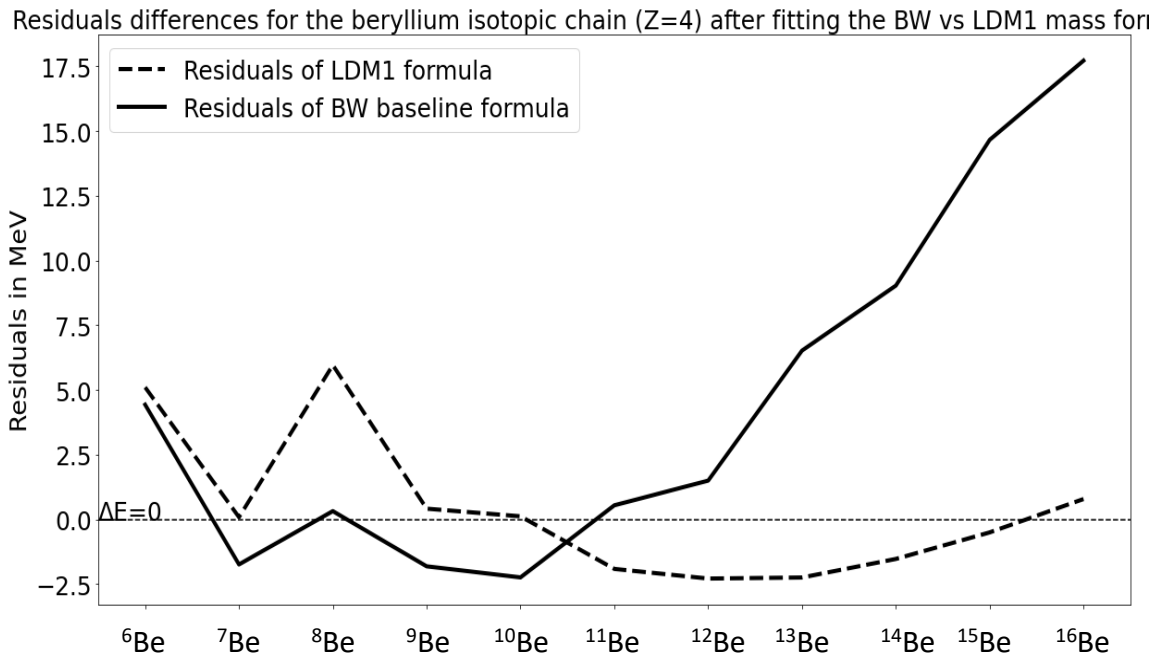

Figure 2.8: *Comparison of the residuals obtained from a linear least squares fit of the BW mass formula (Eq. (5)) and the LDM1 formula (Eq. (7)), for the beryllium isotopic chain.*

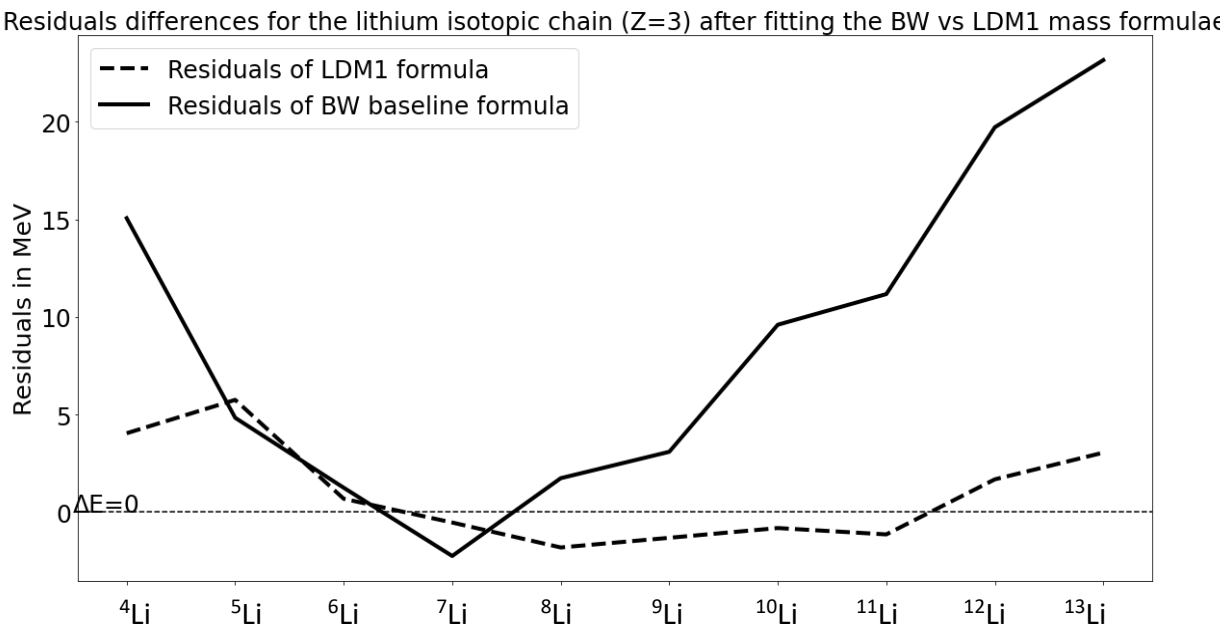

Figure 2.9: *Comparison of the residuals obtained from a linear least squares fit of the BW mass formula (Eq. (5)) and the LDM1 formula (Eq. (7)), for the lithium isotopic chain.*

2.5 The importance of 3N forces:

One of the most critical questions in nuclear physics is to understand the nuclear forces acting between the nucleons from first principles [126]. Towards this direction, the aim is to develop a unified description for all the nuclear systems composed artificially, in the laboratory as well as in cosmos based on the underlying forces among the nucleus [127]. In this context, the development of a systematic and consistent way to describe the interplay between nucleonic interactions in many-body systems have concentrated all the theoretical efforts for many years. Particularly, the focus lies on the development and application of microscopic many-body approaches that include three-nucleon (3N) forces [128]. Thus, nuclear theory has entered an exciting era of structure and reaction calculations driven by several developments in many-body methods and theories, which aim to explain phenomena and nuclear properties based on nuclear forces [40].

The role of the three-nucleon forces in nuclear systems, where more than two nucleon interactions are involved, is of major importance for the proper description of nuclei [126]. The concept of the 3N forces and their impact on observables was known a long time ago, from the early twenty century [129]. The importance of inclusion of the three-body forces in the calculations of a trinucleon system was identified in the mid of 1980's [130,131]. Two nucleon interactions alone were not sufficient to describe the experimental binding energy for nuclei with mass number A = 3, ^{3}H and ^{3}He [130]. Hence, three-body calculations had to be taken into consideration. In this way, an understanding of several phenomena, such as the structure of nuclei and nuclear reactions, can be achieved by entirely considering two nucleonic interactions coupled with three-nucleon forces [132]. To this end, consistent two-nucleon and three-nucleon interactions have been established as new standard inputs in several theoretical approaches [7]. In the standard meson-exchange theory [133], three body forces arise readily as well as in nucleonic interactions from Chiral Effective field theory (EFTs) which has a connection to the underlying theory of Quantum Chromodynamics (QCD) [134,135].

At the most basic level, the strong force is explained by QCD involving the quark–gluon interactions. Although Lattice QCD can predict properties of some nucleon states, the detailed description of many-nucleon systems based on QCD has not been achieved yet.

Chiral effective field theory provides estimates of contributions of interactions between nucleons using a scheme parametrized taking into account long-range pion exchange contributions and shorter-range contact interactions. These contributions manifest as nucleon-nucleon, three-nucleon and even many-body interactions. The appearance of three-body and other many body interactions is due to the composite nature of nucleons. Nucleons are not elementary particles and then they can be effected by external forces which distort their constituents. An interesting study which reviews the importance of chiral effective field theory in understanding the three-nucleon forces and making unique predictions for even higher order many-body forces are presented in Ref. [1].

Chiral effective field theory interactions are considered the theoretical microscopic input for ab-initio theories. Recently, significant progress has been made in the development of ab initio theories. This progress was greatly advanced by notable expansions in the following fields: nuclear interactions, development of better many body theories, vast increased computational power and use of improved algorithms, renormalization group methods [136,137].

Although, the application of the two nucleon interactions in many body theories is relatively straightforward and already established, the calculation of 3N forces has still unknown territories. Difficulties arise in creation of original conceptual models and their subsequent implementation. This framework is extensively analysed in Ref. [136] and references therein.

The inclusion of at least three-body forces in theoretical models is of paramount importance for an understanding of plenty of phenomena not only in several domains of nuclear physics but also in nuclear astrophysics [1]. Particularly, several studies point out the key role of three-nucleon forces in the predictions of neutron and proton drip lines as well as in understanding the properties of neutron-rich matter which is of great importance for the structure of neutron stars.

Three-nucleon forces have to be included in theoretical calculations for explaining phenomena and addressing questions related to the formation and evolution of the nuclear structure [1]. The first evidence of this was the investigation of the dripline in oxygen isotopes where the 3N forces make the nucleus ^{24}O doubly magic and a dripline nucleus [127,138,139,140,141]. Similar studies conclude that 3N forces significantly contribute for the magic neutron number N=28 [142]. Particularly, the so called ''oxygen anomaly'' has been explained in Ref. [127] using three-nucleon forces acting in few-body systems and is illustrated in Fig. 2.10:

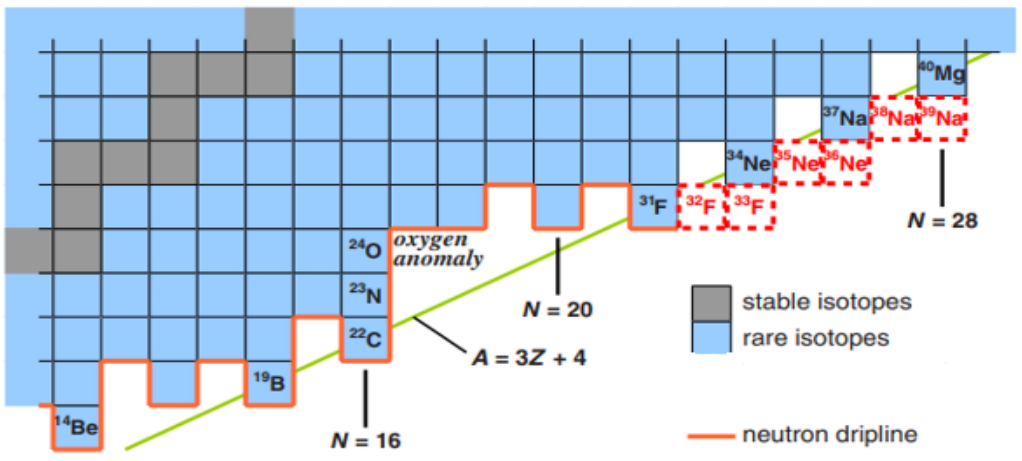

Figure 2.10: *The location of the oxygen anomaly in the neutron drip line is presented. Some isotopes of the most neutron-rich nuclei are also highlighted as well as the location of the neutron drip line corresponds to the fluorine and neon isotopic chains. Adapted from Ref. [6].*

The oxygen anomaly cannot be reproduced in shell model calculations that include only microscopic nucleon-nucleon interactions. The instability observed in oxygen isotopes with mass number from A=25 to A=28, has been attributed to the repulsive interactions among excess neutrons and thus are responsible for the change to the position of the neutron drip line from ^{28}O to the experimentally observed ^{24}O [127]. Additionally, other many-body correlations that may also have an impact in the oxygen anomaly, have been reported in Ref. [6] and it is considered that they are resulting from the dineutron correlation [143,144] and continuum coupling [145].

In a similar manner, the magic nature of the neutron number N=28 and its origin was investigated for the doubly magic nucleus ^{48}Ca [142]. On the contrary, among the well-understood magic numbers N = 2,8,20, the magic number N=28 could not be reproduced using theoretical approaches which involved only two-nucleon interactions. The outcome of theoretical calculations revealed that the origin of the N=28 magic number is attributed to the three-body forces which manifest as repulsive interactions between two valence neutrons [142]. In this way, the magic character of N=28 in the doubly magic nucleus ^{48}Ca, leads to a high 2+ excitation energy as well as to an enhanced magnetic dipole transition strength [142].

The later findings related to the oxygen and calcium neutron-rich isotopes established even more the importance of investigating the neutron-rich matter in terms of many-body interactions and developing relevant theories.

Additionally, neutron drip lines are particularly important in addressing questions on the r-processes which occur in the formation of the heavy elements in neutron-stars mergers [18]. Therefore, mapping and investigating the location of neutron rich regions accurately based on the effect of three-nucleon forces on stability is important [1].

Neutron-rich matter physics are distinguished by the wide range between extreme situations. In very low densities, where the distance between particles is large, the systems' properties depend on S-wave scattering and the effects of nuclear forces are not significant. This state resembles that of cold atomic gases. In intermediate densities, the energy-density, which is a function of the properties of nuclear matter, is used to describe the physics of neutron-rich nuclei which is important to determine the synthesis of heavy elements. In the other end, at higher densities, far away from the nuclear densities, scarce information exists on the properties and composition of nuclear matter. Three-body forces are needed to explain the neutron-rich matter's properties at nuclear densities. Specifically, three-nucleon forces direct the saturation of symmetric nuclear matter [146,147]. Also, three-nucleon contributions, although they are small, are considered important for the equation of state (EQS) of neutron-rich matter and consequently for the symmetry energy and its density as well as the neutron stars' structure [1].

Chapter 3

Methodology

The purpose of this chapter is to present the research design and philosophy adapted for the investigation of the present research topic.

Particularly, the research steps as well as the different computational tools and strategies that were assigned for the data interpretation are described.

Once the overarching rationale of the investigated topic is presented, the most important findings of this research are included in the results' section.

3.1 Research Strategy:

3.1.1 Research Approach:

Starting from the general form of the BW mass formula, local fits were conducted in order to get an optimum set of coefficients, which satisfies our theoretical aims. By the term 'local fit', it is meant a fit which involves nuclei with specific characteristics such as only doubly magic nuclei, only symmetric (N=Z) or asymmetric (N≠Z) subsets of nuclei, fits restricted to groups of nuclei (precisely measured nuclei or nuclei in certain atomic mass regions etc.). As it was previously discussed in subsection (2.4.2), the BW formula, which predicts binding energies of nuclei, incorporates the standard volume, surface, coulomb and asymmetry terms, a_v , a_s , a_c , a_a, respectively, while the pairing coefficient , a_p, is added as free or fixed parameter in the fit, for a slight better description of the residuals when needed.

In the present analysis, a residual is defined as the difference between an experimental value and the corresponding predicted binding energy. Specifically, each experimental value is approximated by a theoretical prediction, thus according to the definition a corresponding residual is calculated. The residuals are considered as an important optimization tool for the validation of a theoretical approach. By conducting a fit of a model to experimental data and then calculating the residuals, the adapted phenomenological approach can be validated.

Once the theoretical formulation and the experimental binding energy data was chosen, a fit to the binding energy data followed. When a fitting procedure was completed, the results of the fit were the estimated coefficients and the residuals.

Following visual inspection of the residuals, it should be no surprise if the predictions are somehow poor as the BW mass model has limited predictive power and misses important underlying physics. However, as it was stated in the introduction, this was not the point of interest here. The focal point is the behavior of the residuals examined for even-even nuclei

chains bound at each end by doubly magic nuclei. These nuclei groups were chosen to reproduce, the also previously observed [117], parabolic-like shape of the residuals calculated between two doubly magic nuclei.

At this point a reference should be made to the exclusive use of the even-even nuclei - nuclei with an even number of both protons and neutrons - in the following analysis. In general, even-even nuclei are considered more stable configurations. This is also reflected in the pairing term of the BW baseline formula, where even-even nuclei give rise to an increase in the binding energy which is also explained by the nuclear shell model. On the contrary, and according to the nuclear shell model, in an odd mass number nucleus unpaired nucleons or holes exist which result into additional interactions among the nucleons.

The present work was realized according to the discrete steps:

1) The BW formula was fit to the experimental binding energies of the traditional doubly magic nuclei and the resulting parameters were used in the steps below.
2) The residuals of the doubly magic nuclei were calculated.
3) The residuals of interest were those which corresponded to doubly magic nuclei in the edge of selected nuclei chains.
4) The residuals in the ends of the selected atomic mass chains (residuals of doubly magic numbers) should have both close values, ideally near zero values. From now on this basic assumption should be referred as first condition.
5) Using the BW formula with the already estimated parameters, the residuals for even-even nuclei bound by doubly magic numbers were evaluated.
6) If these residuals appeared in a parabolic-like shape, we consider this as the second condition that should be satisfied for proceeding to the next steps.
7) If the first condition (step 4) and the second condition (step 6) were satisfied, the analysis proceeded with the fit of the BW formula enriched with two additional terms which has been assumed to be related to NN and 3N forces. This fit was applied to the same even-even nuclei as in step 5.
8) The derived residuals should minimize the observed parabolic-like shape described in step 6.

The above steps are presented schematically in the following Fig. 3.1:

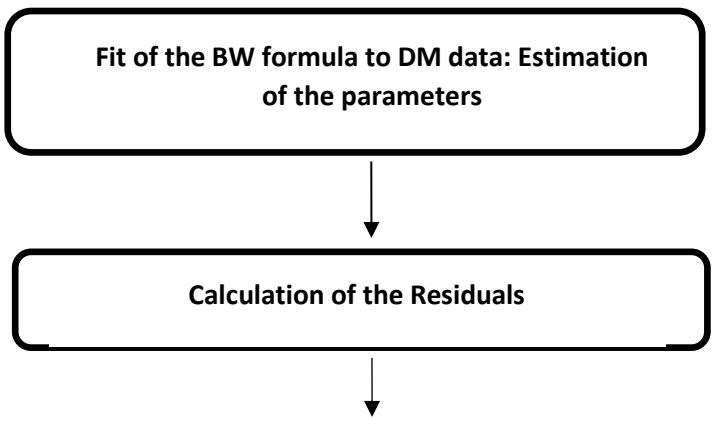

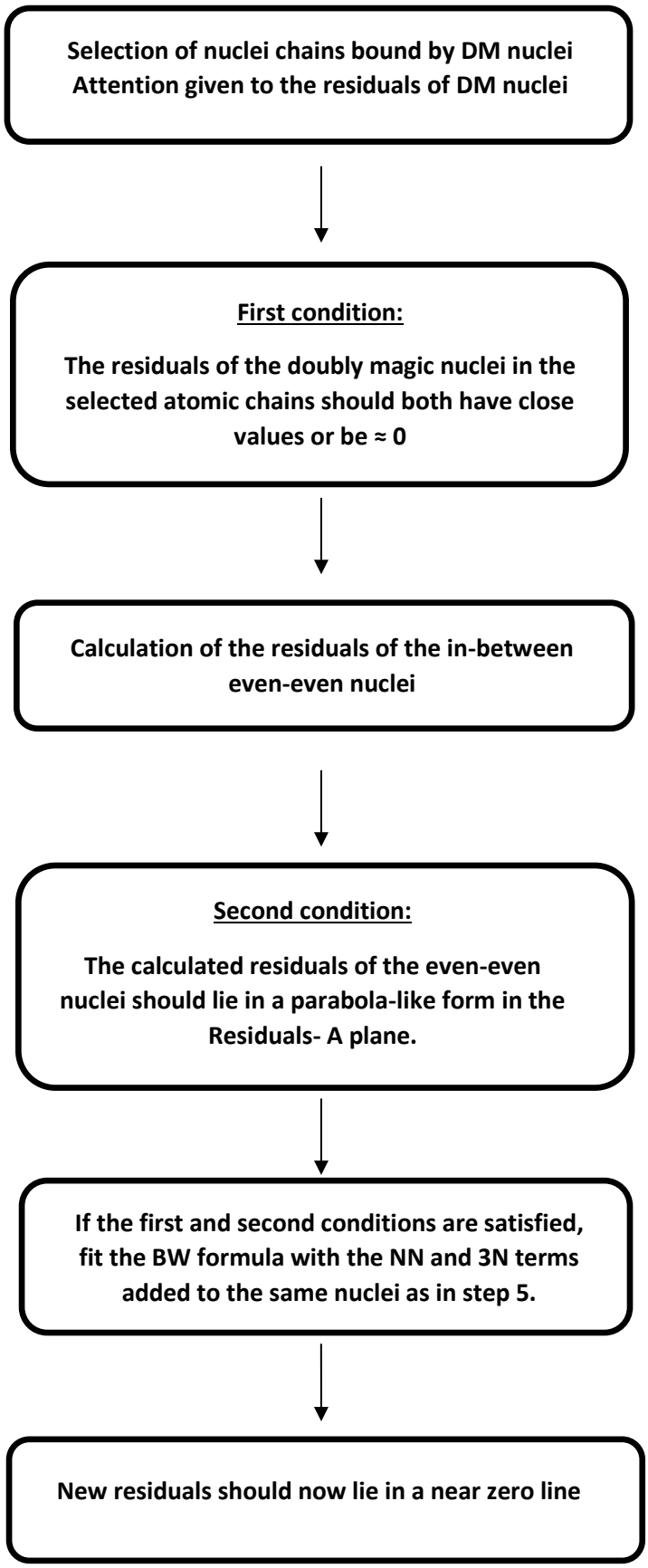

Figure 3.1: *Schematic representation of the research steps followed in this work.*

A repeated routine of the above steps were also occurred when the LDM1 formula was also used to fit the traditional doubly magic nuclei plus the doubly magic nucleus ^{24}O.

It is necessary at this point to start introducing the suggested valence-shell corrections and identify how the modified BW formula, with the inclusion of these two additional terms, contributes to the description of the parabolic trend of the atomic masses. By modified BW formula is meant the enriched BW baseline formula, neglecting or not the pairing contribution, plus the additional microscopic valence shell corrections, that has been assumed to be given due to NN and 3N body forces, and is presented as follows:

$$BE(N,Z) = a_v * A - a_s * A^{\frac{2}{3}} - a_c * \frac{Z*(Z-1)}{A^{\frac{1}{3}}} - a_a * \frac{(N-Z)^2}{A} + a_p * \delta(N,Z) + NN + 3N \quad (10)$$

The first terms a_v, a_s, a_c, a_a (with or without a_p) of the modified BW formula refers to the nuclear energy part of the corresponding BW baseline formula and they remain the same in terms of mathematical expressions.

The mathematical expression of the suggested additional terms, NN and 3N terms, as well as their physical interpretation are extensively discussed in the upcoming subsection (3.1.2). Also, as the fit was applied only to the even-even nuclei, the delta function of the Eq. (10) can be simplified as:

$$BE(N,Z) = a_v * A - a_s * A^{\frac{2}{3}} - a_c * \frac{Z*(Z-1)}{A^{\frac{1}{3}}} - a_a * \frac{(N-Z)^2}{A} + a_p * \frac{1}{A^{1/2}} + NN + 3N \quad (11)$$

From now on the notation ‘M’ next to BW mass formula, BWM, indicates that a fit was conducted after the inclusion of the microscopic valence-shell corrections, given by the NN and 3N terms, to the nuclear energy part of the BW baseline mass model.

The criterion for an improvement between the initial BW residuals and the residuals given by the modified BW formula Eq. (11), is a decreasing trend in the plot of the residuals versus the mass number of the nuclei.

The theoretical framework of the present research study is only a phenomenological approach where closed-shell configurations provide a convenient approximation and one can assume their neighboring nuclei into a valence-configuration space. The viability of this approach has been previously demonstrated in several publications [7] and it is characterized as an effective approach. The strategy introduces inert cores and treats the effects which are maybe resulted by the NN and 3N forces, as a consequence of the interactions of a smaller number of valence nucleons lying between the two closed shells.

To this end, we consider the doubly magic nuclei, as inert cores and then we let the valence nucleons of the even-even magic (or not) nuclei to be affected by what has been assumed to be given by two and three body forces. It is an approximation which simplifies the problem.

By considering inert cores and NN and 3N forces in the valence space, the theoretical approach and assumption of the present study will be applied to specific atomic mass regions and not to all nuclei.

3.1.2 Physical and Mathematical explanation of the suggested valence-shell corrections:

Having described in detail the phenomenological approach of this work, attention should be given to one important characteristic feature which drives the formalism of the proposed terms related to the valence shell corrections which have been assumed to be due to the two nucleon and three nucleon forces. The mathematical expressions of the NN and 3N terms, included in Eq. (11), can reproduce the parabolic pattern that should be observed in the residuals of the selected atomic mass region, starting, and finishing to closed shells (doubly magic nuclei). Specifically, the in-between residuals of nuclei, as it was stated, should lie in a form resembling a parabola, reaching a maximum in the middle of the shell. From now on, the notation 'DM' will be used as a shortcut for the 'Doubly Magic' nuclei. In the following Fig. 3.2, a schematic representation of the expected parabola of the residuals calculated between two DM numbers, using the Eq. (5), in a selected nuclide chain, is given:

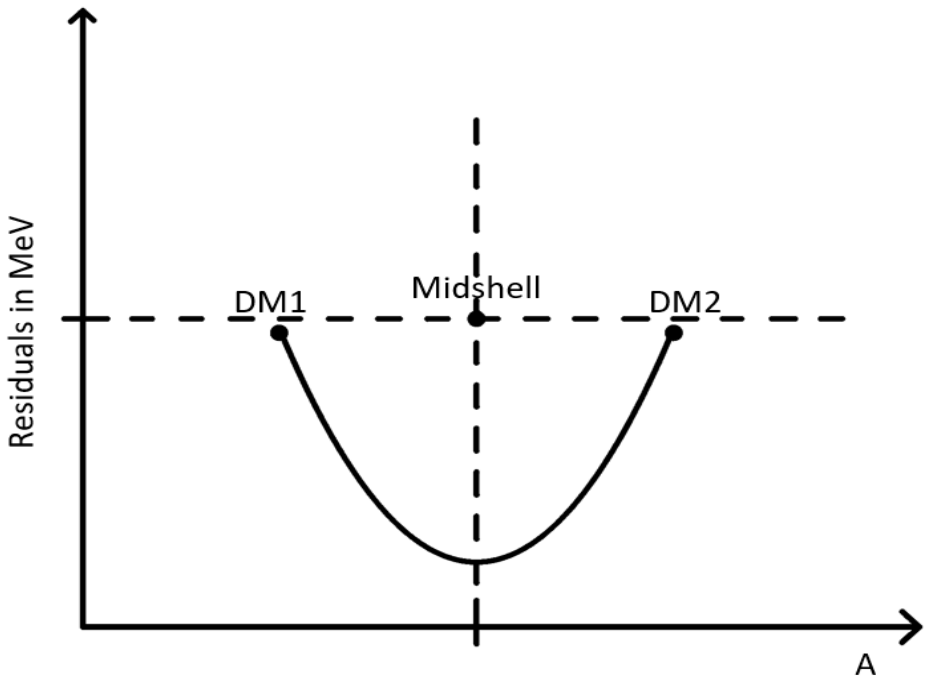

Figure 3.2: *Expected parabola of residuals calculated using the BW baseline formula (Eq. (5)), between two DM numbers (DM1 and DM2), in a selected nuclide chain.*

Therefore, the mathematical expressions of the proposed terms should present a parabolic function or in other words a U-shaped curved line. With such a way, the suggested terms are mathematically comparable with the residuals of the even-even nuclei which also expected to follow a parabola.

So, the question is, what are the physical quantities that can be incorporated in the expressions of the proposed terms and follow a U-shaped line?

In several studies shell corrections terms have been proposed from the standpoint of their dependence on the valence nucleons [117,148,149,150]. In like manner, the formalism of the current suggested terms refers to the description of NN and 3N body forces from the base of the independent particle model and is expressed as a function of the valence nucleons. Beyond a doubly magic core the number of valence nucleons are increased up to mid shell, as fill in orbitals of higher energies, and then decreased till they reach the next magic number of neutron and proton forming closed shell orbitals for both protons and neutrons.

This systematic behavior of the valence neutron (or proton) particles or holes counted from the nearest closed shell, is indicated in the structure of the suggested expressions which have been assumed to be provoked due to the two nucleon and three nucleon forces. Indeed, according to our hypothesis, the NN and 3N forces, which are described as a function of the valence nucleons, should be evident in the selected atomic mass regions, in a way which are capable of reproducing the parabolic pattern of the valence particles or holes.

As a result, the phenomenological shell-model interactions of NN and 3N forces that have been proposed in this research and describe the behavior of the valence nucleons between two closed shells, are mathematically expressed through the equations :

$$NN = B * [n * (n-1)] \tag{12}$$

$$3N = D\ * [n * (n-1) * (n-2)] \tag{13}$$

where B and D are free parameters to be estimated from the fit as before and n is the number of valence nucleons (particles or holes) of each nucleus counted from the nearest closed shell.

Evidently, the microscopic terms of NN and 3N terms, given by the Eqs. (12) and (13), respectively, are linear in the number of valence particles (or holes). They are parametrized employing the valence nucleons which given by the sum of the valence protons (n_p) and valence neutrons (n_n) counted from the nearest closed shell.

By construction, the formulas representing the NN and 3N contributions lie on a parabola as a function of valence nucleons. Starting from a closed shell configuration for both protons and neutrons, the valence particles for nuclei behind the mid-shell follow an increasing trend, while valence holes, correspond to nuclei approaching the next doubly magic shell-closure, are gradually decreased their number.

The NN and 3N terms have a clear physical interpretation which is comparable to the proton behavior due to Coulomb repulsion. Particularly, the NN term shows that each of the n valence nucleons interacts with the $(n-1)$ others. The same logic is applied to the 3N term, where it is considered that a valence nucleon interacts with the others $(n-1)*(n-2)$ but not with itself.

Firstly, the estimation of the number of valence protons and neutrons is necessary for the calculation of the total number of valence nucleons n as defined by the expressions of NN and 3N forces, Eqs. (12) and (13),respectively.

The calculation of the number of the valence neutrons of a nucleus can be estimated using the following Eqs. (14) and (15) based on two main conditions. Starting from a doubly magic shell closure, the first condition indicates that if the number of neutrons of a nucleus is smaller or equal to the number of neutrons of the mid shell nucleus, then the Eq. (14) should be used. In this case, valence particles are counted from the nearest closed shell. In contrast, if the number of neutrons contained in a specific nucleus is greater than the number of neutrons of the mid shell, then the Eq. (15) is valid. Similar expressions hold for the number of valence protons n_p. The formulas for the calculation of the valence neutrons (or protons) are also reported in Ref. [38].

- $If\ N \leq N_{med}\ :\ n_n = N - N_c$ (14)
- $If\ N > N_{med}\ :\ n_n = N_{c+1} - N$ (15)

where N is the number of neutrons (or protons) corresponds to a particular nucleus, N_c symbolizes the first closed shell – right behind the formation of the valence space – and corresponds to the traditional magic numbers of neutrons or protons:

$$N_c = 2, 8, 20, 28, 50, 82, 126 \quad (16)$$

and their mid closures:

$$N_{med} = 5, 14, 24, 39, 66, 104 \quad (17)$$

Also, the N_{c+1} is the number of magic neutrons (or magic protons) of the next nearest closed shell.

Although the mathematical expressions of NN and 3N terms described by the Eqs. (12) and (13), respectively, present the bottom line of the current formalism in terms of the physical interpretation, transformations to their mathematical expressions were necessary to be applied. The interesting thing here is to understand the reasons behind these changes. Several fits and tests have been made which drove the investigation towards this direction and to the application of the relevant corrections to their initial formulas.

To start with, modifications are applied to the mathematical functions of NN and 3N body forces so as to make them reflect the right correlations between the nucleons. Once the inert core has been specified and the valence space is introduced, correlations between the active nucleons should be generated in the U-shaped line in such a way where their strength will be more notable in the beginning and softer around the mid shell. In order to get such mathematical expressions that produce satisfactory results for both NN and 3N terms, it is essential to minimize the slope originating in the previous formulas, Eqs. (12) and (13).

The minimization of the slope permits to reproduce the right concept of interactions between the nucleons in the parabolic plot and introduces corrections to their behavior especially around the mid shell. The initial expressions of NN and 3N terms, Eqs. (12) and (13), respectively, show a sudden overshooting of the correlations among the valence nucleons around the mid shell while at the same time do not account for the proper strength of nucleonic interactions right after the doubly magic shell core.

Therefore, it is found that a correct representation of the correlations of the valence nucleons between two closed shells can mathematically expressed through the following equations:

$$\mathrm{NN} = \mathrm{B} * (\mathrm{n_{max}} *(\mathrm{n_{max}} -1)) - (\mathrm{n_{max}} - \mathrm{n})*(\mathrm{n_{max}} - \mathrm{n} - 1) \quad (18)$$

$$3\mathrm{N} = \mathrm{D} * (\mathrm{n_{max}} *(\mathrm{n_{max}} - 1)*(\mathrm{n_{max}} - 2))-(\mathrm{n_{max}} - \mathrm{n})*(\mathrm{n_{max}} - \mathrm{n} - 1) * (\mathrm{n_{max}} - \mathrm{n} - 2) \quad (19)$$

where similarly, B and D are parameters to be estimated from the fit, the notation n refers to the number of valence particles (or holes) for each nucleus counted from the nearest closed shell and $\mathrm{n_{max}}$ corresponds to the valence nucleons of the mid-shell nucleus. The notation $\mathrm{n_{max}}$ reflects the fact that the mid-shell nucleus has the maximum number of valence nucleons in the U-shaped line.

If one examines the connection between the mathematical expressions of the initial NN and 3N terms (Eqs. (12) and (13)) and the final ones (Eqs. (18) and (19)), it is evident that these expressions are not so different. Particularly, although the final expressions of NN and 3N (Eqs. (18) and (19)) are written relevant to the valence nucleons of the mid shell, the strength of NN and 3N terms, as expressed initially by the Eqs. (12) and (13), is still there.

As an example, an instructive and inspirational point which drove the research towards in modifying the initial mathematical expressions of NN and 3N terms, was the trend of the residuals, given by a fit of Eq. (11), for the even-even nuclei between the two closed shells ^{100}Sn and ^{132}Sn. Particularly, for a better understanding of the physical reasons which altered such modifications, it is worth deserved to include some relevant plots for a visual inspection of the behavior of each function based on the number of the valence particles of each nucleus. Particularly, a comparison of the plots generated by the initial NN and 3N terms, Eqs. (12) and (13), and the new ones, described from the Eqs. (18) and (19), are presented afterwards in Figs. 3.3 and 3.4, respectively. In this example the valence particles, correspond to the even-even nuclei between the DM closed shells, ^{100}Sn and ^{132}Sn, are shown. As the interest lays on

comparing the mathematical functions of NN and 3N terms, before and after the appropriate changes, the parameters B and D was assumed to have a value equal to 1 keV.

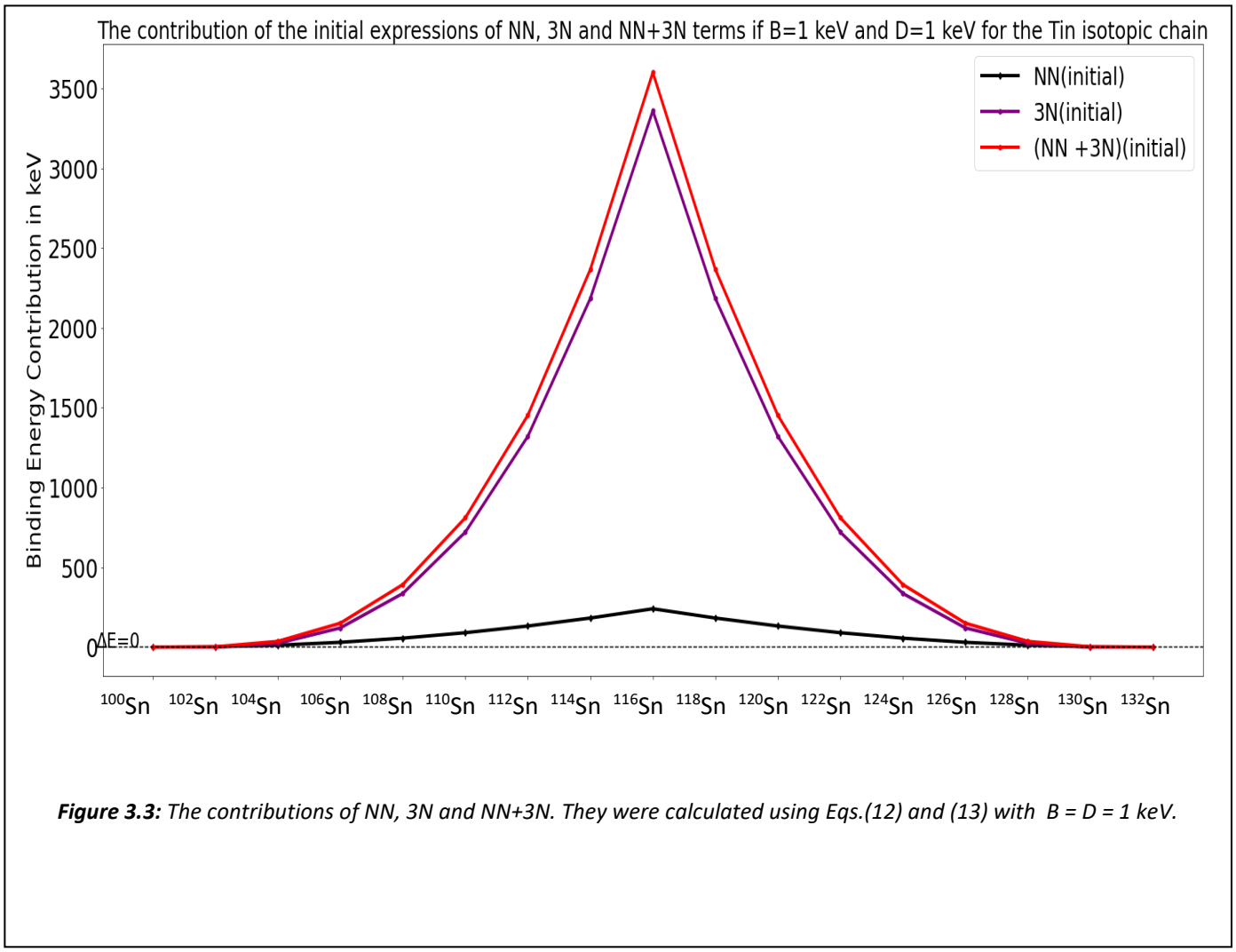

Figure 3.3: *The contributions of NN, 3N and NN+3N. They were calculated using Eqs.(12) and (13) with B = D = 1 keV.*

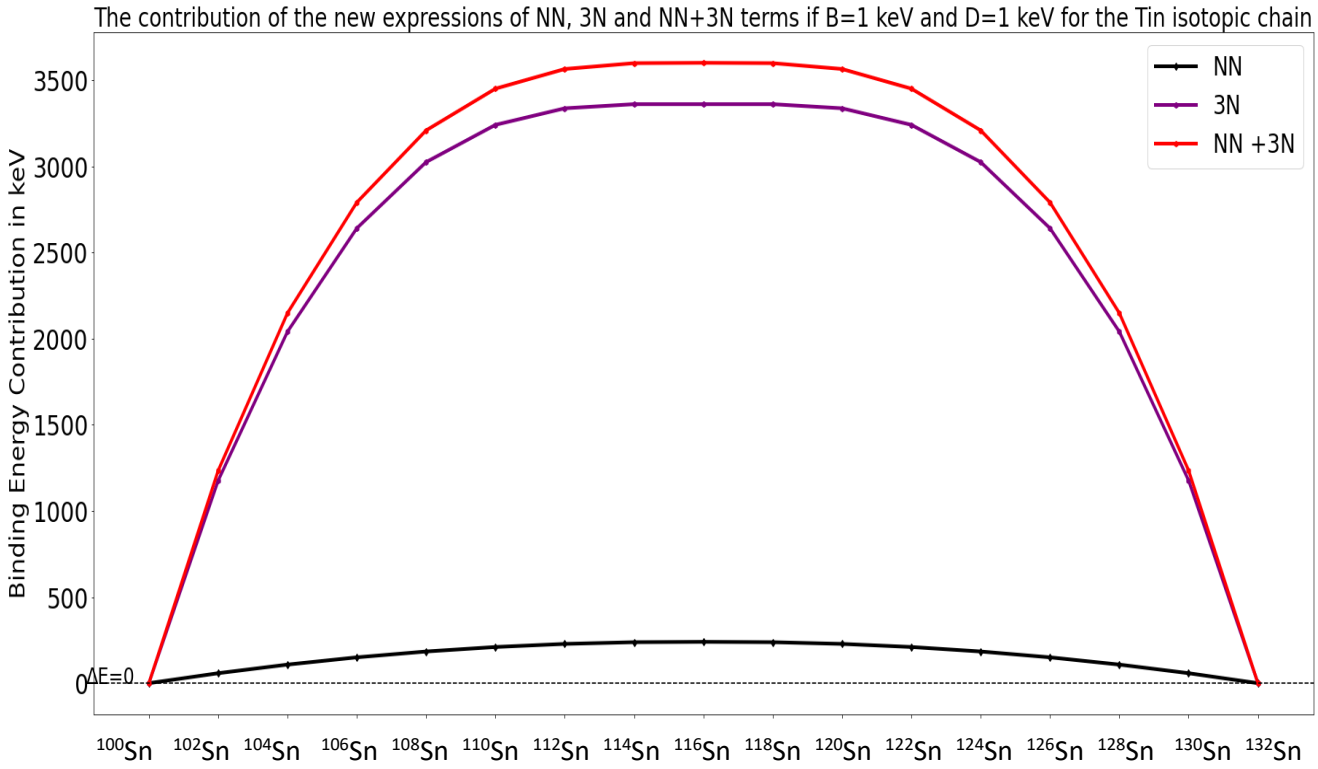

Figure 3.4: *The contributions of NN, 3N and NN+3N terms. They were calculated using Eqs. (18) and (19) with B = D = 1 keV.*

By inspecting the values of the initial NN and 3N expressions, Eqs. (12) and (13), presented in Fig. 3.3, and comparing them with the corresponding outcomes of the final expressions of NN and 3N, Eqs. (18) and (19) of Fig. 3.4, it is obvious that the final functions of NN and 3N have been modified to account more for the valence interactions ranging from zero (inert core, ^{100}Sn) to the start of the valence space and this is the correct physical approach. For instance, if one performs the relevant calculations, in the final expression of NN, the DM nucleus ^{100}Sn with zero number of valence nucleons, suddenly increases its strength from 0 to 58 keV, for the magic nucleus ^{102}Sn, from 58 keV to 108 keV for next nucleus ^{104}Sn and so on. On the other hand, if one looks at the corresponding value of the magic nucleus ^{102}Sn given by the initial expression of NN, it is evident that only a small number of valence nucleonic interactions are generated from the closed shell to first open shell. In addition, at the midshell (around the magic nucleus ^{116}Sn), there is a sudden increasing in the number of correlations. The last statement is not in compliance with the physical interpretation of the suggested correlations.

It is evident that the initial mathematical expressions of NN and 3N, presented in Fig 3.3, consider a stronger effect of valence interactions around the midshell while underestimate the valence interactions right after the DM shell closures. Applying the appropriate transformations to their initial functions, the NN and 3N expressions of Fig. 3.3, are now

capable to describe the correlations between the valence nucleons giving a stronger picture at the edge and softer at the midshell. In such a way, the new final expressions have a slope which reflect that in the midshell all the correlations have been already generated. Therefore, the U-shaped line is now smooth around the midclosure magic nucleus, ^{116}Sn. Therefore, in the results section, the analysis related to the expressions of the Eqs. (18) and (19), is only considered.

Given that the background theory of these expressions has been fully presented, it is important to make a remark on a practical component of the data analysis related to the calculations. As it is already pointed out, by construction the NN and 3N terms are expressed as a function of the valence nucleons. Therefore, a code which is applicable to calculate the valence particles or holes for all the nuclei, it was necessary to be produced. The same code can also be applied efficiently to a larger dataset such as the entire mass16.txt file which includes both odd and even numbers of neutrons and protons. The main thing is to correctly define which are the magic numbers of shell closures for protons and neutrons as well as their mid shells and then based on the Eqs. (14),(15),(16),(17) to construct the problem. The code was written in python programming language, and it is able to print output data of valence neutrons or valence protons or valence nucleons for a nucleus with N neutrons and Z protons. The latter is presented in the Appendix B of the present thesis and was named as 1st code. Also, a more simplified and sorter version of the same code was produced for the calculation of the valence nucleons. This code is also included in the Appendix B and was named as 2nd code. However, in this code changes to the number of protons, Z, and mass number, A, should be applied manually and then the code can generate the valence nucleons (particles or holes). It is important to acknowledge that both codes constructed based on the equations presented in the paper [38].

3.1.3 Regions of Interest:

The selected atomic mass regions, where the BW estimated parameters were applied and the residuals were calculated, should contain even-even nuclei either of the same isotonic or isotopic magic chain or any other chain in the nuclear chart which necessarily is characterized by the presence of two doubly magic nuclei for the application of the analysis' steps described in the subsection (3.1.1). The first closed shell and its higher energy successive. From now on, these selected atomic mass regions are named as regions of interest.

As an example , the calcium isotopic chain includes the doubly magic nucleus calcium-40 (^{40}Ca) while the next confirmed doubly magic nucleus, in the same chain, is calcium-48 (^{48}Ca). In a similar manner, more atomic mass regions, such as the tin chain (from the doubly magic nucleus ^{100}Sn to doubly magic nucleus ^{132}Sn), two diagonal chains (from the doubly magic nucleus oxygen-16 (^{16}O) to doubly magic nucleus ^{40}Ca and from ^{40}Ca to doubly magic nucleus nickel-56 (^{56}Ni)) as well as one isotonic chain of N=28 (from ^{48}Ca to ^{56}Ni), can also be used to test the present theoretical framework as they are in step with the forementioned rule. The term diagonal, which was coined in this work, refers to nuclei chains between two DM nuclei numbers, which are called so because of their appearance in the N-Z plane, also having the property N=Z. These two diagonal chains belong to the light and medium atomic mass regions of the nuclear chart.

However, as we are only interested in even-even nuclei that are included between two doubly magic nuclei, only a few atomic mass regions are currently available for testing our theory due to the lack of experimental atomic mass data for the doubly magic nuclei.

As shell closures were considered the traditional magic numbers which correspond to proton or neutron numbers equal to 2,8,20,28,50,82 and 126. Due to the limited availability of atomic mass data for doubly magic nuclei, the heaviest isotopic chain that can be utilized to apply the present theoretical framework, is the tin (Sn) chain. However, the heaviest doubly magic nucleus that is involved in the fitting procedure of the DM nuclei is the lead-208 (^{208}Pb) with 82 protons and 126 neutrons.

Following the description of the profile of the regions of interest, one could wonder about one more atomic mass region which follows the rule of two doubly magic nuclei along the same isotopic chain, but it is not included in the analysis. In general, the truth is that one can consider at least two more chains of even-even nuclei which lie between two doubly magic nuclei.

One of these chains corresponds to the Helium isotopic chain which includes the two doubly magic nuclei, helium-4 (^{4}He) and helium-10 (^{10}He). Although fits have been conducted to the DM nuclei when the ^{4}He and ^{10}He were also involved, it was concluded that a fit, without taking into consideration very light nuclei, gives more considerable results for our case study.

Therefore, very light nuclei with mass number smaller than A=16 were not considered in the final results of the analysis. Also, as stated before, the simple liquid-drop concept, as formulated from the BW mass formula, is not capable to predict very light nuclei as well as very exotic heavy nuclei and thus fits to a restricted dataset, or in subsets of this dataset, with mass number ranged from A=16 to A=208, were mainly performed.

Additionally, one more isotopic chain was tested in terms of our theoretical approach. This isotopic chain corresponds to the oxygen isotopes. Starting from the first doubly magic shell core, oxygen-16 (^{16}O), valence nucleons of even-even nuclei are considered in the valence space, until the next experimentally confirmed doubly magic nucleus, oxygen-24 (^{24}O) to be reached. The results from this fit as well as the theoretical formulation that was used for the inclusion of the DM nucleus ^{24}O, are presented in the results' chapter.

Based on the instructive Fig. 3.5 of chart of nuclides, a schematic representation of each of the selected atomic mass regions including the even-even nuclei lay between two traditional doubly magic shell closures, is also given. Particularly, the regions of interest were the calcium chain (Z=20) (Fig. 3.6), the tin chain (Z=50) (Fig. 3.7), the two diagonal chains (Figs. (3.8) and (3.9 (RHS))) and the isotonic chain (N=28) (Fig.(3.9 (LHS)). In these regions, the best parameter's fit were applied, and the BW calculated residuals (initial) were compared with those obtained considering the additional NN and 3N expressions.

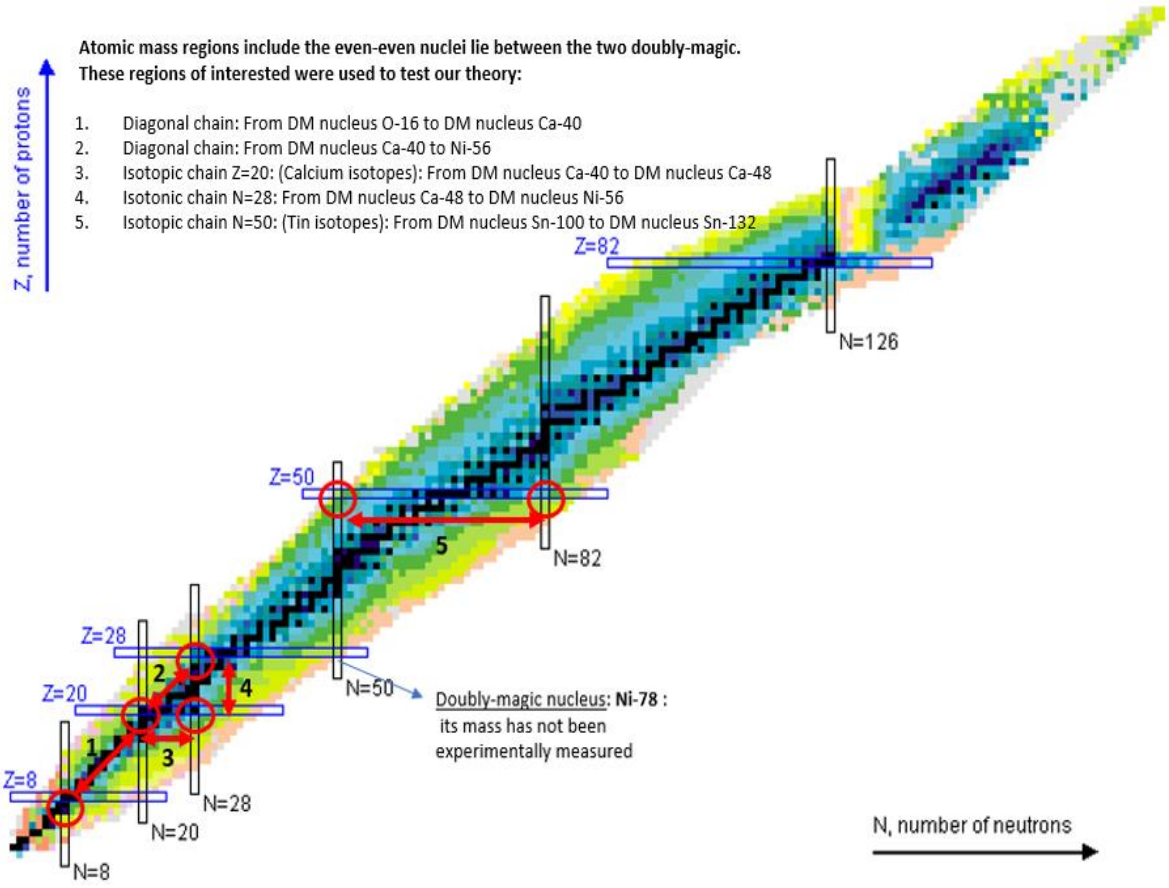

Figure 3.5: *Graphical presentation of the five main regions of interest, depicted on the nuclear chart, used for testing the current theoretical framework. Image source [151].*

Calcium Isotopic Magic Chain (Z=20):

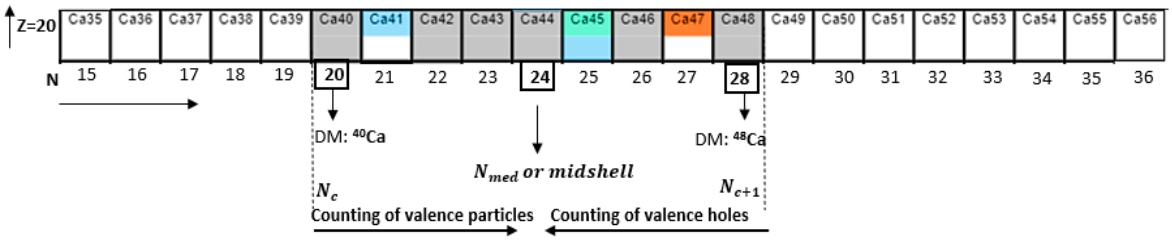

	^{40}Ca	^{42}Ca	^{44}Ca	^{46}Ca	^{48}Ca
Valence Nucleons	0	2	4	2	0

Figure 3.6: *The magic chain Z=20 of the calcium isotopes. It is one of the regions of interest, where even-even nuclei included between the two DM nuclei, ^{40}Ca and ^{48}Ca, were used to apply the present theoretical framework. The arrows assist to understand the process of counting valence particles or holes starting from the nearest closed shell. Nuclear chart data were taken from Ref. [152].*

Tin Isotopic Magic Chain (Z=50):

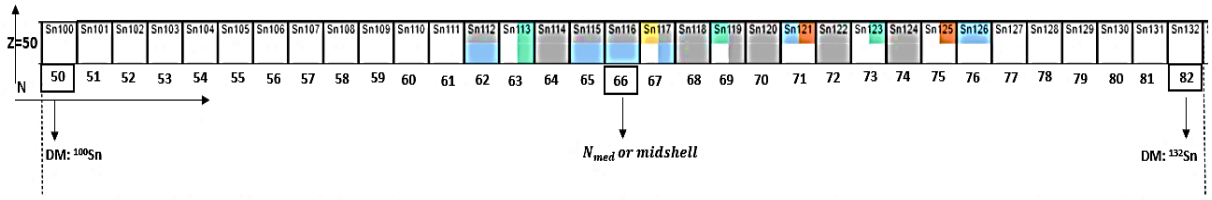

	^{100}Sn	^{102}Sn	^{104}Sn	^{106}Sn	^{108}Sn	^{110}Sn	^{112}Sn	^{114}Sn	^{116}Sn	^{118}Sn	^{120}Sn	^{122}Sn	^{124}Sn	^{126}Sn	^{128}Sn	^{130}Sn	^{132}Sn
Valence Nucleons	0	2	4	6	8	10	12	14	16	14	12	10	8	6	4	2	0

Figure 3.7: *The magic chain Z=50 of the tin isotopes. It is one of the regions of interest, where even-even nuclei included between the two DM nuclei, ^{100}Sn and ^{132}Sn, were used to apply the present theoretical framework. The arrows are used as it was explained in Fig. 3.6. Nuclear chart data were taken from Ref. [152].*

Diagonal Chain from the DM nucleus ^{40}Ca to DM nucleus ^{56}Ni

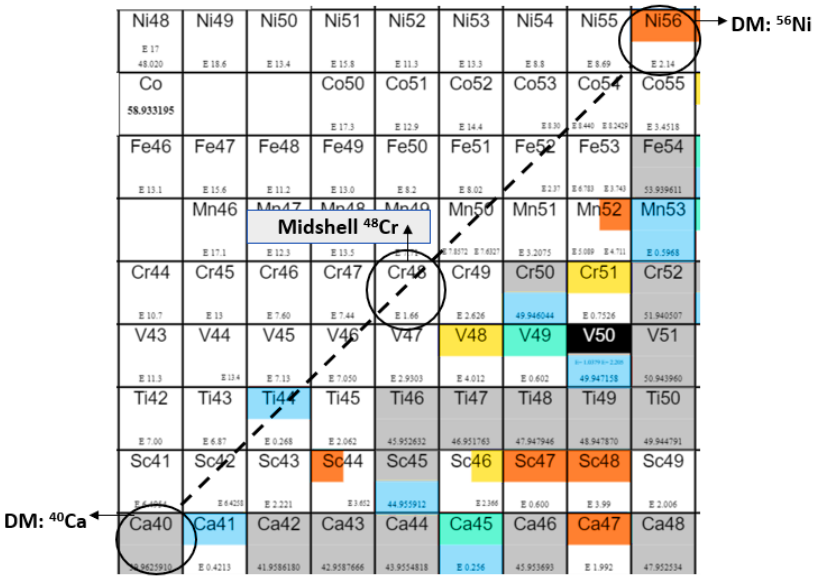

Figure 3.8: *The diagonal chain from the DM nucleus ^{40}Ca to DM nucleus ^{56}Ni. Region of interest, where even-even nuclei included between the two DM nuclei, were used to apply the present theoretical framework. Nuclear chart data were taken from Ref. [152].*

Isotonic Chain N=28

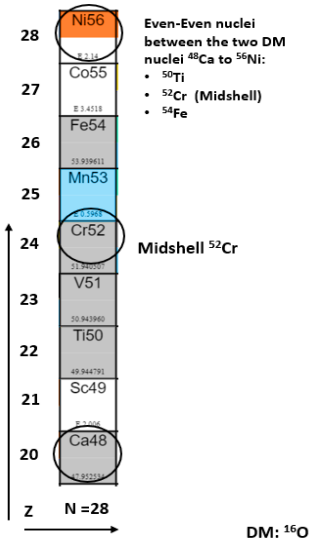

Diagonal Chain from the DM nucleus ^{16}O to the DM nucleus ^{40}Ca

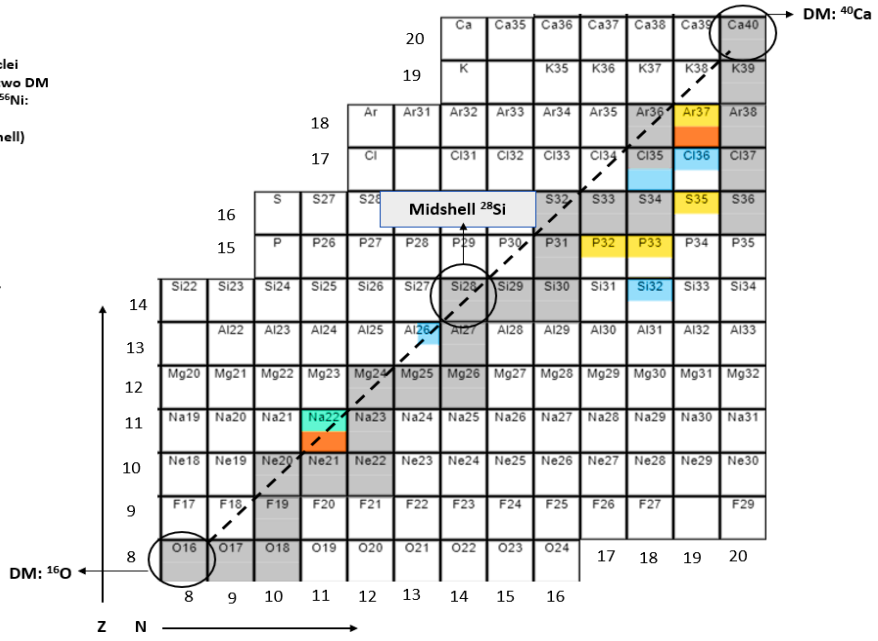

Figure 3.9: *At the LHS: The isotonic magic chain N=28. Region of interest, where even-even nuclei included between the two DM nuclei, ^{48}Ca and ^{56}Ni, were used to apply the present theoretical framework. Nuclear chart data were taken from Ref. [152]. At the RHS: Presentation of the diagonal chain from the DM nucleus ^{16}O to the DM nucleus ^{40}Ca. Region of interest, where even-even nuclei included between the two DM nuclei, were used to apply the present theoretical framework. Nuclear chart were taken from Ref. [152].*

3.1.4 Experimental Inputs:

The BW mass formula, Eq. (5), provides a convenient starting point for the description of the nuclear systems and also was used as a baseline for the application of the present theory. The model is described by a set of 5 parameters which some of them can be slightly varied depending on the needs of the calculations. Details about the structure of the model and its underlying theoretical basis can be found in subsection (2.4.2).

In this work, the parameters of the BW formula were obtained by using the comprehensive database of nuclear masses, which is the atomic mass evaluation generally referred to as AME2016 and was published in March 2017 [2,3]. However, the most up-to-date atomic mass evaluation is the one given by the AME2020 [55,56] and includes updated information to the experimental data recorded in the previous AME2016 database. Updated experimental data of the AME2020, were only used for comparison purposes, when needed, and for certain nuclei. This was mainly to identify any possible changes to the accuracy of the experimental measurements compared to the last published database. A detailed explanation of the reasons and the importance of a more precise determination of atomic masses will be further discussed in an upcoming section (3.3).

The AME2016 table, which lists atomic and not nuclear masses, contains the best values for atomic masses and their uncertainties. Information on the evaluation philosophy and general procedures for the implementation of the mass measurements, are briefly given in section (2.3) of the present thesis. An extended description is also provided in the Refs. [2,3]. Estimates for unknown masses were made by extrapolation from neighboring known data [53] and are also included in the mass table.

A reference has already been made to the inherent relationship of nuclear masses and binding energies. In the present analysis, the quantity of interest is the binding energy of atomic nuclei. The mass tables contain the values of atomic masses and other derived quantities. The binding energies of nuclei can easily be derived once one knows the nuclear or atomic masses Eqs. (1),(2) and (3),(4), respectively. The binding energies are reported in the mass table in keV units, while the atomic masses are given in mass units and all the rest physical quantities also in energy units.

The results of the present work were obtained using only the experimentally measured nuclei – several reported masses and their uncertainties are extrapolated from systematics and marked with the symbol # in place of the decimal point were not taken into account. In the mass list, information relevant to the mass excess of each nucleus are also given which is an alternative way to look at binding energy. However, columns which record data corresponding to the mass excess (keV), beta-decay energy (keV), atomic masses (micro-u) as well as their accompanied uncertainties, are not considered in the process of analysis.

A typical page of the atomic mass table AME2016 is presented in the Fig. 3.10. Several physical quantities, which are shown, correspond to experimental and extrapolated atomic mass data.

1N-Z	N	Z	A	EL	O	MASS EXCESS (keV)		BINDING ENERGY/A (keV)		BETA-DECAY ENERGY (keV)		ATOMIC MASS (micro-u)	
0 1	1	0	1	n		8071.31713	0.00046	0.0	0.0	B- 782.347	0.000	1 008664.91582	0.00049
-1	0	1	1	H		7288.97061	0.00009	0.0	0.0	B- *		1 007825.03224	0.00009
0 0	1	1	2	H		13135.72176	0.00011	1112.283	0.000	B- *		2 014101.77811	0.00012
0 1	2	1	3	H		14949.80993	0.00022	2827.265	0.000	B- 18.592	0.000	3 016049.28199	0.00023
-1	1	2	3	He		14931.21793	0.00021	2572.680	0.000	B- -13736#	2000#	3 016029.32265	0.00022
-3	0	3	3	Li	-pp	28667#	2000#	-2267#	667#	B- *		3 030775#	2147#
0 2	3	1	4	H	-n	24621.127	100.000	1720.449	25.000	B- 22196.211	100.000	4 026431.868	107.354

Figure 3.10: *Extract from the atomic mass data compilation (AME2016) [125]. The decimal point was replaced by # for (non-experimental) estimated values.*

These atomic mass data are part of the atomic mass evaluation AME2016 table and are included in the mass16.txt file, accessible online, and was used as the main data file for the present research work. The source of mass16.txt file for downloading can be found in Ref. [125] and is provided by the Atomic Mass Data Center (AMDC).

In Fig. 3.10, it is observed that some measured experimental binding energies accompanied with zero values of uncertainties. As reported in Ref. [3], a zero value should be considered as an uncertainty smaller than 0.5 eV or 0.0005 keV. This is an important feature that one should take into consideration, especially in the case of a weighted least squares fit. The definition of the 'chi-squared' function reflects that the values of the weights should be necessarily different from zero, otherwise the 'chi-squared' cannot be solved. Hence, in case of using a software programme to carry out calculations or developing a code to solve analytically or numerically the regression problem, an error indication will be observed in the used algorithm.

In the original AME2016 text file [125], the total number of experimental and extrapolated atomic mass data are 3435 and correspond to ground state masses [2]. From them, the 2497 nuclei are experimental measured values while the rest 938 nuclei correspond to extrapolated mass data. As previously explained, the latter were neglected from the present analysis. It is also quite interest to emphasize the variation in the magnitude of uncertainties for different nuclei included in the mass table. A table shown the most accurately determined atomic masses of 16 nuclides is presented in Ref. [3]. The atomic masses for these nuclei correspond to values of uncertainties of less than 1 eV. It is worth noting that the doubly magic nucleus oxygen-16 (^{16}O) is in the list of the most precisely measured nuclei. Also, in the first published article [2] of the atomic mass evaluation, AME2016, a distinction of the 2497 experimental atomic mass data based on the magnitude of their uncertainties is noted. Particularly, it is written that there is an accuracy greater than 0.1 keV for 111 nuclei, while 378 and 1477 of them are determined with a precision greater than 0.1 keV and 10 keV respectively.

Additionally, special care should be also given in the case of including the experimental uncertainties in the fitting procedure, as one should be cognizant of the presence of 153 nuclei which are not precisely determined and have values of uncertainties larger than 100 keV. In

such case, the more dominant nucleus is the more well determined than the rest participating in the fitting procedure. An extensive explanation of the last statement will be given in the upcoming section (3.3).

The reading of the data file is made using the Python programming language. Once the file has been accessible, cleaning and restructuring of the raw material of mass16.txt file was performed so as to simplify its version and applied appropriate adjustments to its physical quantities, when needed.

To this end, the quantity 'total binding energy in MeV' (BE (keV)) was calculated from the binding energy per particle (BE/A (keV)) and a change to the energy units was also made, from keV to MeV. It should be noted that the fit is not affected by this change. It is just a scale of factor in terms of units. The value of uncertainty accompanied each of the experimental binding energy should also be adjusted accordingly to the modifications occurred to the latter value. On the contrary, when a linear regression fit of the BW form of binding energy per particle to the entire mass16.txt file, is occurred and compared with a second fit of total binding energy, the difference between the best fit coefficients obtained by these two fits, is quite considerably different. The reason behind this difference will be explained in the upcoming section (4.4). The last statement shows the importance of always choosing an appropriate scale for the data before the start of the analysis.

It should be also stressed that considering a fit to the quantity total binding energy instead of binding energy per particle and vice-versa, one should also apply the appropriate modifications to the mathematical expressions of BW baseline formula (Eq. (5)) or LDM1 formula (Eq. (7)), by multiplying (or diving) with the mass number A each term of the equations.

Also, specific sets of nuclei which were considered inappropriate for the present analysis were removed (such as very light nuclei of hydrogen isotopes, extrapolated nuclei etc.) and a file which contains only experimental inputs of a particular interest to the current investigation was used. These nuclei are the even-even nuclei and are in total 649. Consequently, the data presented in Table 3.1, were adapted as the main input of the present work, which then it was used to generate further restricted data sets as well as to extract nuclei of particular interest in terms of their characteristics, such as the doubly magic nuclei.

	N	Z	A	El	BE/A(keV)	un(keV)	BE/A(MeV)	un(MeV)	BE(MeV)	unT(MeV)
0	2	2	4	He	7073.9150000	0.0000000	7.0739150	0.0000005	28.2956600	0.0000020
1	4	2	6	He	4878.5190000	0.0090000	4.8785190	0.0000090	29.2711140	0.0000540
2	2	4	6	Be	4487.2470000	0.9080000	4.4872470	0.0009080	26.9234820	0.0054480
3	6	2	8	He	3924.5200000	0.0110000	3.9245200	0.0000110	31.3961600	0.0000880
4	4	4	8	Be	7062.4350000	0.0040000	7.0624350	0.0000040	56.4994800	0.0000320
...	...	...	...	...	...	...	...	...	...	...
644	154	106	260	Sg	7342.5620000	0.0790000	7.3425620	0.0000790	1909.0661200	0.0205400
645	156	106	262	Sg	7341.1850000	0.1350000	7.3411850	0.0001350	1923.3904700	0.0353700
646	156	108	264	Hs	7298.3750000	0.1090000	7.2983750	0.0001090	1926.7710000	0.0287760
647	158	108	266	Hs	7298.2730000	0.1450000	7.2982730	0.0001450	1941.3406180	0.0385700
648	160	110	270	Ds	7253.7750000	0.1780000	7.2537750	0.0001780	1958.5192500	0.0480600

649 rows × 10 columns

Table 3.1: *Data for even-even nuclei extracted from Ref. [125]. After modifying the column of binding energy per particle in keV (BE/A(keV)) and its corresponding uncertainty (un(keV)), the columns which correspond to the total binding energy and its uncertainty, BE(MeV) and unT(MeV) are shown, respectively.*

3.2 Regression Analysis:

The BW baseline mass formula has been extended to account for microscopic shell corrections that has been assumed to be due to the NN and 3N terms as a function of valence nucleons. Using the raw data of experimental binding energies, provided by AME2016, different local fits, included exclusively even-even nuclei across the nuclear landscape, were conducted to get the most optimal set of parameters for the description of the parabolic shape observed in atomic mass regions between two doubly magic nuclei. Having described the theoretical approach, it is important to introduce basic concepts and methods of regression analysis used to fit continuous functions corresponded to nuclear mass formulas.

Among numerous fits that have been performed for the estimation of the best fit parameters, a focus has only been given to cases which are able to generate fit coefficients which satisfy the main conditions of the present phenomenological approach. These cases are mainly oriented to the fit of the DM nuclei. Ideally, the aim is to be found a set of coefficients which is applicable to reproduce the parabolic trend of the even-even nuclei between two doubly shell closures, for all or at least for the majority of the even-even nuclei of the regions of interest. Tracing a unified set of best parameters towards the regions of interest was investigated.

The goal of the regression analysis is to find the relationship between the dependent variable or outcome or response value Y_i , as its value is said to depend on the value that X_i,

which is called the independent or predictor variable, takes on [153], according to equation follows:

$$Y_i = f(X_{i,}\, a) + e_i \tag{20}$$

where i indicates a series of data, a is a vector presents the unknown parameters and e_i is an error term or the residual variable which shows the imperfection in the actual relationship between the data and the model.

In other words, the key point is to quantify the relationship between the explanatory variable (or variables) and the response variable. When changes to the values of the independent variable are performed, the interest lays to observe how these modifications have affected the response variable. By performing a regression analysis and extracting the relationship between the Y and X variables, predictions are used as a guidance for capturing missing variables that should be added to the model. Therefore, additional terms, when needed, it is necessary to be added in a regression model so as to take into consideration other important factors that theoretically should affect the quality of the model. If the number of independent variables used to describe the forementioned relationship, are two or more, the model is a multiple regression model.

The nuclear mass formulae fall into the category of the multiple regression models. Starting from the simplest BW nuclear mass model, a parameterization of the data was made. The BW mass formula, which is described by the Eq. (5), is a model which is linear in parameter space. It depends on five parameters that are the a_v, a_s, a_a , a_c, a_p which multiple some functions of N and Z. The physical explanation of each term has already been described in the subsection (2.4.2).

By using the data points given by the even-even nuclei of AME2016 database, different fits to the BW function were performed to make predictions for values of Y and therefore to provide information on the mutual interaction between the experiment and theory. Hence the goal of data fitting is to find the best values of parameters which fully match the observations with the theory.

Specifically, in 1829, it was proved by Carl Friedrich Gauss that it is convenient and mathematically correct to say that the best fit minimizes the sum of the squares of the errors between the data and the fit regression model [154]. The latter is called the method of ''least-squares'' or ordinary least-squares (OLS). The ordinary least-squares method gives us the most precise estimates of the parameters compared to other unbiased estimation methods [153].

In the present research, a particular focus is given to the ordinary linear regression where the fitting procedure is generalized to be considered as a linear algebra problem (exact solution in matrix notation) or when a numerical solution is applied for the estimation of the optimal parameters (i.e., via gradient descent algorithms).

Nowadays powerful support through analytical computational tools for the use of OLS and other specialized least-squares methods are available. Ideally, a numerical tool should be able to provide an increasing numerical precision in the determination of the unknown parameters as well as to achieve accurate treatment in the estimation of the parameter's uncertainties and their corresponding correlations.

There are many different techniques to perform regression analysis. Some widely popular methods include resampling techniques like bootstrapping and cross-validation [122,155]. With resampling techniques, the true estimator is approaching.

In case of the BW liquid-drop model, a multiple linear regression analysis is applied to approximate the solution of an overdetermined system of linear equations. The idea is that the set of parameters that is obtained from the best fit should minimize the sum of the squares of the residual errors between the experimental data, y_i, and the model. In case of a nuclear model the equation which describes the model is written as $\sum_j c_j\,(x_i)\,a_j$. The last equation means that the model includes j number of functions, $c_j(x_i)$, which depends on j number of parameters, a_j. The x_i refers to the individual data of the used dataset.

The minimization can be performed analytically using the general form of the ''chi-squared'' function:

$$x^2 = \sum_i \frac{(y_i - \sum_j c_j(x_i) a_j)^2}{\sigma_i^2} \tag{21}$$

The difference between the observations and the predicted values is given by the error term, e_i, including in the numerator and should be as small as possible. However, it is unlikely that the predictions made by the regression line will precisely follow the observations. The last statement reveals the imperfect relationship between the inputs data and the theoretical predictions which is often caused by factors such as missing of independent variables or systematic effects due to systematic or statistical uncertainties etc. [156]. An interesting study towards an understanding of the uncertainties in scientific measurements is also given in Ref. [156].

Thus, given the expression of the x^2 function, Eq.(21), and the variance in the denominator, one can perform the linear regression fit having two possible choices. The first choice is to consider that the least squares fit treats each observation equally in determining the parameters, by applying equal weight to each of the experimental inputs. This is the case of equal and non-correlated measurement error, and the error or weight matrix is an identical matrix [154]. The OLS procedure assigns a weight of $w_i = \frac{1}{\sigma_i^2}$ equal to 1 for each observation.

The second option is to weigh some observations more heavily than others. This procedure is known as a weighted least squares (WLS) and the resulting parameter estimates are called weighted least squares estimates. The WLS is a generalization case of ordinary least squares and is usually applied to stabilize the variance of the residuals to satisfy the standard regression assumption of homoscedasticity which means constant variance [153, 157]. Also, a weighted least squares fit can provide a solution of limiting the influence of outlying observations on the regression analysis [157]. As will be proved later, the last statement was also one of the indications that paved the way for drawing appropriate conclusions on the fitting method that should follow for the rest of the analysis. An extended reference on the impact of uncertainties in the fitting procedure is also presented in the next section.

When a WLS procedure is applied, the observations will get less weight and therefore their impact in the fitting procedure will be less, compared with experimental inputs with smaller values of uncertainties and thus greater weight. In other words , large values of error variances corresponded to low-accuracy data, are weighed less in the fit, while observations which are precisely determined should be more heavily weighted.

In mathematics, some problems can be solved either analytically or numerically. The minimization of x^2 function, Eq. (21), can be performed analytically [122]. The relationship between the data and the parameters of a linear model can be always written as a matrix-vector product. As the chi-squared minimization is in fact the maximum-likelihood estimator (MLE) of the function parameters a_j, if we derive respect to them and set to zero as standard MLE, the Eq. (21) is written:

$$\sum_i c_j\,(x_i)\left[\frac{y_i-\Sigma_j c_j a_j}{\sigma_i^2}\right] = 0 \tag{22}$$

And the matrix notation can be used to express the Eq. (22):

$$0 = C^T V^{-1} y - C^T V^{-1} C a \tag{23}$$

$$C^T V^{-1} y = C^T V^{-1} C a \tag{24}$$

$$a = (C^T V^{-1} C)^{-1} C^T V^{-1} y \tag{25}$$

which concludes to the following x^2 estimator of the parameter vector â:

$$\hat{a} = (C^T\, V(y)^{-1}\, C)^{-1} C^T V_y^{-1} * \; y = M * y \tag{26}$$

where the V_y is the error matrix or covariance-variance matrix or variance matrix for the measured values y, in this case the experimental binding energies taken from the mass table AME2016, and C is the matrix that contains the functions of the linear model, independent variables of the nuclear model [122].

The regression routines of most statistical software packages have options on performing a weighted or unweighted least squares fit. The data analysis was performed using minimization methods applied in Python programming language. Particularly, several minimization methods are used to estimate the best values of parameters. Where applicable, more than one of the minimization techniques presented below, were tested to check the validity of the fit by comparing the outcomes. Indeed, analytical solutions are very important for evaluating numerical codes. Actually, an exact solution is a straightforward method to solve the problem and estimate the best fit parameters once the matrix C of Eq. (26) is defined. Following the estimation of the best fit parameters, the results should be tested with each of the outcomes of the numerical solutions. In such a way the sensitivity of each algorithm can be assess as well as their ability to make reliable estimations of their parameters, associated uncertainties, and correlations.

The minimization methods and routines that were followed for the determination of the best fit parameters in this work, briefly are presented below:

i. **Analytical Solution:**
The minimization of the x^2 function, Eq. (21), is performed analytically using the matrix notation given by the Eq. (26). The matrices multiplication presented in this equation can simply be performed by making use of the built-in-functions in Python. The code is adapted by Ref. [122].

ii. **Curve Fitting from Python:**
The code is modified to perform a least squares minimization method to determine the model's parameters. The routine is called ''curve fit'' and it is provided by the SciPy.Optimize package.
The code is adapted by Ref. [122].

iii. **LMFIT library:**
'Lmfit' provides a high-level interface mainly for non-linear optimization and curve fitting problems in python [158]. This function imports a 'Model' function and provides a useful statistical report with information including the chi-square value, the values of the parameters, their uncertainties etc.

iv. **MINUIT:**
It is a tool for the estimation of the minimum value of a multi-parameter function analyzing the shape of the function around the minimum [159]. Here, the iminuit which is a Jupyter-friendly Python interface for the Minuit2 C++ library [160] maintained by CERN's ROOT, was used as an alternative minimization method.

It is also worth mentioning that each of the minimization routines described above, can generate the best values of parameters as well as their corresponding uncertainties. The uncertainties were calculated by the variances of the diagonal elements of the covariance-variance matrix. Particularly, the square root of the variance gives the uncertainty for each of the parameters. The covariance-variance matrix provides plenty of information related not only to the error on the parameters but also the covariance between the one parameter and the other, through its off-diagonal terms. In other words, it provides access to the so called 'Pearson correlation coefficient'. Particularly, given two data sets X and Y, with N elements each, the covariance matrix is defined as :

$$cov(X,Y) = \frac{1}{N}\sum_i (X_i - \bar{X})(Y_i - \bar{Y}) = \overline{XY} - \bar{X}\bar{Y} \quad (27)$$

where $\overline{XY}$ is the average value of the product $X\ Y$ of the two data, $\bar{X}$ is the average value of the data X and similarly, $\bar{Y}$ is the average value of the data Y.

As an example, considering the following 2x2 covariance matrix (Σ) of x and y vectors:

$$\Sigma = \begin{bmatrix} \sigma_{xx} & \sigma_{xy} \\ \sigma_{yx} & \sigma_{yy} \end{bmatrix} \quad or \quad \begin{bmatrix} {\sigma_x}^2 & \sigma_{xy} \\ \sigma_{yx} & {\sigma_y}^2 \end{bmatrix} \quad (28)$$

where $\sigma_x \; and \; \sigma_y$ are the standard deviations of x and y, respectively, σ_{xx} ($or \; {\sigma_x}^2$) and σ_{yy} ($or \; {\sigma_y}^2$) are the variances of x and y, respectively and the σ_{yx} = $(\sigma_{xy})^T$ = cov(x,y), applying the Eq. (27).

If the x and y are uncorrelated, the off-diagonal elements of the covariance-variance matrix (Σ), presented in Eq. (28), are zero and then a variance matrix is formed.

The Pearson's correlation coefficient is written as:

$$r_{x,y} = \frac{cov\,(X,Y)}{\sigma_x \sigma_y} \tag{29}$$

Therefore, from a covariance-variance matrix, one can easily have access to a symmetric and square matrix which is known as 'correlation matrix' and gives valuable information about the correlations presented between different terms of the BW baseline formula. It provides a critical assessment related to the physics that the model is applicable to grasp considering this set of the physical parameters. It can also uncover relationships and mutual influence of terms that maybe have not previously observed.

It is important to note that in case of employing the fit using one from the minimization routines described above, special care should be given to whether we fit a linear or nonlinear model. Numerical solutions are widely used for complex models and nonlinear models. In such cases one should pay attention to the physics of the model and therefore to optimize as much as possible the fitting. If the model is linear and contains simple terms, a numerical solution is also a simple way to perform the fitting procedure.

In the case of fitting a linear model, it can be proved that we have only one minimum. This means that if the routine converges, the right minimum point has been found. However, this is not always the case when one deals with nonlinear models where typically they have more than one minimum.

Particularly, when an automatic routine is used for performing the fitting procedure, attention should be given in defining the starting points [122]. A numerical solution requires initial guesses to be inserted in the code for each of the values of the parameters. In the fit of a nonlinear model, there is often the case where one minimizes the chi-squared function, the code generates the minimum but still the data are not reproduced. In this case, there are some factors that need to be examined for identifying what causes the wrong predictions. The first is that either the model is wrong, or the starting guesses result the problem. The fitting routine is automatic and therefore the user does not have the control of the procedure directly.

There are several nonlinear nuclear models which require a careful approach towards this justification. In order to resolve the problem of starting points, the analysis of the chi-square surface can be performed so as to identify if the generated minimum is a local minimum or an absolute minimum [122]. An alternative method to resolve the problem is to change the algorithm used for the fit.

In the present research analysis, the macroscopic part of nuclear mass models such as the ones given by the Refs. [38,112] were also tested to identify whether they satisfy the main

conditions of the adapted phenomenological approach. As it is already pointed out, in case of a nonlinear nuclear mass model, the fitting procedure was evaluated each time by modifying the starting points of the parameters. Also, the outcomes obtained by different minimization routines such that presented above, were compared. If these evaluation methods led to outcomes which produce similar values of best parameters, the approximation of the fitting process is good.

However, the interest of the results section lay only to present fits of the macroscopic part of nuclear mass formulas, among those tested, which were applicable to satisfy the needs of the current theoretical approach.

3.3 Uncertainties in the observables:

Once the minimization method was applied and the parameters were determined, one can easily compute the residuals. The residuals can give us an idea about the discrepancy between the model and the data. Therefore, large discrepancies are a strong indicator of the regression model's quality. Such deviations in the model's behavior can be influenced by a poor fit or the quality of the model. The BW mass formula is a linear model in parameter space so there is only one minimum, and it is certain that a numerical or exact solution is applicable to generate the correct values of best coefficients.

In the case of the liquid-drop model, it is beyond doubt that the model is inaccurate, providing a poor approximation of the reality. It is a not well-constructed model where the typical error estimate is hundred times larger than the experimental variances of observables. Particularly, the average deviations of the BW baseline formula give values in order of MeV, while the typical experimental uncertainties range between a few tens of keV, but also can have an uncertainty value in order of eV [57].

Thus, the BW formula is far worse than the error obtained by the uncertainties of the experimental binding energies. Although significant achievements have been made in reproducing the mass of the nuclei across the nuclear chart, with a rms in order of keV, shell corrections should still be included in the fit. To this end, it is clear that for performing the least-squares fitting procedure, one should also decide whether or not there is a point to include the experimental uncertainties in the fit.

It is obvious that the dependence of the results on the weights will be significant. Considering the uncertainties of the experimental binding energies, while neglecting correlations between them, it is expected that binding energies, having greater values of uncertainties, lose their impact over the regression [161]. In general, imprecise measurement uncertainties and model imperfections are the two main sources that cause poor predictions and thus discrepancies between the observed values and the theoretical ones [162].

Therefore, applying weights to the data can have a significant effect on the accuracy and thus the estimated results. In this work, both a weighted and an unweighted least squares fit

were applied to find the most optimal set of parameters. After investigation of the given results and performing several tests to understand the impact of the uncertainties in each fit, conclusions were made. Upon evaluation of the conclusions, it was finalized that an unweighted least squares fit is the only 'natural' choice for the current research. An analytical explanation on the reasons that drove us to this conclusion will be presented in the chapter 4 of the results.

Also, it is necessary to clarify from the beginning, if the experimental quantities involved in the fit are considered as correlated or uncorrelated. It is usually essential to make the assumption that the experimental observables are statistically independent values, which determined and entered the mass table as absolute measurements. In this way, the measurement error related with one observable is considered as statistically unassociated with the measurement error in all other observables.

To this end, in case of performing a weighted least squares fit, in a matrix notation, the weight matrix of the Eq.(26) is the variance matrix , and its off-diagonal terms are zero. Particularly, here, the experimental nuclear binding energies are considered as uncorrelated measurements and either we deal with an unweighted least squares fit or with weighted least squares fit, the error matrix of the Eq.(26) is always a variance matrix, where Vy is equal or different to the identical matrix for the case of an unweighted or weighted least squares fit respectively.

Chapter 4

Results

After an analytical representation of important aspects of the present phenomenological approach and research strategy, the most important results obtained by the analysis are presented in this chapter. An investigation related to an appropriate fit, which is capable to reveal the parabolic like trend of the magic (or not) nuclei between the two doubly shell closures, was continuously conducted. Once the latter is satisfied the inclusion of the extra valence-shell corrections, assumed to be due to the presence of NN and 3N forces, were added to the model so as to describe the captured shape.

As already outlined, the BW baseline equation as well as the modified liquid-drop mass formula (LDM1) was tested for their ability to reproduce the main conditions of the current work. Therefore, modifications to the existed terms of the BW formula, such those described by the LDM1, were used as alternative adjustments in performing the analysis and describing the parabolic shape of the residuals by introducing the additional terms of NN and 3N in the examined atomic mass chains.

Any other case mentioned as tested in previous sections and its related analysis is not presented in the results' chapter, it is evident that it does not satisfy the purposes of this project. However, when required, critical evidence points that assist in constructing and directing a concrete analysis strategy will be discussed.

4.1 The BW Mass Formula Fits:

4.1.1 Weighted Least Squares Fit to binding energy data for the DM nuclei (A ≥16):

A search for an appropriate set of parameters which is able to satisfy the two main conditions of the present phenomenological approach, was started by performing a weighted least-squares fit of the BW baseline mass formula to the traditional DM nuclei of AME2016 mass table. In such a way, there are not valence-shell interactions. Particularly, fits to the DM nuclei were restricted for A ≥16. At this point a reminder is given to the exclusion of the very light nuclei from the fitting procedure as the BW baseline formula is not capable to grasp the properties of such nuclei since it purely approximates a system composed of a few particles.

The best values of parameters and their accompanied uncertainties, as determined after a weighted least squares fit of the BW multi-parameter function of Eq. (5) to the traditional DM nuclei data are presented in the following Table 4.1.

Weighted least squares Fitting to the DM nuclei for A ≥16				
1) Fitting on the total binding energy (BE(MeV)) **2) Using the BW baseline formula of Eq. (5)** **3) Including the experimental uncertainties: 'unT(MeV)'** **4) Considering the pairing term (ap) as free parameter** **5) Minimization method: scipy.optimize.curve_fit**				
a_v (MeV)	**a_s (MeV)**	**a_c (MeV)**	**a_a (MeV)**	**a_p (MeV)**
24.66 ± 0.53	45.04 ± 1.59	1.33 ± 0.03	46.02 ± 1.45	194.80 ± 9.84

Table 4.1: *Best values of parameters from the weighted least squares fitting of the BW mass formula, Eq.(5), to the DM nuclei for A ≥ 16 , including the pairing contribution.*

Comparing the fit parameters of Table 4.1 with corresponding parameters from the literature it can be seen that the DM fit produced considerably different results. Even if the fit was repeated unweighted, still the resulting parameters differ significantly. Notice should be given to the value of the pairing term which was estimated 1 order of magnitude greater than the reported in literature. This should be explained from the independence of pairing term in closed shells nuclei as it was also reported in Ref. [112]. Although a search in the literature was made aiming to detect results from relevant studies, which were exclusively focused on fits of nuclear mass models to DM nuclei, no such investigations were found. Indicatively, the Table 4.2 presents a compilation of different values of parameters that were estimated in previous works which included all or subsets of nuclides of different atomic mass evaluations. This Table 4.2 was included in the present analysis for comparison purposes.

Comparison of the best fit coefficients of the BW mass formula (MeV) as obtained from different studies								
Coefficients in MeV	**AME**	**Fit**	**Restricted Dataset**	**a_v (MeV)**	**a_s (MeV)**	**a_c (MeV)**	**a_a (MeV)**	**a_p (MeV)**
Ref. [163]	2016	BE	A≥16	14.64	14.08	0.64	21.07	11.54
Ref. [38]	2003	BE	All the 2149 nuclei reported in Ref. [177]	15.67	17.70	0.71	23.07	12.73
Ref. [144]	2003	BE	All the mass table	15.777(53)	18.34 (17)	0 .710 (3)	23.21(10)	12 (2)
Ref. [120]	2003	BE	Subset of 1931 nuclei	15.8	18.3	0.714	23.2	12.0
Ref. [164]	2012	BE	A > 14	15.69 ± 0.025	17.75 ± 0.08	0.713 ± 0.002	23.16 ± 0.06	11.8 ±0.9

Table 4.2: *Comparison of the best values of coefficients of the BW mass formula terms as obtained by different authors. The column 'Fit' contains the experimental values of the total binding energy (BE) in MeV to which the BW formula is fitted.*

Following this conclusion, the reasons which affect the results of the best fit parameters, in case of fitting the DM nuclei, considering the conditions of the fit shown in Table 4.1, was investigated. As already referred in subsection (2.4.2), an independence of the pairing term in the vicinity of closed shell nuclei is reported in Ref. [112].

To this end, a weighted least squares fit to the DM nuclei for A ≥16 was repeated for the BW baseline formula, Eq. (5), but now neglecting the pairing contribution and the results of the best fit coefficients are shown in the following Table 4.3.

Weighted least squares Fitting to the DM nuclei for A ≥16				
1) Fitting on the total binding energy (BE(MeV)) **2) Using the BW baseline formula of Eq. (5)** **3) Including the experimental uncertainties: 'unT(MeV)'** **4) Without including the pairing term (ap)** **5) Minimization Method: scipy.optimize.curve_fit**				
a_v (MeV)	**a_s (MeV)**	**a_c (MeV)**	**a_a (MeV)**	**a_p (MeV)**
14.17 ± 0.18	13.51 ± 0.37	0.60 ± 0.26	17.30 ± 0.83	-

Table 4.3: *Best values of parameters from the weighted least squares fit of the BW mass formula to the DM nuclei for A ≥16, without including the pairing term (ap) in the fitting procedure.*

By inspecting the set of the best values of energy coefficients of Table 4.3, the results arising from the weighted regression of the BW baseline formula can be evaluated. The best fit coefficients can also be compared with those obtained from fits of Table 4.2 so as to detect possible extreme values in the estimated parameters or their corresponding uncertainties.

Especially, when the parameters accompanied with large values of uncertainties, it is a clear indication that they are not well determined by the experimental data. In general, the smaller the value of the parameters' uncertainties, the more confidence one can have about the sample values that used as estimates for the fit coefficients [153]. In addition, parameters with large values of uncertainties, completely lose their impact over the regression analysis [161] and are necessary to be removed from the fitting procedure as they can cause misleading to the error analysis [57]. Therefore, in the present research work, the parameters along with their accompanied uncertainties were always considered as a rough indicator for the evaluation of the accuracy and reliability of the parameters as well as the population used to make the estimates [153].

It is of substantial interest that the best values of parameters, given in Table 4.3, differ significantly from those of Table 4.1. Thus, it is concluded that the pairing contribution should be removed from the regression analysis.

Also, as noted earlier in subsection (2.4.2), one can come across with different forms of pairing term in the literature [120]. The form of pairing term, which was adapted in the present analysis, is given by the Eq. (6). However, two more terms related to the pairing expressions can been described by: $\delta(N,Z) = A^{-k}\ with\ \mathrm{k}\epsilon\ \left\{\frac{3}{4}, 1\right\}$. Although an investigation was made to reveal any possible improvements to the estimated parameters using there alternative expressions of pairing term, no significant contribution and changes to the results were identified.

The optimum values of parameters were determined using the minimization routine SciPy Curve fitting from Python. In the current research analysis, the scipy.optimize.curve_fit is the main automatic routine which is used for the representation of the results. This numerical solution was also compared with the exact solution of the chi-squared function in matrix notation, Eq. (26), but as it was expected no differences were detected in the estimation of the parameters. The BW baseline formula is a simple case of a linear model in parameter space and the automatic routine should be able to easily detect that one minimum. In such case, the search for the minimum through an automatic routine is a quite easy and straightforward process.

In addition, many more automatic routines were checked for their ability to extract the results, when needed. Particularly, the best fit coefficients generated by the automatic routine 'scipy.optimize.curve_fit' of Table 4.3, were compared with other numerical routines such those presented in section (3.2). As an example, in Table A.1 given in Appendix A, one can find the outcomes of the fit coefficients corresponded to different minimization methods. These values of parameters were all determined after a weighted least squares fitting to the DM nuclei for A ≥16 was performed, using the BW baseline formula but without including the pairing contribution.

From the outcomes of Table A.1, one can conclude that the values of the best fit coefficients are quite similar, and no large divergences occur between the estimated parameters of different linear regression methods (numerical solutions and exact). Particularly, it is observed that the 'Lmfit library' from python and the minimization routine 'MINUIT' generate the same results of best fit coefficients, while the results of exact solution and 'scipy.optimize.curve_fit' are also in totally agreement.

However, it is visible that the MINUIT gives significantly smaller values of parameters uncertainties. The uncertainty in regression parameters depends on the sensitivity of the regression method. The estimation of the parameter's uncertainties employing an exact solution can solve conflicts arise from different numerical solutions.

After the estimation of the parameters given in Table 4.3, the residuals of the DM nuclei can be determined. In the present analysis, the residuals were calculated by the difference:

$$Residuals = BEexperimental\ (MeV) - BEtheoretical\ (MeV) \tag{30}$$

In the present analysis, the experimental total binding energy is noted as 'BE(MeV)' and its corresponding theoretical value as 'LD (MeV)' .

Particularly, the focus is set on the values of the residuals which correspond to the pairs of the doubly magic nuclei of the regions of interest, presented in the following Table 4.4:

Residuals of Doubly Magic Nuclei of the Regions of Interest in MeV for a Weighted Least Squares Fit of the BW formula to the DM nuclei for A ≥16									
Diagonal Chain from ^{16}O to ^{40}Ca		Diagonal chain from ^{40}Ca to ^{56}Ni		Calcium Isotopic chain: Z=20		Isotonic chain: N=28		Tin Isotopic chain: Z=50	
^{16}O	^{40}Ca	^{40}Ca	^{56}Ni	^{40}Ca	^{48}Ca	^{48}Ca	^{56}Ni	^{100}Sn	^{132}Sn
Residuals in MeV									
0.001	-0.089	-0.089	6.769	-0.089	0.044	0.044	6.769	16.108	5.549

Table 4.4: *The residuals from the weighted least squares fit of the BW formula to the DM nuclei binding energies which correspond to the edge of the regions of interest. The blue header columns contain the residuals of the doubly magic closed shells of the diagonal chain ^{16}O to ^{40}Ca, the burgundy red header columns the residuals of the DM nuclei of the diagonal chain ^{40}Ca to ^{56}Ni, the orange, purple and green header columns contain the residuals of the DM nuclei of the calcium, isotonic (N=28) and tin chains, respectively.*

By a visual inspection of the pairs of Table 4.4, it is evident that the DM nuclei which correspond to the Calcium isotopic chain and the diagonal chain from ^{16}O to ^{40}Ca are the only regions of interest where the first condition of the present phenomenological approach is satisfied. Particularly, the two DM nuclei ^{40}Ca and ^{48}Ca have approximately the same values of residuals. Similar behavior follows the residuals of the DM nuclei of the diagonal chain from ^{16}O to ^{40}Ca. In contrary, one can observe that the rest of the chains do not follow this rule having pairs of DM nuclei with large values of discrepancies between them. Also, the residuals of the DM nuclei are shown in the following Fig. 4.1 for a better visualization and understanding of the obtained values:

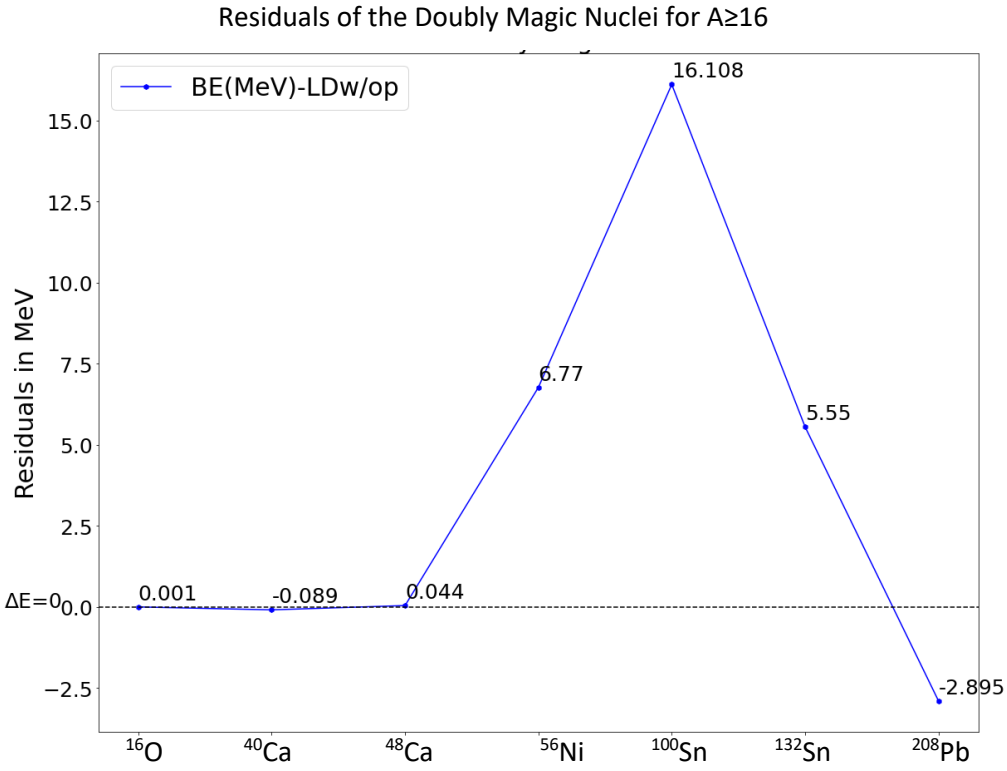

Figure 4.1: *Residuals of the weighted least squares fit of the BW mass formula to the binding energies of the DM nuclei when the pairing term is neglected. The estimated values of binding energies are noted as 'LDw/op'.*

A question that immediately arises by looking at the residuals of Fig. 4.1 is which are the factors that force the value of the residual of the nucleus ^{100}Sn to be so high compared to all the rest. While the light region of DM nuclei seems to be predicted quite well, having residual values close to zero, one can observe a clear imbalance in estimates. There is a clear overestimation of the DM nucleus ^{100}Sn by the fitting procedure. During the conduction of the present analysis, considerable time was consumed towards an understanding of the weights' effects on the outcomes. Particularly, different tests were made for identifying the role of each nucleus in the weighted least squares fit and concluding about the possible choices related to the experimental uncertainties that one has in the regression formalism. In the present thesis, only the most important tests are included.

Dependence of the results on the weights is obvious when different kinds of measurements are included in the fitting procedure and their accompanied experimental uncertainties have different magnitudes. It should be born in mind that the predictions obtained by a weighted least squares fir are significantly affected by the choice of the nuclei and their uncertainties, as some nuclei account more in the fit than others.

The standard procedure of weighting the data with the inverse square of the measurement uncertainty, clearly shows that more weight and thus more importance is given to the more accurately determined nuclei, while less precisely nuclei receive less importance in the fit. The last statement is the focal point here. By looking at the residuals of Fig. 4.1, the light region of the DM nuclei performs better since we have uncertainties that are way smaller and thus more important. Especially, the DM nucleus ^{16}O has a very precisely known experimental value, while the experimental value of the DM nucleus ^{100}Sn is not so well determined. Therefore, we concluded that this is what makes the fit shifting towards the light region trying to make better predictions for these light nuclei rather than the heavy ones.

Additionally, in Ref. [165], it is also pointed out the role of the DM nucleus ^{100}Sn as a critical nucleus that imposes modifications to the weighted least-squares fitting procedure. Particularly, it concludes that the DM nucleus, ^{100}Sn, is an important nucleus that needs to be measured more accurately.

Also, as it has already been seen, when the pairing contribution is included in the fit of the DM nuclei, the results of the coefficients are strange, and the values of parameters are far from the reported ones given by the relevant literature (Table 4.2). For this reason, in the case of the DM nuclei, a fixed value of 12 MeV for the parameter ap was adopted which then it was multiplied by $\frac{1}{A^{1/2}}$.

The fixed value of 12 MeV is reported in several papers. Particularly, in Ref. [117], which is a review on different fits of terms of the semi-empirical mass formula, is mentioned that the pairing term coefficient is calculated between 9.62 and 11.81 MeV ~ 12.0 MeV. Also, in Refs. [116,120], the value of a_p = 12 MeV is reported after performing a least-squares fit.

In addition, in the present analysis, an unweighted least squares fit was performed to the mass16.txt file, which included all the 2494 odd and even nuclei, using the minimization method MINUIT and a pairing term value of 12.0 MeV was estimated. The results are shown in the Table A.2 of the Appendix A.

From this point on and for the rest of the analysis, the 12 MeV fixed value of pairing parameter is adopted. Therefore, a weighted least squares fit of the BW baseline formula, Eq.

(5), to the DM nuclei was repeated for the estimation of the best values of parameters, but now including the pairing coefficient as a fixed parameter. The calculated residuals are presented in the following Fig. 4.2:

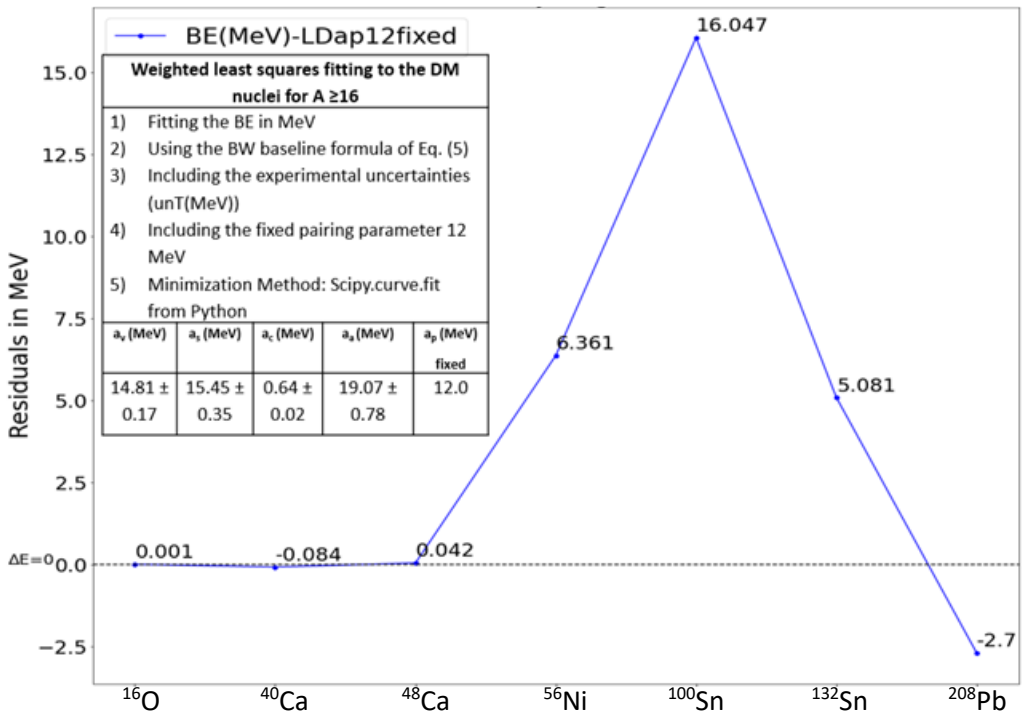

Figure 4.2: *Residuals of the weighted least squares fit of the BW baseline formula to the DM nuclei binding energies, when a fixed value of 12 MeV was assigned to the pairing parameter. Also, the best values of the estimated parameters are presented.*

Comparing the values of residuals obtained when the pairing term is considered - or not- as a fixed parameter equal to 12 MeV in the weighted least squares regression, it can be seen that its contribution is insignificant as it was expected for doubly magic nuclei. The residuals of the DM nuclei are slightly minimized by the inclusion of the pairing term; however, no important improvements was occurred in the overall performance of the residuals for the case of the weighted least squares fit.

In the first test, the idea was to replace the actual values of experimental uncertainty of ^{100}Sn and ^{132}Sn, with a very small uncertainty (= 10^{-10} MeV) at least three orders of magnitude smaller than the smallest of the rest uncertainties of the other DM nuclei, which remained the same. Once these modifications were applied, a weighted least squares fit of the BW baseline formula to the traditional DM nuclei for A ≥16 was repeated, considering the value of 12 MeV for the pairing parameter. An inspection of the residuals obtained from this fit is necessary to present for uncovering the close links between the experimental uncertainties of the most and less accurate DM nuclei during a weighted least squares fitting. To this end, the plot of the

residuals related to this test, which is named 'Test 1', is shown in Fig. 4.3. Also, the estimated parameters are reported in Table A.3 of the Appendix A.

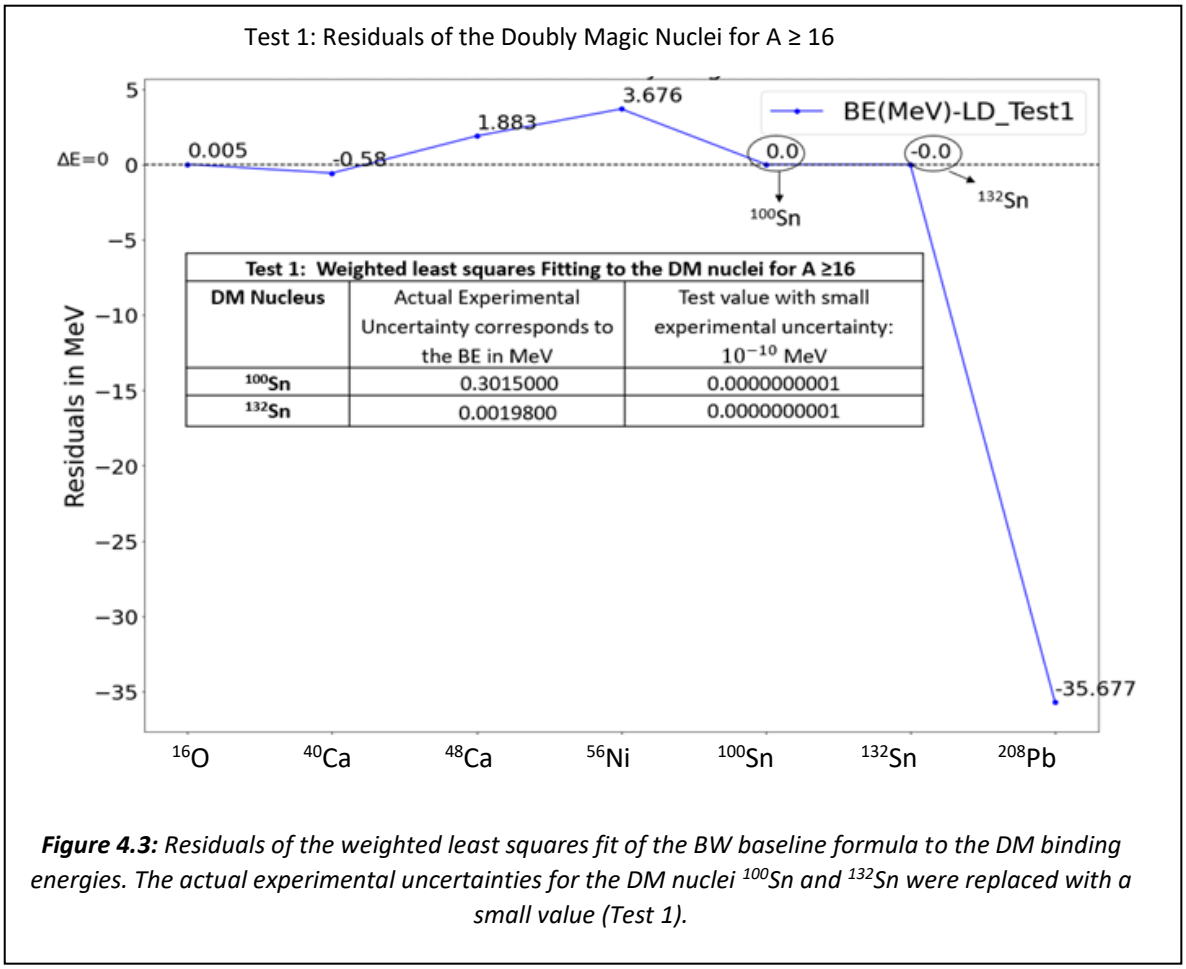

Figure 4.3: *Residuals of the weighted least squares fit of the BW baseline formula to the DM binding energies. The actual experimental uncertainties for the DM nuclei ^{100}Sn and ^{132}Sn were replaced with a small value (Test 1).*

Taking into consideration the results obtained by the Test 1, it is evident that the residuals very much depend on the choice of the weights. The fit is driven by the uncertainties assigning more importance to more precisely known nuclei. In this case, the well-determined light nuclei are predicted very accurately from the fitting procedure. In addition, the DM nuclei ^{100}Sn and ^{132}Sn have completely changed their behavior compared to their residual values of Fig. 4.2. Particularly, the fit assigns now more importance to the prediction of the DM nuclei ^{100}Sn and ^{132}Sn while overestimates the residual values of the DM nucleus ^{208}Pb. As it can be observed from the Fig. 4.3, the difference between the experimental and theoretical binding energies corresponding to the DM nuclei ^{100}Sn and ^{132}Sn is exactly zero. However, this is unlikely the case due to several factors which significantly influence the fit, such as measurement errors, systematic or random, underlying missing theory of the model etc. Here, it is certain that there is an underestimation of the residual values of the DM nuclei of ^{100}Sn and ^{132}Sn caused by the extremely small values of experimental uncertainties of Test 1. It is also worth mentioning that this is more of an issue when the sample size used in the estimation procedure is too small.

An additional test, Test 2, was also conducted to test the influence of the experimental uncertainties in the present dataset of the DM nuclei. Particularly, if the DM nucleus ^{100}Sn is completely removed from the fitting procedure, one can ascertain that almost nothing changes in the results. The latter indicates that the fit considers as an outlier the DM nucleus ^{100}Sn and thus ignores its impact in the weighted least squares procedure. The residuals' plot associated with this fit is presented in the following Fig. 4.4.

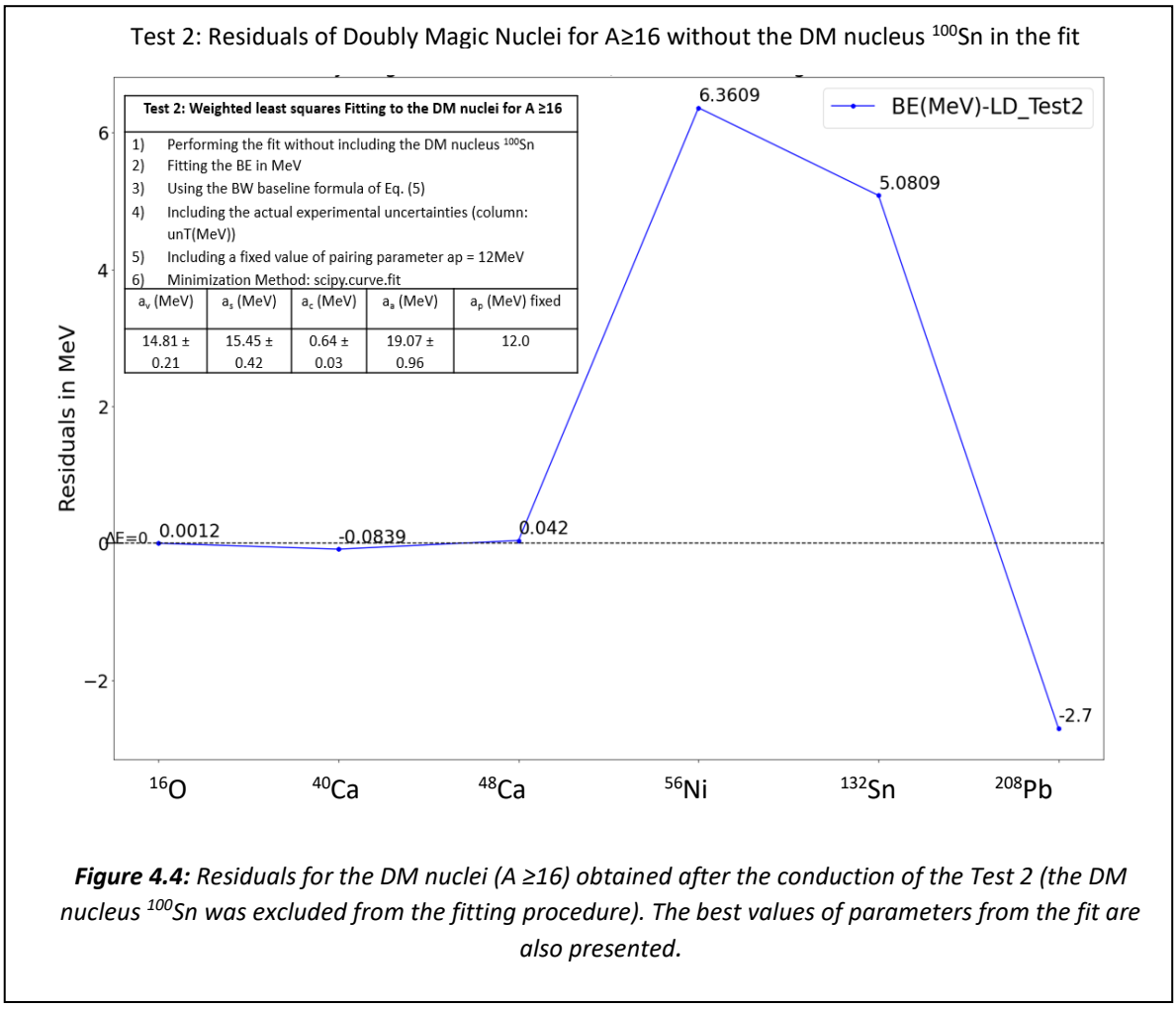

Figure 4.4: *Residuals for the DM nuclei (A ≥16) obtained after the conduction of the Test 2 (the DM nucleus ^{100}Sn was excluded from the fitting procedure). The best values of parameters from the fit are also presented.*

Furthermore, one more test, Test 3, is presented here which aims to show the inherent connection between the weights of the observables and their importance in the estimation of the parameters and thus the residuals. In this fit, it was assumed that the light nuclei have a greater value of uncertainty. Particularly, the DM nuclei: ^{16}O, ^{40}Ca and ^{48}Ca, which are considered as the most precisely measured nuclei of the DM dataset, have now a value of uncertainty equal to 0.1 MeV. The rest of the uncertainties of the DM nuclei remained the same. The results obtained from the Test 3 show that the fit is shifting towards to the nuclei which are most precisely determined. In Table A.4 presented in the Appendix A, the estimated parameters are shown, while in the following Fig. 4.5, the residuals associated with this fit are presented. It is now clear, that the weights have a big dependence on the estimated residuals

of the DM nuclei dataset. Their behavior is driven by the choice of the experimental uncertainties and therefore the weights.

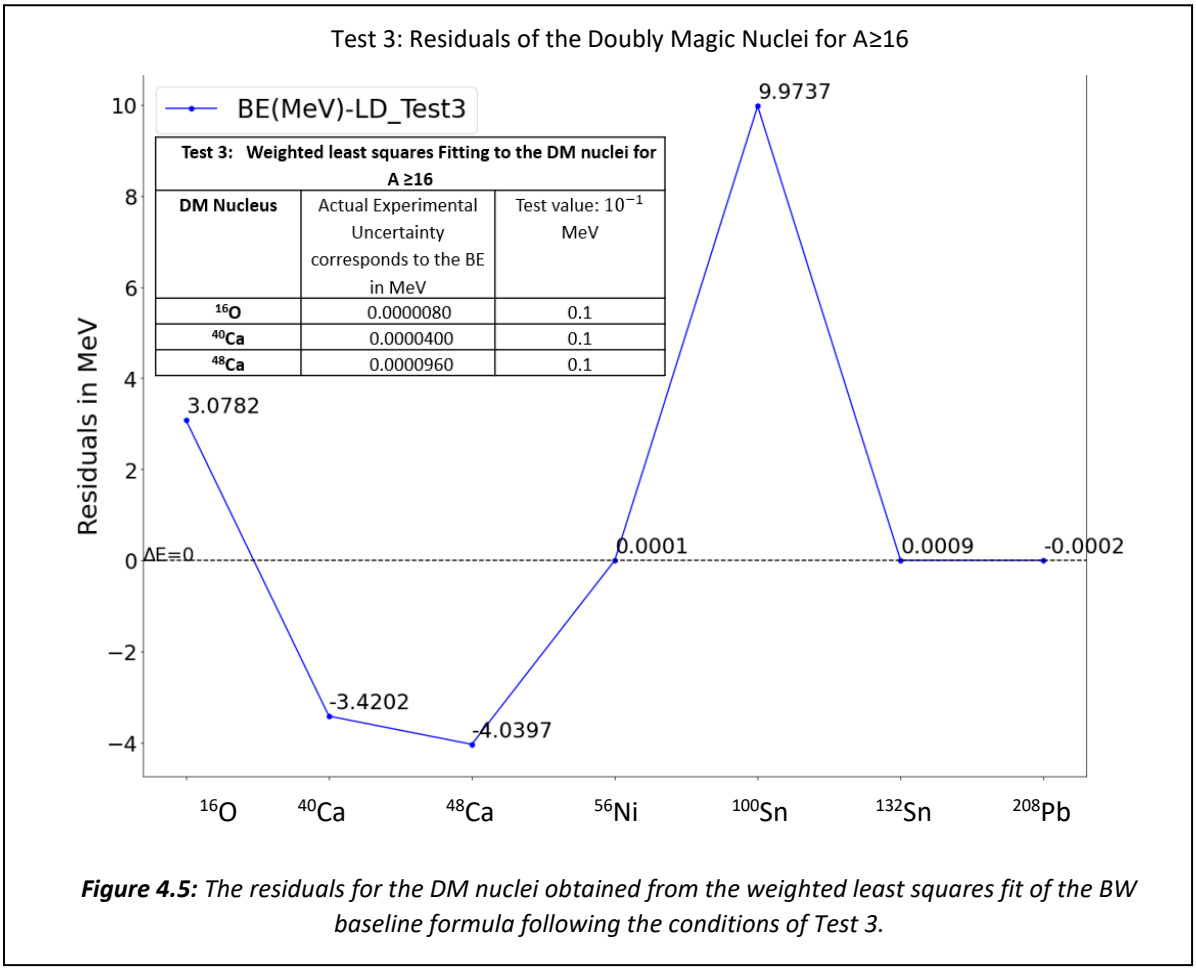

Figure 4.5: *The residuals for the DM nuclei obtained from the weighted least squares fit of the BW baseline formula following the conditions of Test 3.*

After analyzing the data of the Tests 1, 2 and 3, the close dependence of the least-squares fitting procedure on the weights is evident. Therefore, conclusions are made regarding what the next steps should be in the regression analysis. An unweighted least squares fitting appears to be the only 'natural' choice of weights, $W_j = 1$, considering the current availability and precision of the DM nuclei included in the AME2016 mass table. More precise measured atomic mass data for DM nuclei are necessary to be made in the future if one wants to consider the experimental uncertainties in the fitting procedure.

In addition, two graphical ways were used to show the imbalance presented in the magnitudes of experimental uncertainties of the traditional DM nuclei for A ≥16 and are presented in Fig. A.1 of Appendix A. Particularly, a histogram was utilized to emphasize the large difference in the values of experimental uncertainties between the DM nucleus ^{100}Sn and the rest of the DM nuclei. The box-and-whisker plot was also adapted as an alternative way to detect outliers. In the case of including the experimental uncertainties in the fitting procedure, it can be also visually proved that the experimental uncertainty correspond to DM nucleus ^{100}Sn is an outlier.

Moreover, a reference has already been made to the fact that the AME2016 is an out-of-date database and the most recent released atomic mass evaluation AME2020 is now available for use. The focus lies in identifying any significant changes that have been occurred to the experimental measured values of the DM nuclei and their corresponding uncertainties. Particularly, an inspection of the experimental uncertainty of the not well-determined DM nucleus, ^{100}Sn, is required so as to detect any possible improvement on its measured value. The result was that although there is a slight decrement in the value of its uncertainty, from approximately 0.3 MeV to 0.2 MeV, it is a minor change that cannot bring significant enhancements in the weighted regression analysis of the DM nuclei dataset.

4.1.2 Unweighted Least Squares Fit to binding energy data for the DM nuclei (A ≥16):

A conclusion has already been made regarding the insufficiency of the weighted least squares fitting procedure to satisfy the first condition of the present phenomenological approach. To this end, an unweighted least squares fit of the BW baseline formula (Eq. (5)) to the DM nuclei for A ≥ 16 was conducted. It should be mentioned that an unweighted least squares regression analysis is adapted for the rest of the analysis assuming equal weight to all the experimental data of $\sigma_i^2 = \sigma^2(N,Z) = 1\ MeV^2$ [166].

In Ref. [117], an unweighted least squares fit to all the nuclei included in the AME2003 mass table was reported using the BW baseline formula and without taking into consideration the contribution of the pairing term. The fit is made considering the total binding energy and a slight difference to the expression of the coulomb term can also be observed. The difference is related to its numerator, and it is extensively discussed in the section (4.4) of the present investigation. In Table A.5 presented in the Appendix A, the estimated values of parameters for this fit is included as well as the best fit coefficients obtained using different minimization methods to fit the DM nuclei. The results of the fit taken by the Ref. [117] are only included for comparison purposes. It should be stressed that the sample size between the two studies - Ref. [117] and the present analysis- is very different. Therefore, although there is no expectation for making the same estimations, extreme differences between the values of the estimated parameters cannot be acceptable.

The following Table 4.5 includes the conditions of the unweighted least squares fit to the DM nuclei for A ≥16 as well as the best values of the estimated parameters. The value of pairing parameter was inserted in the regression analysis as fixed and set to 12 MeV. Also, it should be stressed that if one compares the values of the optimum parameters of Table 4.5, with the best values of coefficients of Table A.5, where the pairing term is totally neglecting from the fit, it is concluded that its contribution in the fit is not large. However, the pairing contribution as fixed parameter was included in the rest of the analysis as it succeeds to bring

the values of the DM nuclei - edge of the regions of interest- a bit (although not significantly) close to each other.

An Unweighted Least Squares Fitting to the DM nuclei for A ≥16				
1) Fitting the BE in MeV **2) Using the BW baseline formula of Eq. (5)** **3) Without Including the experimental uncertainties** **4) Including the pairing term as fixed parameter a_p=12 MeV** **5) Minimization Method: scipy.curve.fit**				
a_v (MeV)	**a_s (MeV)**	**a_c (MeV)**	**a_a (MeV)**	**a_p (MeV) fixed**
16.86± 1.36	20.65± 3.75	0.79±0.10	26.81± 4.16	12.0

Table 4.5: *Best values of parameters from the unweighted least squares fit of the BW mass formula to the DM nuclei for A ≥16, with 12 MeV assigned to the pairing term coefficient.*

Re-applying the previous strategy as for the unweighted least squares fit, the values of the residuals correspond to the DM nuclei of the regions of interest, should satisfy the first condition of the present theoretical approach. Therefore, in the following Table 4.6, the results of the residuals are presented as pairs based on which region of interest, they are found in. Also, in Fig. 4.6, the residuals of the DM nuclei are shown.

Residuals of Doubly Magic Nuclei of the Regions of Interest in MeV for an Unweighted Least Squares Fit of the BW baseline formula to DM nuclei for A ≥16									
Diagonal Chain from ^{16}O to ^{40}Ca		Diagonal chain from ^{40}Ca to ^{56}Ni		Calcium Isotopic chain: Z=20		Isotonic chain: N=28		Tin Isotopic chain: Z=50	
Residuals in MeV									
^{16}O	^{40}Ca	^{40}Ca	^{56}Ni	^{40}Ca	^{48}Ca	^{48}Ca	^{56}Ni	^{100}Sn	^{132}Sn
3.72	-4.06	-4.06	-1.85	-4.06	-3.08	-3.08	-1.85	4.08	3.51

Table 4.6: *The residuals from the unweighted least squares fit of the BW formula to the DM nuclei binding energies which correspond to the edge of the regions of interest. The blue header columns contain the residuals of the doubly magic closed shells of the diagonal chain ^{16}O to ^{40}Ca, the burgundy red header columns the residuals of the DM nuclei of the diagonal chain ^{40}Ca to ^{56}Ni, the orange, purple and green header columns contain the residuals of the DM nuclei of the calcium, isotonic and tin chains, respectively.*

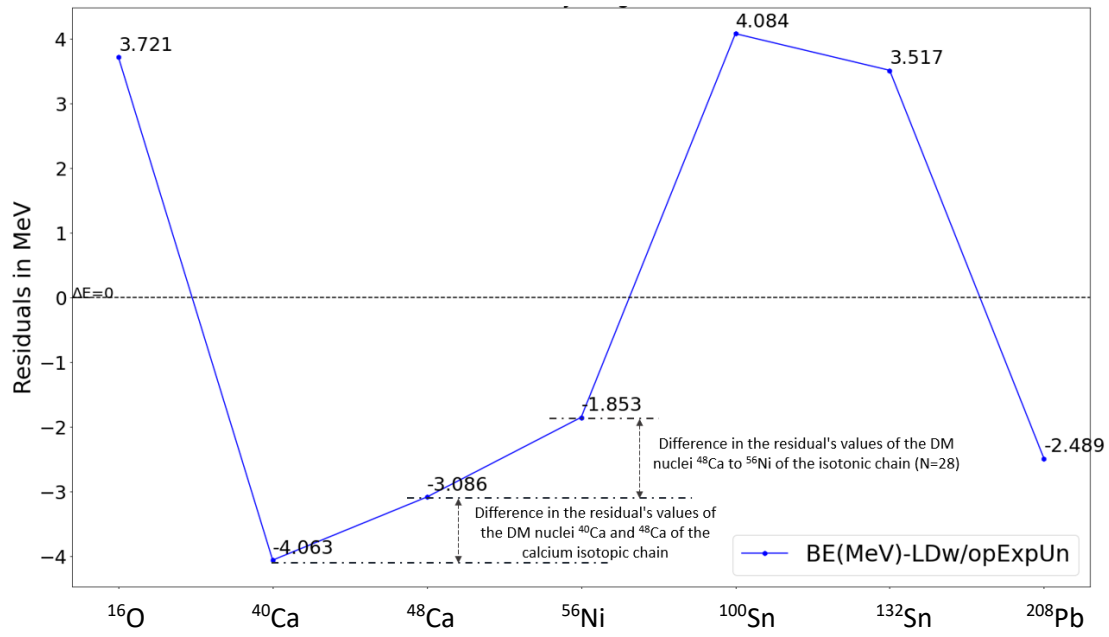

Figure 4.6: *The residuals for the DM nuclei (A≥16) obtained from the unweighted least squares fit of the BW baseline formula, assigning the value of 12 MeV to the pairing term coefficient.*

Following the research steps described in the subsection (3.1.1), the residuals of the DM nuclei correspond to the edge of the regions of interest should start and finish from approximately the same point. By visual inspection of the residuals of Fig. 4.6, it is clear that the first condition is satisfied at least for the three out of five atomic mass regions. Particularly, the calcium and tin isotopic chains appear to have almost equal values of residuals. The same behavior is also followed for the residuals correspond to the DM nuclei of the isotonic chain (N=28), even though they present a difference of approximately 1.23 MeV. These small differences between the DM shell closures of the regions' edge is a first indication for the suitability of the estimated parameters of Table 4.5 to reproduce the investigated parabolic shape in these atomic mass regions. Although the first condition is satisfied, the best values of parameters is also necessary to satisfy the second condition. Therefore, it is important to verify if the even-even magic nuclei lay between the DM nuclei of tin, calcium and isotonic chains, can reproduce a U-shaped line. In addition, it should be noted that the two diagonal chains do not align with the first rule and due to this reason, the analysis associated with these chains is not included here. Additional terms or refinements to the BW baseline formula should be considered which are able to reproduce the symmetry energy of the even-even nuclei of the diagonal chains. As they are all symmetric nuclei, terms that account more for N=Z nuclei than the asymmetric ones, should be considered in the fit.

It is important to make an additional observation regarding the residuals' values of the tin, calcium and isotonic (N=28) chains. As an example, by inspection of the residuals of the DM nuclei ^{40}Ca and ^{48}Ca, it can be seen that although these DM nuclei have almost equal values of residuals, they do not start from zero. The phenomenological approach of the present investigation assumes some inert cores and a valence space configuration. It is expected that the start point should be zero where no valence nucleons interactions occur and then valence interactions start to be taken into consideration with the increase of the valence space. Although this is only a phenomenological approach and not an exact solution of the problem, a strategy which aims to bring the residuals of the DM nuclei to zero was adapted. This is an artificial method applied to all the nuclei along the regions of interest, when needed. Particularly, the idea is to subtract a reference nucleus from all the experimental as well as calculated binding energies which correspond to the even-even nuclei of the regions of interest and their edge (two DM nuclei). The reference nucleus is always one of the DM nuclei included in this chain and all the calculations are taken relevant to this DM nucleus.

In what follows, the best fit parameters presented in Table 4.5, were applied to the even-even nuclei included between the DM nuclei of tin, calcium and isotonic (N=28) chains. If the second condition is satisfied, a comparison between the BW residuals (initial) and the residuals obtained from the fit of the BWM formula (Eq. (11)), is conducted for the evaluation of the results and relevant plots are presented.

1) Calcium isotopic chain (Z=20):

First, the best parameters applied to the even-even nuclei which lie between the two DM nuclei ^{40}Ca and ^{48}Ca. By only inspecting the residual's values, column 'BE(MeV)-LD(MeV)' of the following Table 4.7, one can conclude that the fit parameters are applicable to reproduce values of residuals which resemble a parabola.

Here, the DM nucleus ^{40}Ca was used as a reference nucleus and thus its experimental and theoretical value was subtracted by the rest of the nuclei included in the dataset. Thus, the residuals (initial) that were used in the fit were all relative measurements. This is an artificial approach which was used to force the residuals of the DM nuclei ^{40}Ca and ^{48}Ca to start from zero or as close to zero as possible.

The Eqs. (31),(32),(33) present the steps, which were followed, when the reference nucleus ^{40}Ca is subtracted from the rest of the even-even magic nuclei up to DM nucleus ^{48}Ca.

$$BEnew(exp) \quad = \text{BEexp}(^{A}\text{X'}) - \text{BEexp}(^{40}\text{Ca}) \tag{31}$$

$$BEnew(theor) = \text{BEtheor}(^{A}\text{X'}) - \text{BEtheor}(^{40}\text{Ca}) \tag{32}$$

then the final residuals relevant to the reference DM nucleus ^{40} Ca are:

$$B\text{W\_Residuals} = BEnew(exp) - BEnew(theor) \quad (33)$$

where the notation ^{A}X' refers to an even-even nucleus with mass number A, lays between the two DM nuclei ^{40}Ca and ^{48}Ca.

The following Table 4.7 shows the residuals of the even-even nuclei from ^{40}Ca to ^{48}Ca, before ('BE(MeV)-LD(MeV')) and after ('BW_Residuals') the subtraction of the experimental and theoretical value of the DM nucleus ^{40}Ca from the experimental and theoretical values of the rest of the nuclei.

Nucleus	**LD (MeV) (or BEtheor.)**	**BE(MeV)-LD (MeV)**	**(BEexp(^{A}Ca)-BEexp(^{40}Ca)) MeV**	**(BEtheor(^{A}Ca)-BEtheor(^{40}Ca)) (MeV)**	**BW_Residuals = (BE(^{A}Ca)-BE(^{40}Ca)) - (BEtheor(^{A}Ca)-BEtheor(^{40}Ca)) MeV**
^{40}Ca	346.115	-4.063	0.000	0.000	0.000
^{42}Ca	370.680	-8.784	19.844	24.565	-4.721
^{44}Ca	390.643	-9.683	38.908	44.528	-5.620
^{46}Ca	406.610	-7.837	56.721	60.495	-3.774
^{48}Ca	419.087	-3.086	73.949	72.972	0.977

Table 4.7: *The best fit parameters of Table 4.5 were applied to the even-even nuclei from ^{40}Ca to ^{48}Ca. In such a way, their theoretical binding energies in MeV (LD(MeV)) as well as the residuals (BE(MeV)-LD(MeV)) were calculated. The column '(BEexp(^{A}Ca)-BEexp(^{40}Ca)) MeV' shows the results after the subtraction of the experimental binding energy of ^{40}Ca from the experimental binding energies of the rest of the magic nuclei. Similar calculations for the theoretical binding energies and are presented in column ' (BEtheor(^{A}Ca)-BEtheor(^{40}Ca)) (MeV)'. Finally, the new residuals relevant to the reference nucleus ^{40}Ca are shown in the last column, 'BW_Residuals'.*

Following the estimation of the residuals for the even-even nuclei from the DM nuclei ^{40}Ca to ^{48}Ca, an additional fit of the BW baseline formula plus the NN and 3N valence-shell corrections (Eq. (11)) was made. Specifically, the parameters of the BW baseline formula were set to values determined by the previous fit of the BW formula to the DM binding energies. Therefore, the modified BW formula includes extra two terms which are the independent variables, X and k, while B and D are the free parameters to be estimated. The 'BW_Residuals' column of Table 4.7 are the dependent variables. At this point, it is important to mention that the X and k variables are the predictors which correspond to the following analytical expressions:

- From Eq. (18) :

Expressing the NN term as:

$$\mathrm{NN} = \mathrm{B} * (\mathrm{n_{max}} *(\mathrm{n_{max}} -1)) - (\mathrm{n_{max}} - \mathrm{n})*(\mathrm{n_{max}} - \mathrm{n} - 1)$$

where

$$\mathrm{X} = \left(\mathrm{n_{max}} * (\mathrm{n_{max-1}})\right) - (\mathrm{n_{max}} - \mathrm{n}) * (\mathrm{n_{max}} - \mathrm{n} - 1) \quad (34)$$

and

- From Eq. (19) :

Expressing the 3N term as:

$$3\mathrm{N} = \mathrm{D} * (\mathrm{n_{max}} *(\mathrm{n_{max}} - 1)*(\mathrm{n_{max}} - 2))-(\mathrm{n_{max}} - \mathrm{n})*(\mathrm{n_{max}} - \mathrm{n} - 1) * (\mathrm{n_{max}} - \mathrm{n} - 2)$$

where

$$\mathrm{k} = (\mathrm{n_{max}} *(\mathrm{n_{max}} - 1)*(\mathrm{n_{max}} - 2))-(\mathrm{n_{max}} - \mathrm{n})*(\mathrm{n_{max}} - \mathrm{n} - 1) * (\mathrm{n_{max}} - \mathrm{n} - 2) \quad (35)$$

Starting with Eq. (11), with a_p = 12 MeV, and re-arranging terms, the following equation is derived:

$$BE(N,Z) - \left(a_v * A - a_s * A^{\frac{2}{3}} - a_c * \frac{Z*(Z-1)}{A^{\frac{1}{3}}} - a_a * \frac{(N-Z)^2}{A} + 12.0 * \frac{1}{A^{\frac{1}{2}}}\right) = NN + 3N \quad (36)$$

Substituting the NN and 3N terms from Eqs. (18) and (19), the following Eq. (37) is derived:

$$BE(N,Z) - \left(a_v * A - a_s * A^{\frac{2}{3}} - a_c * \frac{Z*(Z-1)}{A^{\frac{1}{3}}} - a_a * \frac{(N-Z)^2}{A} + 12.0 * \frac{1}{A^{\frac{1}{2}}}\right) = \mathrm{B} * (\mathrm{n_{max}}*(\mathrm{n_{max}}-1)) - (\mathrm{n_{max}} - \mathrm{n}) * (\mathrm{n_{max}} - \mathrm{n} - 1) + \mathrm{D} * (\mathrm{n_{max}} *(\mathrm{n_{max}} - 1)*(\mathrm{n_{max}} - 2)) - (\mathrm{n_{max}} - \mathrm{n})* (\mathrm{n_{max}} - \mathrm{n} - 1) * (\mathrm{n_{max}} - \mathrm{n} - 2) \quad (37)$$

Using Eqs. (34) and (35), Eq.(37) is simplified as:

$$BE(N,Z) - \left(a_v * A - a_s * A^{\frac{2}{3}} - a_c * \frac{Z*(Z-1)}{A^{\frac{1}{3}}} - a_a * \frac{(N-Z)^2}{A} + 12.0 * \frac{1}{A^{\frac{1}{2}}}\right) = B * X + D * k \quad (38)$$

The last equation is equivalent to:

$$or \qquad BW\_Residuals = B * X + D * k \quad (39)$$

using the last Eq. (39) the parameters B and D were determined by fitting to the BW_Residuals values.

In addition, an extra fit considering only the contribution of NN term was applied so as to identify its strength in the fitting procedure. In this case, the fitted Eq. (39) is now written as:

$$BW\_Residuals = NN \quad => \quad BW\_Residuals = B * X \tag{40}$$

At this point it should be noted that an exclusive fit of the BWM formula when only the 3N contribution is included in the fit, was not taken into consideration here, as its contribution was found to be insignificant.

Once the minimization process of the Eqs. (39) and (40) was completed, the best values of parameters B and/(or) D were estimated and then the residuals were calculated. It is of utmost importance to evaluate how these residuals are behaving compared to the initial ones.

The inclusion of NN and 3N terms in the BW mass formula should be able to describe the parabolic trend between the two doubly magic numbers. A judgement on the latter is made based on how well the NN and 3N terms can capture the parabolic-like shape of the BW_Residuals.

The BW_Residuals (initial residuals) are plotted against the even-even nuclei included between the two DM nuclei of ^{40}Ca and ^{48}Ca. The BW_Residuals in MeV are described by the blue line color plot of the following Fig. 4.7. To visualize the improvement in the description of the parabolic shape, the residuals obtained from the fit of Eq. (39), BW_Residuals-(NN+3N) in MeV, are given by the green color line and plotted in the same graph for comparison purposes. In the same graph, the residuals' values from a fit of Eq. (40), BW_Residuals-NN in MeV, when only the contribution of NN is taken into account, are also shown.

The resulting residuals after the consideration of the NN and 3N microscopic terms in the BW baseline formula appear to approach the zero-line capturing the parabolic-like shape of the blue line color. The residuals' values, which correspond only to NN contribution, Eq. (40), is also presented by the red color line and shows that a better description of the parabolic shape is succeeded when the 3N term also included in the fit.

Calcium isotopic chain (Z=20): Even-Even Nuclei between the DM: ^{40}Ca to ^{48}Ca: BW_Residuals vs BW_Residuals-(NN+3N) vs BW_Residuals-NN

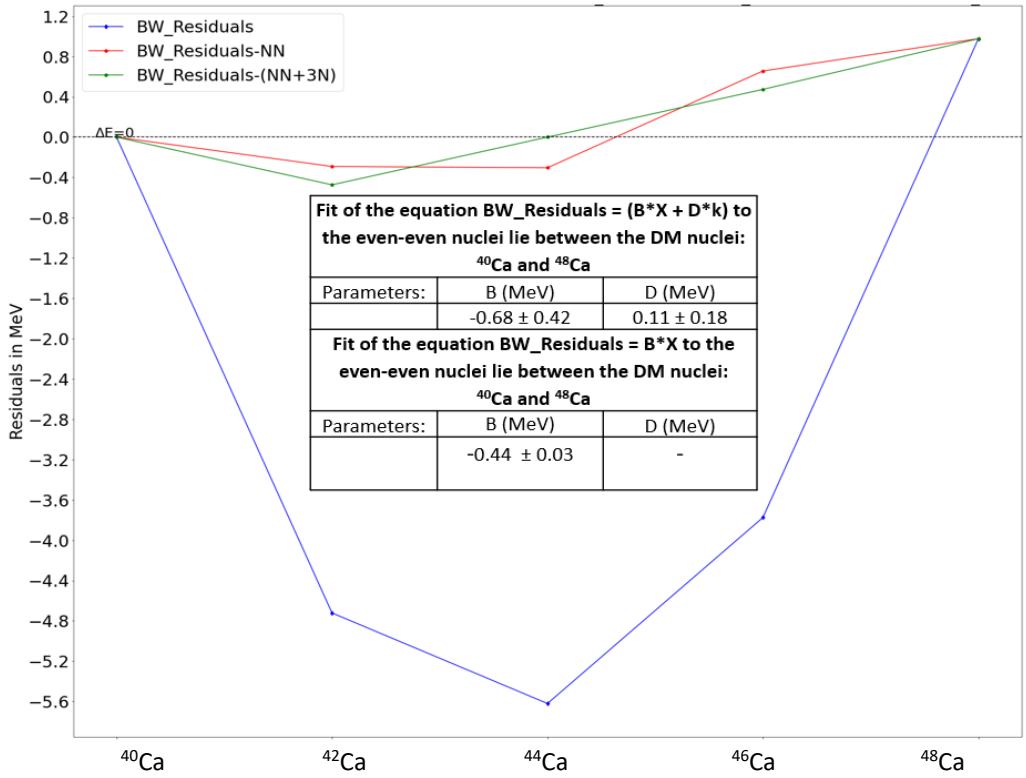

Fit of the equation BW_Residuals = (B*X + D*k) to the even-even nuclei lie between the DM nuclei: ^{40}Ca and ^{48}Ca		
Parameters:	B (MeV)	D (MeV)
	-0.68 ± 0.42	0.11 ± 0.18

Fit of the equation BW_Residuals = B*X to the even-even nuclei lie between the DM nuclei: ^{40}Ca and ^{48}Ca		
Parameters:	B (MeV)	D (MeV)
	-0.44 ± 0.03	-

Figure 4.7: *Residuals of the even-even nuclei between the two DM nuclei ^{40}Ca and ^{48}Ca. Three plots are shown for comparison purposes. The blue line color plot connects the BW_Residuals calculated using the parameters of Table 4.5, the green line corresponds to the residuals obtained after the fit of the Eq. (39) and the red color line shows the residuals' values when the NN contribution is only considered, Eq. (40). The best values of B and/(or) D parameters are also shown.*

2) Tin isotopic chain (Z=50):

An investigation towards the even-even nuclei between the DM nuclei, ^{100}Sn and ^{132}Sn, is presented next. The best fit parameters of Table 4.5 were applied to the even-even nuclei included between the two DM nuclides of the tin isotopic chain and their residuals examined for their ability to resemble a parabola. As it is evident only by inspecting the residuals' values of the following Table 4.8 and specifically the column: 'BE(MeV)-LD(MeV)', the data follow a U-shaped assembly line. Similarly, to the calcium chain, the experimental and theoretical value of the DM reference nucleus, ^{100}Sn, was subtracted from all the experimental and theoretical binding energies of the nuclei included in the dataset of the tin chain. Therefore, the new values of residuals 'BW_Residuals' were calculated relatively to the DM nucleus, ^{100}Sn and a new fit of the Eqs. (39) and (40) was performed for the estimation of the best fit coefficients B and/(or) D. Also, a comparison between the BW_Residuals and the residuals

obtained after the fit of the Eqs. (39) and (40), BW_Residuals-(NN+3N) and BW_Residuals-NN, respectively, are presented in the following Fig. 4.8.

Nucleus	LD (MeV)	BE(MeV)-LD (MeV)	BEexper(^{100}Sn) (MeV)	BEexp(^{A}Sn)-BEexp(^{100}Sn) (MeV)	BEtheor(^{100}Sn) (MeV)	(BEtheor(^{A}Sn)-BEtheor(^{100}Sn)) (MeV)	BW_Residuals (MeV)
^{100}Sn	821.214	4.084	825.297	0	821.214	0	0
^{102}Sn	850.728	-1.636	825.297	23.794	821.214	29.515	-5.720
^{104}Sn	878.188	-6.261	825.297	46.629	821.214	56.974	-10.345
^{106}Sn	903.710	-9.914	825.297	68.499	821.214	82.496	-13.997
^{108}Sn	927.401	-12.746	825.297	89.358	821.214	106.187	-16.830
^{110}Sn	949.362	-14.793	825.297	109.272	821.214	128.149	-18.877
^{112}Sn	969.687	-16.162	825.297	128.228	821.214	148.473	-20.245
^{114}Sn	988.461	-16.888	825.297	146.275	821.214	167.247	-20.972
^{116}Sn	1005.764	-17.083	825.297	163.384	821.214	184.551	-21.167
^{118}Sn	1021.673	-16.722	825.297	179.653	821.214	200.459	-20.806
^{120}Sn	1036.257	-15.718	825.297	195.242	821.214	215.043	-19.802
^{122}Sn	1049.581	-14.057	825.297	210.227	821.214	228.368	-18.141
^{124}Sn	1061.708	-11.748	825.297	224.663	821.214	240.494	-15.831
^{126}Sn	1072.693	-8.809	825.297	238.586	821.214	251.480	-12.893
^{128}Sn	1082.592	-5.218	825.297	252.076	821.214	261.378	-9.302
^{130}Sn	1091.454	-1.168	825.297	264.989	821.214	270.240	-5.251
^{132}Sn	1099.326	3.517	825.297	277.546	821.214	278.113	-0.567

Table 4.8: *The best fit parameters of Table 4.5 were applied to the even-even nuclei from ^{100}Sn to ^{132}Sn. The values of the residuals of the column 'BW_Residuals (MeV)' were derived taking into account the DM reference nucleus ^{100}Sn.*

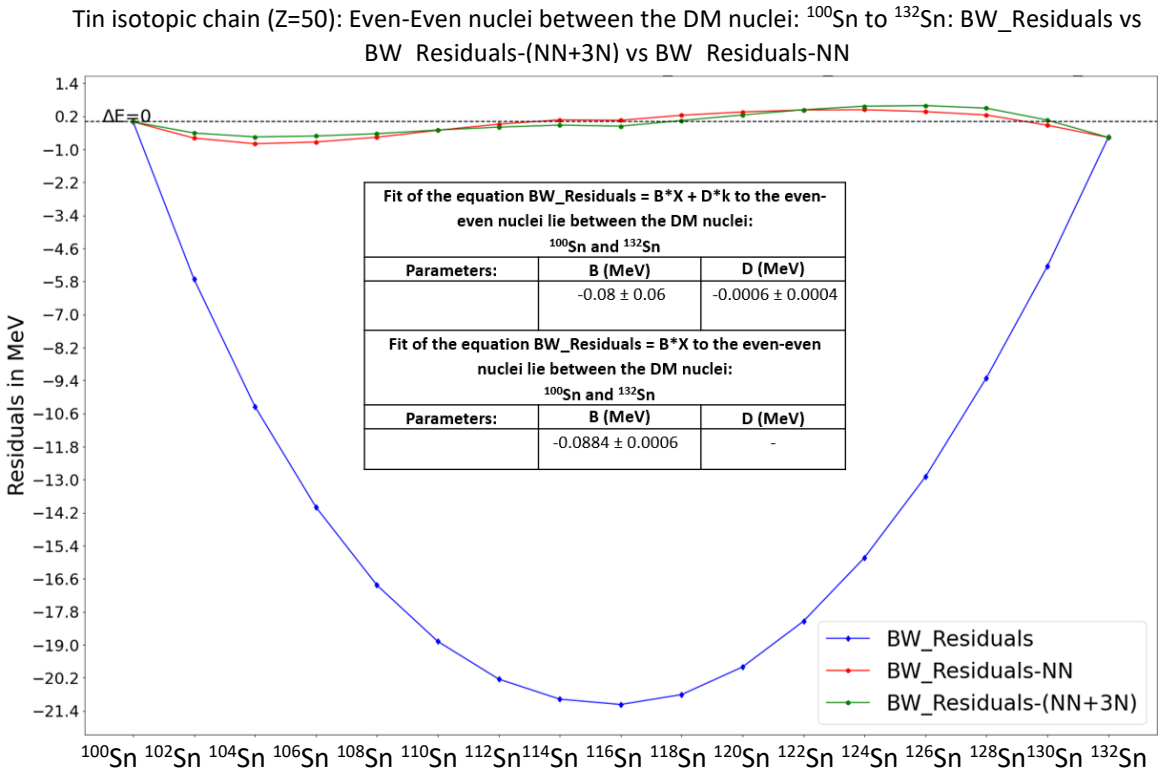

Figure 4.8: *Residuals of the even-even nuclei between the DM nuclei ^{100}Sn and ^{132}Sn. Three plots are shown for comparison purposes. The blue color line plot connects the BW_Residuals calculated using the parameters of Table 4.5, the green line corresponds to the residuals obtained after the fit of the Eq. (39) and the red color line shows the residuals' values when the NN contribution is only considered, Eq. (40). The best values of B and/(or) D are also shown.*

Finally, it becomes apparent that the residuals of the even-even nuclei included between the two DM nuclei, ^{100}Sn and ^{132}Sn, follow a parabolic trend which can successfully described by the inclusion of the NN and 3N valence-shell corrections. The green color line which corresponds to the residuals given by the fitted Eq. (39) has been significantly attributed to the explanation of the parabolic form of the initial residuals. Similar behavior is also found for a fit of the Eq. (40). The inclusion of the valence-shell corrections, due to what is anticipated to be given by NN and 3N terms, in the BW baseline formula serves the purposes of the present theoretical approach.

3) Isotonic chain (N=28):

Repeating the analysis for the isotonic chain N=28, the parameters of the Table 4.5 were applied to the even-even nuclei included between the two DM nuclei ^{48}Ca and ^{56}Ni. The difference between the experimental and theoretical binding energies for these nuclei are presented in the column: 'BE(MeV)-LD(MeV)' of Table 4.9. The in-between residuals of the two DM nuclei, ^{48}Ca and ^{56}Ni, appear to follow a parabola. However, it should be noted that there is still a difference in the residuals' values of the DM nuclei - edge - of the present atomic mass region. In a similar way as before, the experimental binding energy as well as its corresponding theoretical value of the reference DM nucleus, ^{48}Ca, is necessary to be subtracted from each of the experimental and theoretical values of all the rest nuclei of the dataset, respectively. The final residuals are shown in the last column of Table 4.9.

Nucleus	**LD (MeV)**	**BE(MeV)-LD(MeV)**	**BEexper(^{48}Ca) (MeV)**	**(BE(^{A}Ca)-BE(^{48}Ca)) (MeV)**	**BEtheor(^{48}Ca) (MeV)**	**(BEtheor(^{A}Ca)-BEtheor(^{48}Ca)) (MeV)**	**BW_Residuals (MeV)**
^{48}Ca	419.087	-3.086	416.001	0.000	419.087	0.000	0.000
^{50}Ti	445.065	-7.279	416.001	21.785	419.087	25.978	-4.193
^{52}Cr	464.447	-8.095	416.001	40.351	419.087	45.360	-5.009
^{54}Fe	477.861	-6.097	416.001	55.764	419.087	58.774	-3.010
^{56}Ni	485.849	-1.853	416.001	67.995	419.087	66.762	1.233

Table 4.9: *Best fit parameters of Table 4.5 were applied to the even-even nuclei from the DM nuclei ^{48}Ca to ^{56}Ni. The values of the residuals of the column 'BW_Residuals (MeV)' were derived taking into account the DM reference nucleus ^{48}Ca.*

What follows the estimation of the residuals' values for each of the nuclei of Table 4.9, is fits of the BW modified formula given by the Eqs. (39) and (40), to the dataset presented in Table 4.9. In a similar manner as before, the following Fig. 4.9, shows a comparison of the initial residuals, BW_Residuals, and the residuals as obtained after the fits of the Eqs. (39) and (40).

Isotonic chain (N=28): Even-Even nuclei between the DM nuclei: ^{48}Ca to ^{56}Ni : BW_Residuals vs BW_Residuals-(NN+3N) vs BW_Residuals-NN

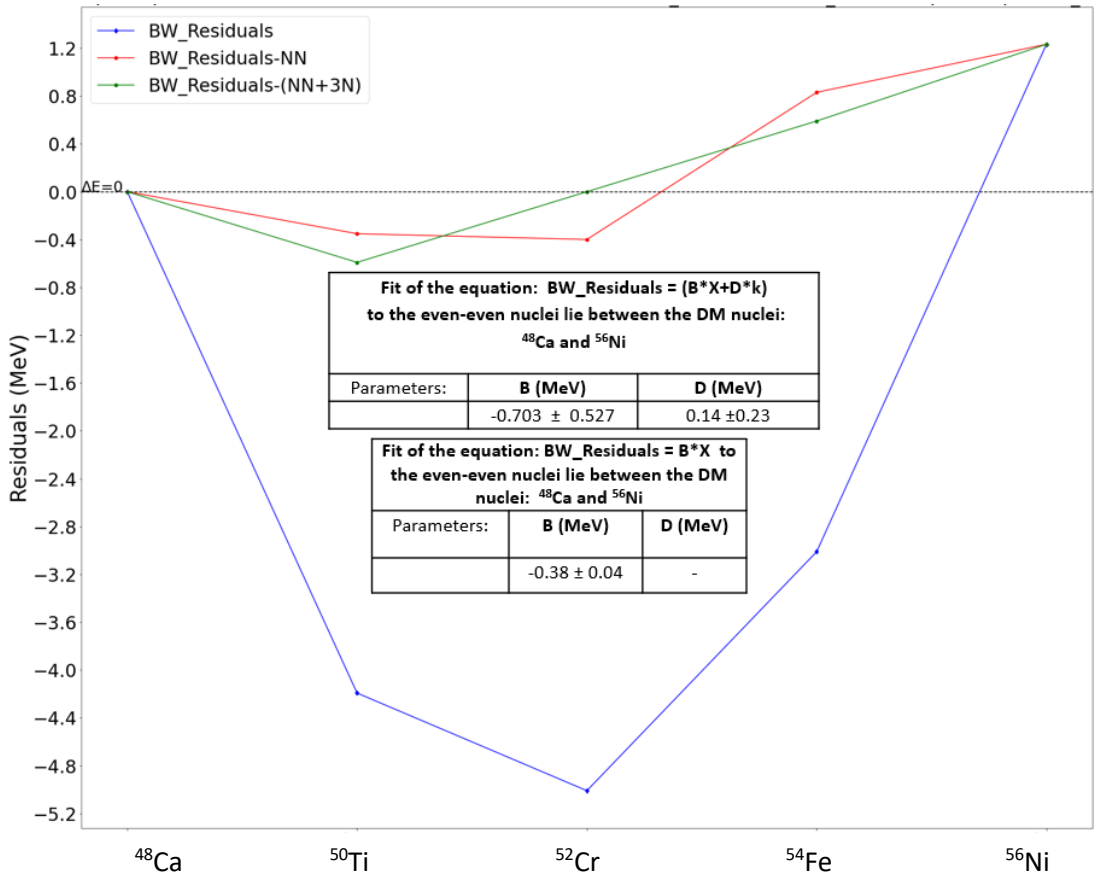

Figure 4.9: *Residuals of the even-even nuclei between the DM nuclei ^{48}Ca and ^{56}Ni. Three plots are shown for comparison purposes. The blue line color plot connects the BW_Residuals calculated using the parameters of Table 4.5, the green line corresponds to the residuals obtained after the fit of the Eq. (39) and the red color line shows the residuals' values when the NN contribution is only considered in the fit, Eq.(40). The values of the best fit parameters are also shown.*

Given the residuals' plots of the last Fig. 4.9, it seems that the inclusion of the valence-shell corrections, given by the NN and 3N terms, minimizes the BW_Residuals, which were calculated using the parameters of Table 4.5 and are depicted in Fig 4.9 connected with a blue line. The latter actually means that is able to describe the parabolic shape of the blue color line. However, it should be emphasized that it is not expected the residuals of green color line to be exact zero. As previously explained, the predicted values cannot be exactly the same as the observed values due to the measurement uncertainties and model imperfections [162].

The overall performance of the case of an unweighted least squares fit of the BW baseline formula to the traditional DM nuclei and also fitting its modified version (BWM) to the regions of interest, is now important to be assessed. First, it was proved that the best fit coefficients obtained from such an unweighted least squares regression, are applicable to reproduce the parabolic behavior of the BW residuals between two DM nuclei. Following the last justification, a fit of the BWM formula, Eq. (39) (and Eq. (40)), towards the even-even nuclei included between the two shell closures, was performed. The findings show that the inclusion of the additional valence-shell corrections of NN and 3N terms are applicable to describe the parabolic shape of the BW residuals for calcium and tin isotopic chains as well as for the isotonic chain (N=28).

At this point, it is important to make a remark on the fit to the dataset restricted to the even-even nuclei of Table 3.1. An unweighted least squares fitting procedure was also applied to the even-even nuclei included in the range of $16 \leq A \leq 208$. Although this case of fitting was tested, such a fit was rejected and considered invalid. Reference has already been made to the inadequacy of the BW baseline formula to account for shell effects and microscopic theory. It is a simple model which only provides valuable information about the bulk properties of nuclear systems. Particularly, in case of conducting a fit of the BW baseline formula to the even-even nuclei for $16 \leq A \leq 208$, open shells of even-even nuclei are not taken into consideration in the model's theory of the BW formula. To this end, the estimated parameters, obtained from such a fit, are considered inappropriate and was not used for further evaluation of our research approach.

In addition, as previously reported, one more isotopic chain can be tested for its ability to reproduce our phenomenological approach, if ones takes into consideration the experimentally approved DM nucleus, ^{24}O. Therefore, the DM nucleus, ^{24}O, was added to the list of the DM nuclei and an unweighted least squares fitting procedure followed. The results showed that the edge of the Oxygen isotopic chain, which correspond to the DM nuclei ^{16}O and ^{24}O, do not satisfy the first condition of the present research strategy. In a similar manner, the residuals' values of the rest of the DM nuclei presented in the list, also do not follow the first rule after the inclusion of the DM nucleus ^{24}O. Therefore, this case of fit is not presented here.

Before proceeding with the rest of the analysis, it should be summarized that more input as well as output data related to the fits of the regions of interest are included in the Appendix A. The input data, residuals' values, theoretical binding energies as well as the contribution of each of the NN and 3N terms, after fitting the Eqs. (39) and (40) to the even-even nuclei of the examined regions of interest, are shown in Tables A.6 to A.11 of the Appendix A.

4.2 The LDM1 Formula Fit:

4.2.1 Fit to the traditional DM nuclei (A ≥16) binding energies and with the addition of the DM nucleus ^{24}O:

As it has been discussed in subsection (2.4.2), an improvement to the expression of the BW baseline formula was suggested by Samanta and Adhikari [124], aiming to explain some light nuclei as well as nuclei far from the line of stability. Particularly, by modifying the asymmetry and pairing terms in the initial BW baseline formula, it identified new magic numbers of Z and N or the disappearance of some of the already known magic numbers.

In the present analysis, the LDM1 formula was only adapted in an attempt to bring the residuals for the pairs of the DM nuclei of the selected regions of interest to similar values so to satisfy the first condition of the present phenomenological approach. To this end, an unweighted least squares fit of the LDM1 formula to the traditional DM nuclei, adding also the newly observed DM nucleus ^{24}O, was conducted. Therefore, the even-even nuclei included between the two closed shells of the oxygen isotopic chain was also examined for their ability to reproduce the current theoretical approach. All the DM entries should also follow the condition A ≥16. The best fit coefficients are presented in Table 4.10.

1) Fitting the BE in MeV
2) Using the LDM1 formula of Eq. (7)
3) Without including the experimental uncertainties
4) Including the pairing term as fixed parameter 12 MeV
5) Minimization Method: Scipy.curve.fit from Python

a_v (MeV)	a_s (MeV)	a_c (MeV)	a_a (MeV)	a_p (MeV) fixed
15.89 ± 0.71	17.98 ± 1.91	0.72 ± 0.05	23.93 ± 2.11	12.0

Table 4.10: *Best fit parameters obtained from the unweighted least squares fit of the LDM1 formula to the DM nuclei binding energies, for A ≥16, including the DM nucleus ^{24}O.*

Once the best fit parameters were calculated, the residuals' values for each nucleus included in the fit was accessed. Particularly, the interest lays in observing the values of the DM nuclei which were included in the regions of interest. The pairs of such DM nuclei are shown in the following Table 4.11 and their residuals' plot in Fig. 4.10, and they should satisfy the first condition.

Diagonal Chain from ^{16}O to ^{40}Ca		Diagonal chain from ^{40}Ca to ^{56}Ni		Isotopic chain: Z=20		Isotonic chain: Z=28		Isotopic chain: Z=50		Isotopic chain: Z=8	
Residuals in MeV											
^{16}O	^{40}Ca	^{40}Ca	^{56}Ni	^{40}Ca	^{48}Ca	^{48}Ca	^{56}Ni	^{100}Sn	^{132}Sn	^{16}O	^{24}O
2.30	-4.31	-4.31	-1.01	-4.31	-4.99	-4.99	-1.01	4.97	4.37	2.30	1.05

Table 4.11: *The residuals from the unweighted least squares fit of the BW formula to the DM nuclei binding energies which correspond to the edge of the regions of interest. The blue header columns contain the residuals of the doubly magic closed shells of the diagonal chain ^{16}O to ^{40}Ca are presented, the burgundy red header columns the residuals of the DM nuclei of the diagonal chain ^{40}Ca to ^{56}Ni, the orange, purple and green header columns the residuals of the DM nuclei of the calcium, isotonic and tin chains, respectively. Also, the residuals for the DM nuclei of the oxygen isotopic chain are shown in red header color.*

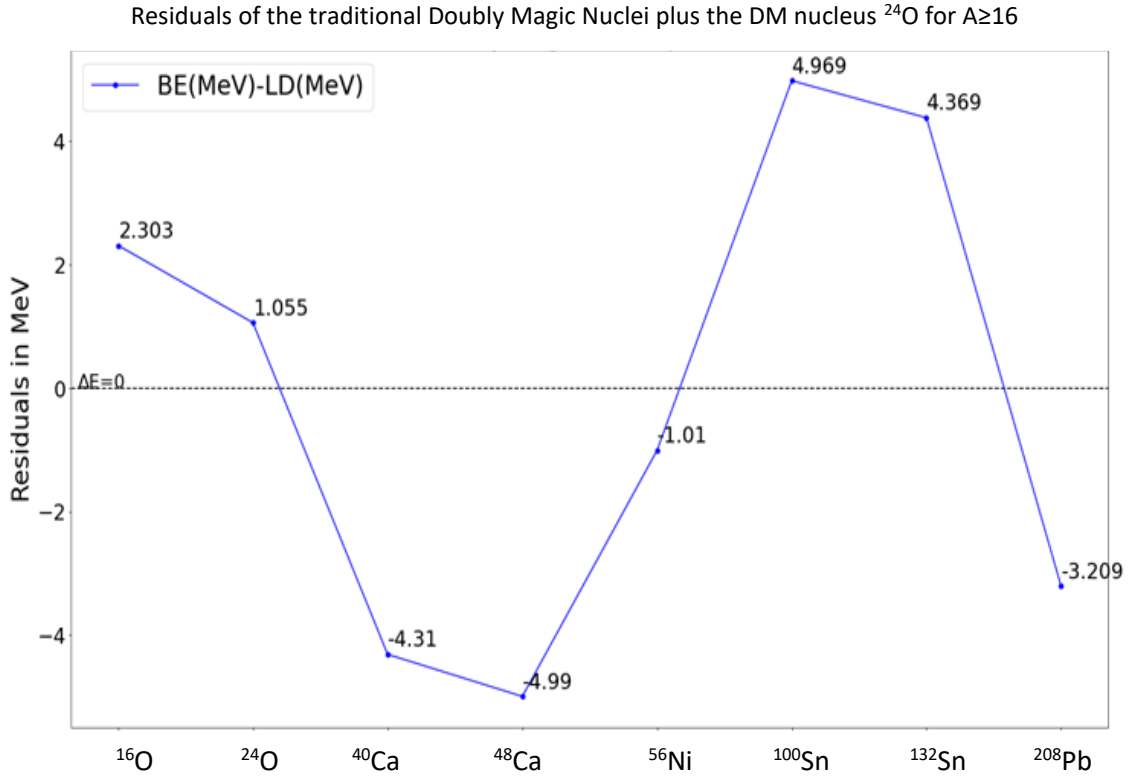

Figure 4.10: *The residual values for the DM nuclei (A ≥16) obtained from the unweighted least squares fit of the LDM1 formula plus the DM nucleus ^{24}O are shown.*

By inspecting the values of the pairs of the DM nuclei, presented in Table 4.11, it is evident that the pairs of the DM nuclei which satisfy the rule of having approximately close values of residuals, correspond to the calcium, tin, and oxygen isotopic chains. On the contrary, one can also notice that there is a big difference in the residuals' values of the DM nuclei of the isotonic chain (N=28) as well as the diagonal chains from ^{16}O to ^{40}Ca and from ^{40}Ca to ^{56}Ni. Particularly, the edge of the isotonic chain (N=28), which correspond to DM nuclei ^{48}Ca and ^{56}Ni, have an absolute difference of approximately 4 MeV between their residuals' values. These chains are not suitable to satisfy the first condition of the present theoretical approach as well as they produce residuals' values of even-even nuclei between closed shells, with inconspicuous parabolic character. Thus, their analysis was omitted from the present work.

In a similar manner as before, first the best fit parameters of Table 4.10, are applied to the calcium, tin and oxygen isotopic chains in order to identify if they can produce residuals which follow a parabolic-like form in compliance with the research steps presented in the subsection (3.1.1). If the latter is true, a fit to the even-even nuclei of these regions of interest using a modified LDM1 formula was conducted. This formula refers to the inclusion of the additional valence-shell corrections given by the NN and 3N terms to the LDM1 formula, Eq.(7). Afterwards, the analysis for the examined regions of interest proceeded in a similar manner like the one presented in the example case with the application of the Eqs. (31),(32),(33). Then the final residuals are derived and named as 'LDM1_Residuals'. The analytical mathematical expression of the modified LDM1 formula is presented next:

$$\mathrm{BE(A,Z)} = \mathrm{a_v} * \mathrm{A} - \mathrm{a_s} * \mathrm{A}^{\frac{2}{3}} - \mathrm{a_c} * \frac{\mathrm{Z}*(\mathrm{Z}-1)}{\mathrm{A}^{\frac{1}{3}}} - \mathrm{a_{sym}} * \frac{(\mathrm{A}-2\mathrm{Z})^2}{1+e^{-\frac{A}{17}}} * \mathrm{A} + \delta \mathrm{n}ew + \mathrm{NN} + 3\mathrm{N} \quad (41)$$

Following exactly the same calculations as for the case of the BW baseline formula and the Eqs. (34) to (37), the parameters B and D were determined with regression analysis using the following equation, which is linear in parameter space with the dependent variable in the left-hand side:

$$LMD1\_Residuals = \ B * X + D * k \quad (42)$$

If only the contribution of NN term is considered, the modified LDM1 expression of Eq. (42) is now written:

$$LMD1\_Residuals = \ B * X \quad (43)$$

Relevant Tables and graphs, obtained for each of the regions of interest, are presented next. The steps followed to obtain the plots of each graph have a similar logic as before and the previous subsections can be revisited for further clarifications, if necessary.

1) Calcium isotopic chain from the DM nucleus ^{40}Ca to DM nucleus ^{48}Ca:

The best fit parameters of Table 4.10 were applied to the even-even nuclei included between the two DM nuclei ^{40}Ca to ^{48}Ca. Then the estimations of the experimental binding energies as well as the residuals correspond to each of the nuclei were calculated and the subtraction of the DM reference nucleus, ^{40}Ca, was also conducted. Once the final residuals' values (LDM1_Residuals) have been determined, an unweighted least squares fit of the modified LDM1 formula, Eq. (42), as well as of Eq. (43), to the even-even nuclei from the DM nuclei ^{40}Ca to ^{48}Ca, was performed. The residuals' plots correspond to such fits are presented in the same graph of Fig. 4.11 for comparison purposes.

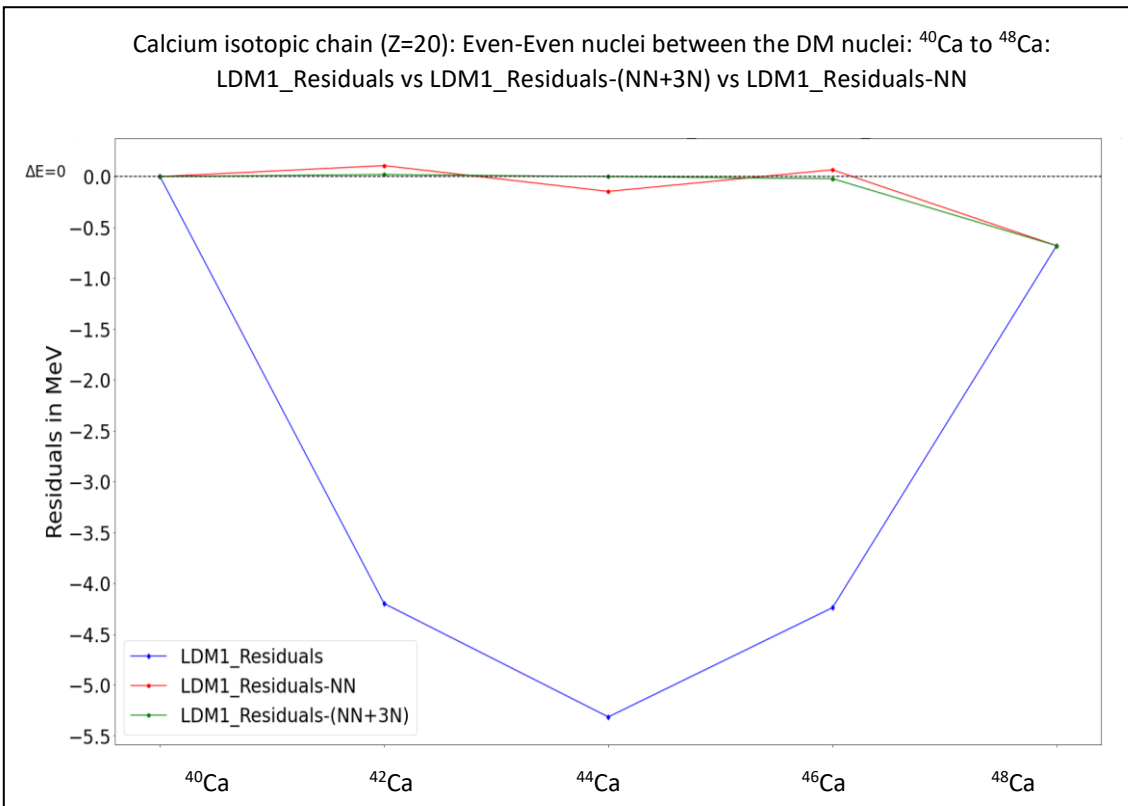

Figure 4.11: *Comparison of the residuals correspond to the even-even nuclei from the DM nucleus ^{40}Ca to ^{48}Ca. The blue color line connects the LDM1_Residuals calculated using the parameters of Table 4.10, the green color line the residuals after fitting the Eq.(42) and the red color plot the residuals after fitting the Eq. (43).*

2) Tin isotopic chain from the DM nucleus ^{100}Sn to DM nucleus ^{132}Sn:

The best fit parameters of Table 4.10 were applied to the even-even nuclei included between the two DM nuclei ^{100}Sn to ^{132}Sn. Then, theoretical values of binding energies as well as the residuals correspond to each of the nuclei were calculated. The experimental and theoretical values of the DM reference nucleus ^{100}Sn was also subtracted from each of the experimental and theoretical binding energies of the DM nuclei, respectively, included in the list of the tin isotopic chain. Once the final residuals' values (LDM1_residuals) have been determined an unweighted least squares fit of the modified LDM1 formula, Eq. (42), as well as the Eq. (43), to the even-even nuclei from the DM nucleus ^{100}Sn to ^{132}Sn, can be made. The residuals' plots of the above fits are all presented in the following Fig. 4.12.

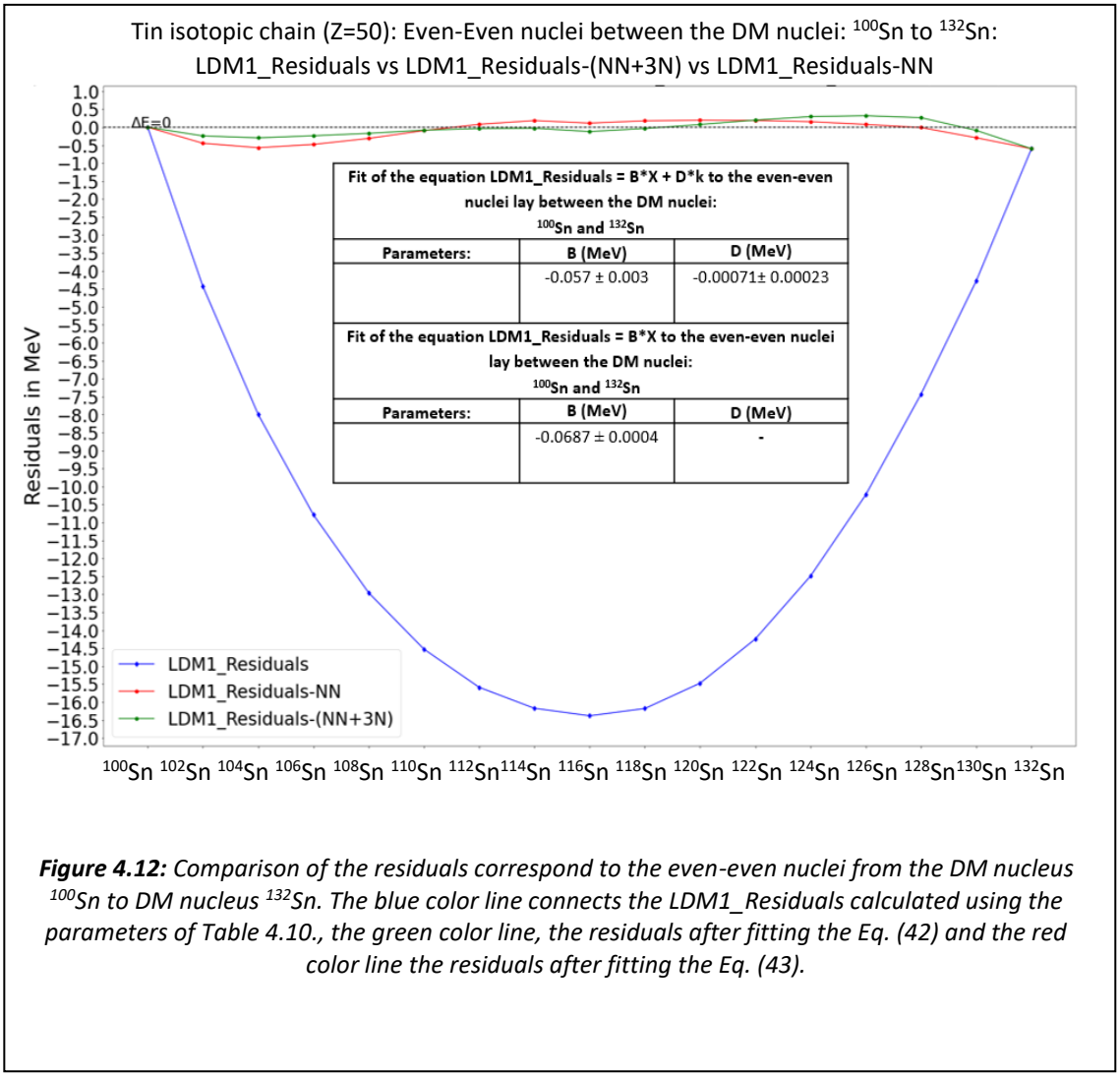

Figure 4.12: *Comparison of the residuals correspond to the even-even nuclei from the DM nucleus ^{100}Sn to DM nucleus ^{132}Sn. The blue color line connects the LDM1_Residuals calculated using the parameters of Table 4.10., the green color line, the residuals after fitting the Eq. (42) and the red color line the residuals after fitting the Eq. (43).*

3) Oxygen isotopic chain from the DM nucleus ^{16}O to DM nucleus ^{24}O:

The best fit parameters of Table 4.10 were applied to the even-even nuclei included between the two DM nuclei from ^{16}O to ^{24}O. Then, the theoretical values of binding energies as well as the residuals correspond to each of the nuclei can be calculated. The experimental and theoretical value of the DM reference nucleus ^{16}O was also subtracted from each of the experimental and theoretical binding energies of the DM nuclei, respectively, included in the list. Once the final residuals' values, LDM1_residuals, have been determined, an unweighted least squares fit of the modified LDM1 formula Eq. (42), as well as Eq. (43), to the even-even nuclei from the DM nucleus ^{16}O up to DM nucleus ^{24}O, can be performed. The residuals' plots, correspond to the oxygen Isotopic chain, are presented in the following Fig. 4.13:

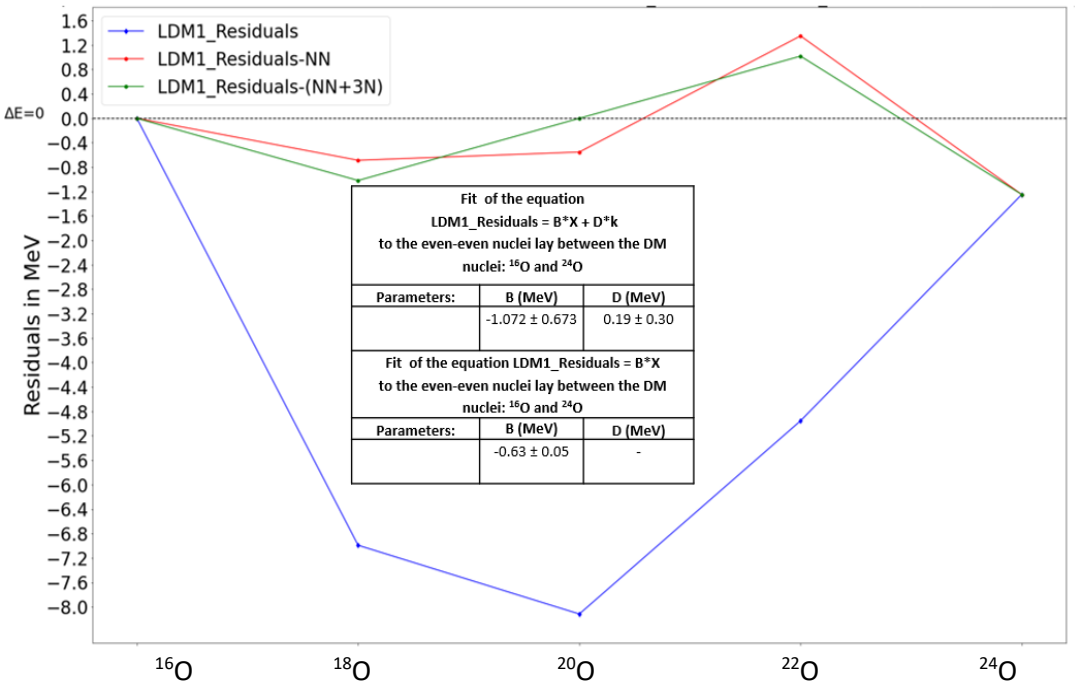

Figure 4.13: *Comparison of the residuals correspond to the even-even nuclei from the DM nucleus ^{16}O to DM nucleus ^{24}O. The blue color line connects the LDM1_Residuals calculated using the parameters of Table 4.10, the green color line the residuals after fitting the Eq. (42) and the red color line plot the residuals after fitting the Eq. (43).*

Considering the results obtained from the above analysis, one can conclude that a fit of the LDM1 formula to the DM nuclei, including the DM nucleus, ^{24}O, generates a set of parameters which is applicable to reproduce the U-shaped line of the residuals for the even-even nuclei between the two DM shell closures. This parabolic-like shape is notable for the

calcium, tin and oxygen isotopic chains. Thus, once a fit of the modified LDM1 formula occurred towards to these atomic mass regions, the parabolic-like behavior can be captured with the inclusion of the NN and 3N terms.

Concluding relevant input as well as output data related to the fits of the LDM1 to the even-even nuclei lie between the DM nuclei of each regions of interest are presented in the Appendix A and in Tables A12 to A17.

4.3 Comparison with Shell Corrections from the literature:

The importance of inclusion shell corrections in the liquid-drop mass formula has been pointed out by many authors from the early years of nuclear physics. Several studies have been made in implementing shell effects to mass models in order to achieve an accurate description of nuclear masses. To this end, several terms of shell corrections have been proposed which are often laborious and challenging to apply.

A simple way to account for shell effects in the liquid-drop mass formula can be found in Refs. [38,111,167,168]. This is based on counting valence nucleons - particles or holes - following the rule of interacting boson model (IBM) [169]. In Refs. [4,99,112,170], one can find a similar approach in adapting such shell corrections to different versions of liquid-drop mass formula so as to achieve a precisely description as well as reliable predictions of nuclear masses especially around closed shells.

To compare the valence-shell corrections of Eqs. (18) and (19), introduced in this work, with a shell correction from the literature, two terms suggested by Ref. [4] were chosen. These terms, which are characterized by simplicity, are expressed as a function of the total number of valence nucleons, particles or holes and are added to the BW baseline formula. Particularly, one of them is linear and the other is quadratic in the number of valence neutrons (n_n) and valence protons (n_p). The linear and quadratic terms are named P and PP, respectively, and are described by the following expressions:

$$P = b1 * \left(n_n + n_p\right) \tag{44}$$

and

$$PP = b2 * \left(n_n + n_p\right)^2 \tag{45}$$

where n_n and n_p are the number of valence neutrons and valence protons respectively and $b1\ and\ b2$ are free parameters to be estimated from the fit. The sum $(n_n + n_p)$ is equal to the total number of the valence nucleons , n , of the nucleus.

Including both the linear and quadratic terms, Eqs. (44) and (45), respectively, the following modified BW mass formula is now written as:

$$BE(N,Z) = a_v * A - a_s * A^{\frac{2}{3}} - a_c * \frac{Z*(Z-1)}{A^{\frac{1}{3}}} - a_a * \frac{(N-Z)^2}{A} + 12 * \frac{1}{A^{\frac{1}{2}}} + P + PP \quad (46)$$

Re-arranging the terms in Eq.(46) and leaving the shell correction in the right-hand side of equation, the Eq.(47) is derived:

$$BE(N,Z) - \left(a_v * A - a_s * A^{\frac{2}{3}} - a_c * \frac{Z*(Z-1)}{A^{\frac{1}{3}}} - a_a * \frac{(N-Z)^2}{A} + 12.0 * \frac{1}{A^{\frac{1}{2}}}\right) = P + PP \quad (47)$$

replacing P and PP terms from the Eqs. (44) and (45), respectively, Eq.(47) is transformed as:

$$BE(N,Z) - \left(a_v * A - a_s * A^{\frac{2}{3}} - a_c * \frac{Z*(Z-1)}{A^{\frac{1}{3}}} - a_a * \frac{(N-Z)^2}{A} + 12.0 * \frac{1}{A^{\frac{1}{2}}}\right) = b1 * \left(n_n + n_p\right) + b2 * \left(n_n + n_p\right)^2 \quad (48)$$

the Eq. (48) is equivalent to:

$$BW\_Residuals = b1 * \left(n_n + n_p\right) + b2 * \left(n_n + n_p\right)^2 \quad (49)$$

It should be also emphasized that the shell correction described by the sum of the Eqs. (44) and (45), is only a simple expression and an upgraded version of the latter has been introduced in the Duflo-Zuker microscopic mass formula [4,96,171]. This updated version proposes the addition of extra terms in the liquid-drop mass formula which considers two-, three- and four-body forces according to the study [99]. For a detailed description of the physical interpretation of each of these terms and their use in the nuclear mass model, one can access the suggested literature.

Considering the BW_Residuals given in Tables 4.7, 4.8, 4.9 correspond to the calcium isotopic chain, tin isotopic chain, and isotonic chain (N=28), respectively, a fit of the Eq. (49) to the even-even nuclei included between the DM shell closures of these chains was conducted. The residual's plots, presented for each of the regions of interest, include a comparison between the initial residuals, BW_Residuals, and the residuals obtained after the fit of the Eq. (49), BW_Residuals-(P+PP).

A judgment on the efficacy of the additional terms P and PP to reproduce the parabolic shape is based on their ability to describe the atomic masses of these particular regions of interest.

The steps followed are exactly the same as previously and the only modification applied is in the interpretation of the modified BW formula which is now given by the Eq. (49). Thus, the phenomenological approach is identical to what has already been introduced.

1) Calcium isotopic chain from the DM nucleus ^{40}Ca to DM nucleus ^{48}Ca:

The analysis starts with the case of the even-even nuclei included between the DM nuclei, ^{40}Ca to ^{48}Ca. A fit of the modified BW mass formula of the Eq. (49) to these even-even nuclei was made and a comparison of the residuals' values are shown in the following Fig. 4.14. In addition, the input and output data are also included in Table 4.12.

Input and Output data

Nucleus	BW_Residuals (MeV)	$n_n + n_p$	$(n_n+n_p)^2$	(P+PP) MeV	(BW_Residuals-(P+PP)) MeV
^{40}Ca	0	0	0	0	0
^{42}Ca	-4.721	2	4	-4.248	-0.474
^{44}Ca	-5.620	4	16	-5.620	0.000
^{46}Ca	-3.774	2	4	-4.248	0.474
^{48}Ca	0.977	0	0	0	0.977

Table 4.12: *The input data and the estimated theoretical and residual values correspond to the even-even nuclei of the calcium isotopic chain.*

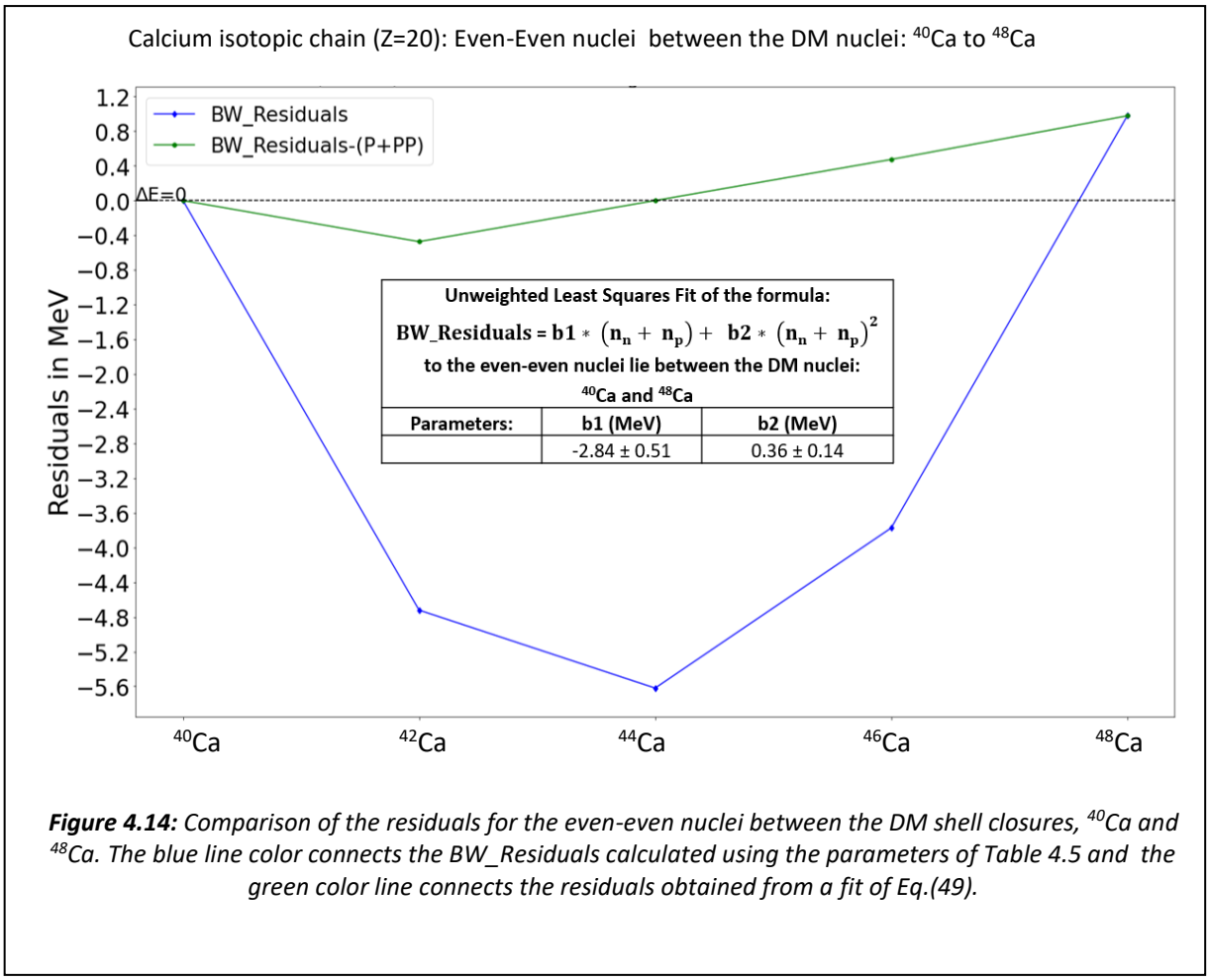

Figure 4.14: *Comparison of the residuals for the even-even nuclei between the DM shell closures, ^{40}Ca and ^{48}Ca. The blue line color connects the BW_Residuals calculated using the parameters of Table 4.5 and the green color line connects the residuals obtained from a fit of Eq.(49).*

2) Tin isotopic chain from the DM nucleus ^{100}Sn to DM nucleus ^{132}Sn:

Similar analysis was followed for the description of the parabolic behavior of the residuals of the even-even nuclei for the Tin isotopic chain, considering the suggested shell correction given by the inclusion of the terms P and PP in the fit. Particularly, an unweighted least squares fit of the Eq. (49) is conducted and the input as well as output data related to this fit has been included in the following Table 4.13. Following the calculation of the residuals, a comparison between the BW_Residuals and the residuals obtained after the fit of the Eq. (49), is presented in the following Fig. 4.15.

Input and Output data					
Nucleus	**BW_Residuals (MeV)**	**$n_n + n_p$**	**$(n_n+n_p)^2$**	**P+PP (MeV)**	**(BW_Residuals-(P+PP)) MeV**
^{100}Sn	0	0	0	0	0
^{102}Sn	-5.720	2	4	-5.209	-0.511
^{104}Sn	-10.345	4	16	-9.677	-0.668
^{106}Sn	-13.997	6	36	-13.404	-0.594
^{108}Sn	-16.830	8	64	-16.390	-0.440
^{110}Sn	-18.877	10	100	-18.635	-0.242
^{112}Sn	-20.245	12	144	-20.139	-0.106
^{114}Sn	-20.972	14	196	-20.903	-0.069
^{116}Sn	-21.167	16	256	-20.925	-0.241
^{118}Sn	-20.806	14	196	-20.903	0.097
^{120}Sn	-19.802	12	144	-20.139	0.338
^{122}Sn	-18.141	10	100	-18.635	0.494
^{124}Sn	-15.831	8	64	-16.390	0.558
^{126}Sn	-12.893	6	36	-13.404	0.510
^{128}Sn	-9.302	4	16	-9.677	0.374
^{130}Sn	-5.251	2	4	-5.209	-0.043
^{132}Sn	-0.567	0	0	0	-0.567

Table 4.13: *The input data as well as the estimated theoretical and residuals' values of binding energies correspond to the even-even nuclei of the tin isotopic chain are presented.*

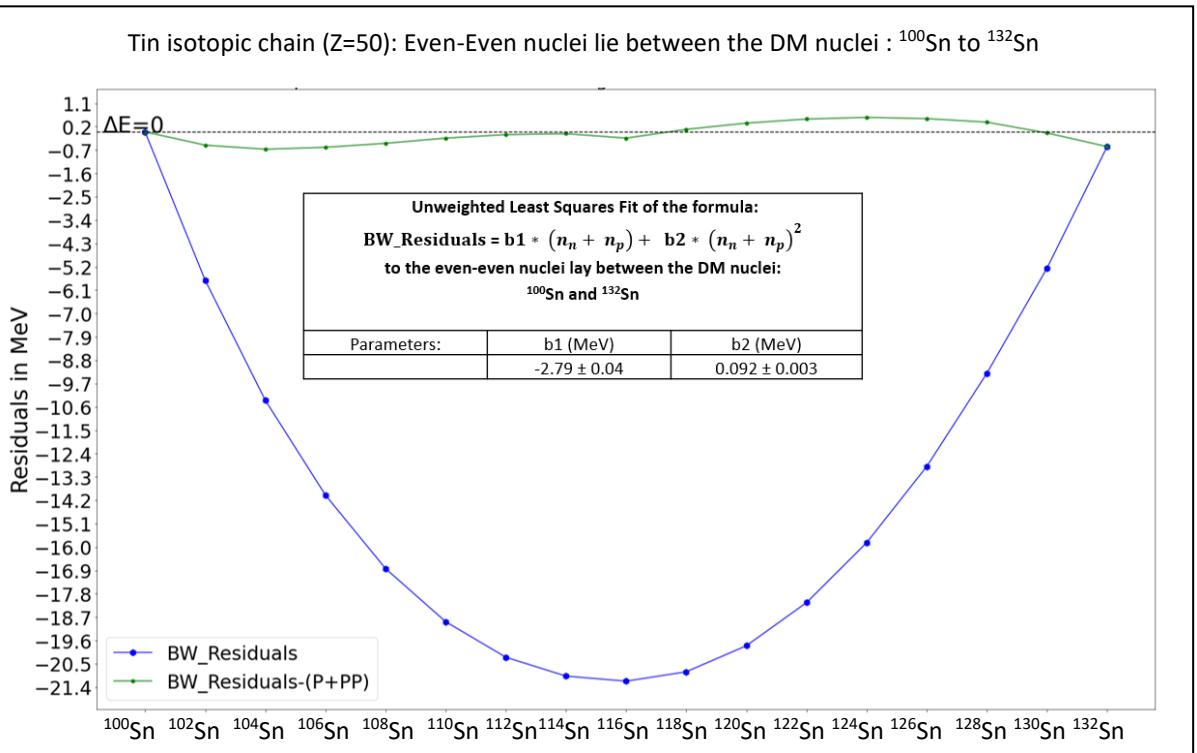

Figure 4.15: *Comparison of the residuals of the even-even nuclei between the DM shell closures, ^{100}Sn and ^{132}Sn. The blue line color connects the BW_Residuals calculated using the parameters of Table 4.5 and the green color line connects the residuals obtained from a fit of Eq. (49).*

3) Isotonic chain (N=28) from the DM nucleus ^{48}Ca to DM nucleus ^{56}Ni:

In a similar manner, a fit of the Eq. (49) to the even-even nuclei which lie between the DM shell closures ^{48}Ca to ^{56}Ni and the calculation of the in-between residuals, can also follow. The input data as well as the output theoretical and residuals' values of binding energies for the even-even nuclei, are shown in the following Table 4.14. Following the calculation of the residuals, a comparison between the 'BW_Residuals' and those obtained by the fit of Eq. (49) is shown up in Fig. 4.16.

Input and Output data					
Nucleus	**BW_Residuals (MeV)**	**$n_n + n_p$**	**$(n_n+n_p)^2$**	**P+PP (MeV)**	**(BW_Residuals-(P+PP)) MeV**
^{48}Ca	0	0	0	0	0
^{50}Ti	-4.193	2	4	-3.602	-0.591
^{52}Cr	-5.009	4	16	-5.009	0.000
^{54}Fe	-3.010	2	4	-3.602	0.591
^{56}Ni	1.233	0	0	0	1.233

Table 4.14: *The input data and the estimated theoretical and residual values correspond to the even-even nuclei of the isotonic chain N=28, from the DM nucleus ^{48}Ca to ^{56}Ni are presented.*

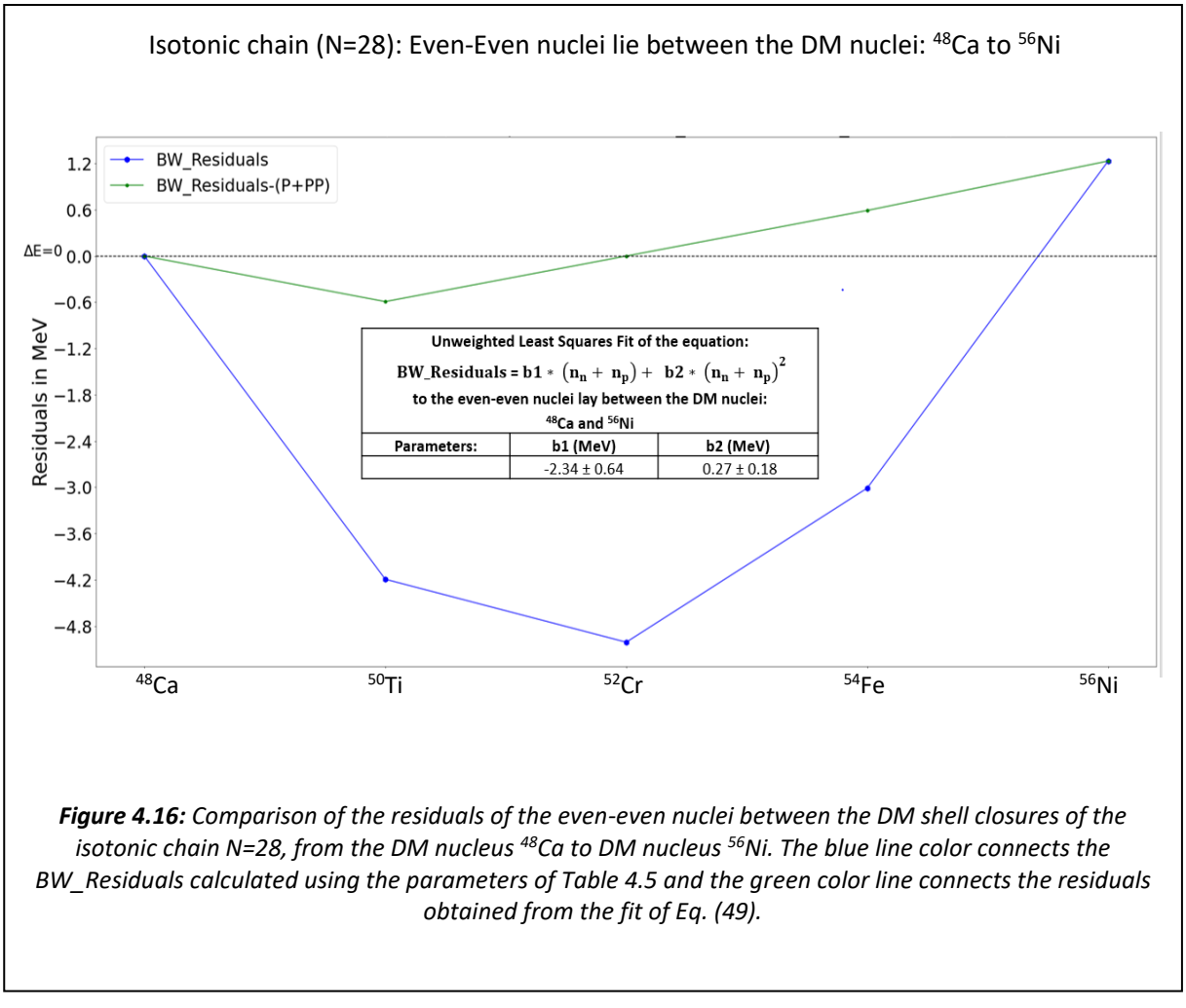

Figure 4.16: *Comparison of the residuals of the even-even nuclei between the DM shell closures of the isotonic chain N=28, from the DM nucleus ^{48}Ca to DM nucleus ^{56}Ni. The blue line color connects the BW_Residuals calculated using the parameters of Table 4.5 and the green color line connects the residuals obtained from the fit of Eq. (49).*

As previously stated in subsection (4.1.2), the set of parameters of Table 4.5, is not applicable to reproduce residuals for the even-even nuclei of the diagonal chains from ^{16}O to ^{40}Ca and from ^{40}Ca to ^{56}Ni, which resemble a parabola. As the main conditions of the current phenomenological approach are not satisfied, a fit of the modified BW formula, Eq. (49), to the even-even nuclei of the diagonal chains, is not considered appropriate and thus is not included here.

Summarizing the case of including the shell correction, described by the P and PP terms, to the BW mass formula, it is evident that these terms are applicable to capture the parabolic-like shape for the in-between residuals of the calcium and tin isotopic chains as well as isotonic chain (N=28).

A comparison between the valence shell-corrections, proposed by the current investigation and those suggested from the literature, incorporating the P and PP terms, show a clear agreement in the description of the parabolic behavior of the residuals. The latter means that the shell correction of P and PP terms, is applicable to reproduce the observed parabolic character of the residuals with a similar manner as the present additional terms of NN and 3N are able to do so. The residuals obtained from a fit of the Eqs. (39) and (49) towards the nuclei of the regions of interest produce residuals for even-even nuclei lie between two DM nuclei, with very similar values.

4.4 General Important Remarks that were detected during the analysis:

Various investigations have been made throughout the conduction of the present research aiming to access a set of best fit parameters which is able to reveal the parabolic shape of the residuals between two DM nuclei and to describe them with the inclusion of the extra NN and 3N terms afterwards. Towards this justification, alternative expressions of the terms of nuclear mass formulas or expansion of the existed ones (obtained from the literature) was conducted. Also, least-squares fits to different atomic mass regions as well as fits of the nuclear mass formulas to the quantity binding energy per nucleon rather than the total binding energy, with or without the incorporation of the experimental uncertainties, were investigated. A presentation of some of the most important conclusions that detected during this analysis are presented herein:

1) It is evident that there is a limited availability of measured atomic mass data corresponding to DM nuclei. Particularly, the traditional doubly magic nuclei of mass16.txt (excluding the very light ones) are seven, four of which correspond to symmetric DM nuclei (^{16}O, ^{40}Ca, ^{56}Ni, ^{100}Sn) and the rest to asymmetric (^{48}Ca, ^{132}Sn, ^{208}Pb). The first concern that arises here has to do with the sample size and the statistical power that needs to be increased for making more reliable estimations. Particularly, if the sample size of the DM nuclei dataset is increased, the statistical power will be enhanced. Collecting enough data is also important for detecting

important association that maybe exist in the population. The ground rule regarding the data sample is that the bigger the sample size, the better the estimations are. However, the latter depends on several factors and further investigations using power analysis techniques are necessary. Correspondingly, there are also limitations for a dataset which includes a large sample size. In Ref. [172], an extensive discussion regarding the sample size and the statistical techniques applied for determining the essential sample size is also presented.

2) In the present analysis several attempts were made for reducing the residuals corresponding to the DM nuclei. To this end, additional terms were added to the BW baseline formula aiming to reproduce the symmetry energy of the even-even nuclei of the diagonal chains. As they are all symmetric nuclei, terms that account for N=Z nuclei should be considered in the fit. Similarly, additional terms were used for fits involving DM nuclei. The list of the traditional DM nuclei, used in the present work, includes four symmetric and three asymmetric nuclei. Different combinations of terms were applied and their ability to reproduce our theory as well as to describe the DM nuclei were evaluated.
As an example, a fit of the BW baseline mass formula to the DM nuclei, when two extra terms are also added in the fitting procedure, will be presented. Particularly, the standard part of the BW baseline formula remains the same and then two extra terms were added. The extra terms are the exchange coulomb term (axc) and the Wigner energy term (aw) reported and explained in Ref. [117].
Thus, the BW baseline formula with a fixed pairing parameter with a value of 12 MeV and the inclusion of the two additional terms, is now given by:

$$BE(N,Z) = a_v * A - a_s * A^{\frac{2}{3}} - a_c * \frac{Z*(Z-1)}{A^{\frac{1}{3}}} - a_a * \frac{(N-Z)^2}{A} + \frac{12}{A^{\frac{1}{2}}} + axc * \frac{Z^{\frac{4}{3}}}{A^{\frac{1}{3}}} + aw * \frac{|N-Z|}{A} \quad (50)$$

If an unweighted least squares fit of Eq. (50) to the traditional DM nuclei is performed, the results of the residuals for the DM nuclei are presented in Fig. 4.17. Also, a comparison between the set of the estimated parameters obtained from the fit of Eq. (50) and the BW baseline formula, Eq. (5), is presented in the following Table 4.15.

Unweighted Least Squares Fit of the Eq. (50) to the traditional DM nuclei for A ≥ 16

1) **Fitting the BE in MeV**
2) **Using the BW baseline formula with the extra terms: axc and aw of Eq. (50)**
3) **Without including the experimental uncertainties**
4) **Including a fixed value of pairing parameter a_p = 12MeV**
5) **Minimization Method: scipy.curve.fit**

a_v (MeV)	a_s (MeV)	a_c (MeV)	a_a (MeV)	a_p (MeV)	axc (MeV)	aw (MeV)
16.69 ± 0.92	20.12 ± 2.65	0.79 ± 0.06	25.21 ± 2.80	12.0 fixed	7.56 ± 2.41	81.29 ± 41.64

Unweighted Least Squares Fit of the Eq. (5) to the traditional DM nuclei for A ≥ 16

1) **Fitting the BE in MeV**
2) **Using the BW baseline formula of Eq. (5)**
3) **Without including the experimental uncertainties**
4) **Including a fixed value of pairing parameter a_p = 12MeV**
5) **Minimization Method: scipy.curve.fit**

a_v (MeV)	a_s (MeV)	a_c (MeV)	a_a (MeV)	a_p (MeV)	axc (MeV)	aw (MeV)
16.86 ± 1.36	20.65 ± 3.75	0.79 ± 0.10	26.81 ± 4.16	12.0 fixed	-	-

Table 4.15: *Comparison of the best values of parameters obtained from fit of Eq.(50) and Eq.(5) to the traditional DM nuclei for A≥ 16.*

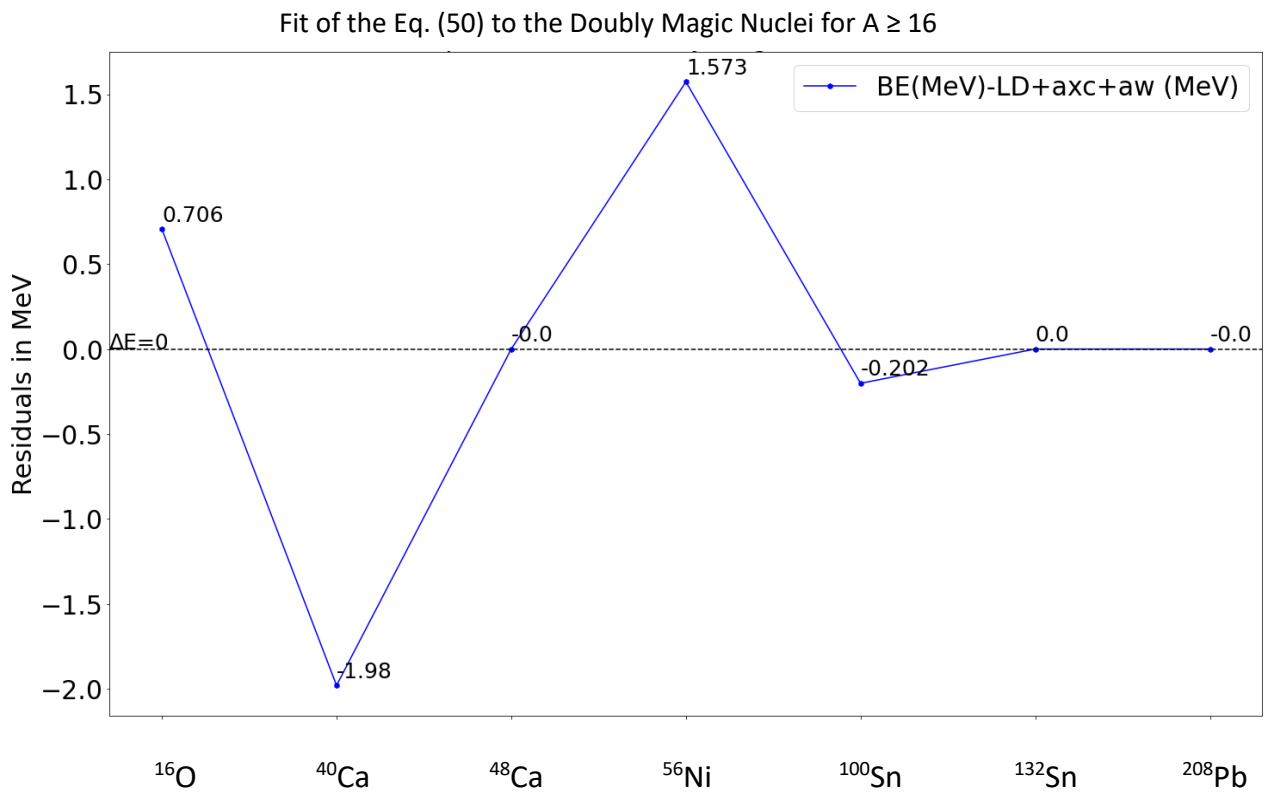

Figure 4.17: *The residuals for the DM nuclei (A≥16) obtained from the unweighted least squares fit of the enriched BW baseline formula, Eq. (50).*

By inspection of the values of the residuals of Fig. 4.17, one can conclude that the residuals are greatly minimized with the inclusion of just two terms in the BW baseline formula.

Despite this fact, one should be skeptical about whether it originates in the real applicability of the model to make reliable estimations of the present observations or other factors influence each term in the model and drive the behavior of the regression analysis.

Particularly, a question arise regarding the overfitting problem which in this occasion may occur due to the small sample size of the DM nuclei. In such a way, it is responsible for the differences between the actual and predicted values, which are exactly zero for some DM nuclei or very close to zero for some others. The standard linear regression considers that the number of the sample observations (n) should be much greater that the number of parameters (p) such that n >> p, so as to make reliable predictions. If the number of the data are almost equal to the number of parameters, n ≈ p, it is often the case where the parameters are forced to follow the data. In addition, it should be noted that the inclusion of the Wigner term in this fit result some asymmetric nuclei to be predicted very accurately compared to some

others. This indicates a clear preference of the fit towards the asymmetric nuclei rather the symmetric.

Also, by comparing the best values of coefficients reported in Table 4.15, it can be seen that the parameters a_v, a_s, a_c, a_a do not differ significantly between the two fits, but they are characterized from a slightly increase in their uncertainties' values.

A special reference should be given to the large value of uncertainty accompanying the estimated parameter of the Wigner term (aw), presented in Table 4.15. This observation implies that the parameter is not well determined. A correlation analysis to identify the role of this parameter over the least squares fitting procedure is also recommended. This will be determined whether it should be eliminated from the analysis.

It is also necessary to be verified if the estimated coefficients correspond to the additional terms ($axc\ and\ aw$) are similar to the ones reported in the relevant literature, Ref. [117]. In Ref. [126], the reported values for the $axc\ and\ aw$ are 2.22(5) MeV and -43.30(222) MeV, respectively. However, in this study an enriched BW formula, involved eleven fit coefficients, are fitted to the entire AME2003 atomic mass table.

Although this analysis cannot be considered for applying our theoretical approach, due to reasons previously explained, it is a good example which provided us with valuable insights and directed the current investigation.

3) The dependence of the least-squares fitting procedure on the weights of the DM nuclei was also evident when a fit to the binding energy per particle was performed instead of the total binding energy. In order to investigate the last statement, it is important to focus on the difference between the fits of these two physical quantities. A fit on the total binding energy seems also to be a reasonable decision for our analysis.

   Naturally, a fit on the total binding energy, assigns more importance to the heavy atomic mass region, while a fit to the binding energy per particle gives more importance to the medium, light nuclei [57,117].

   Therefore, fits to the DM nuclei using the quantities of the total binding energy and binding energy per particle were conducted to determine the changes in the estimated parameters. As it was expected, considerable differences in the values of the best fit parameters were found in the case of an unweighted least squares fit. A Similar investigation in nuclei of the entire AME2003 mass table was reported in Ref. [126], where the results obtained from a fit to the total binding energy significantly differed from those obtained from a fit to the quantity, binding energy per particle.

   However, when in the present work, a weighted least squares fit to the DM nuclei binding energy per particle of BW baseline formula, was conducted, it was found that the best fit parameters do not differ from the results of the best fit parameters of a weighted least squares fit of BW to the total binding energy. This is due to the influence of the weights in the fitting procedure, which result the residuals of the DM nuclei to behave with similar manner either a fit to the total binding energy or the binding energy per particle is performed.

In Tables A.18 to A.23 presented in Appendix A, the residuals for the DM nuclei as well as the estimated parameters for different fit cases are presented.
The outcome generated from these fits significantly contributed to changing the research direction related to the regression analysis.

4) Several studies have considered the expression $\frac{Z^2}{A^{1/3}}$ for the coulomb term, instead of the expression $\frac{Z*(Z-1)}{A^{\frac{1}{3}}}$ which is reported in Eq. (5) and also adapted by the present investigation. However, both of the expressions were tested and a fit to the DM nuclei was repeated using the form $\frac{Z^2}{A^{1/3}}$, so as to evaluate any significant changes to the results of the DM nuclei residuals. The form of the coulomb term $\frac{Z*(Z-1)}{A^{\frac{1}{3}}}$ is a more correct expression in terms of the physical meaning of the Coulomb energy. Particularly, although the Z^2 form is widely used in several studies [23,117,163,165,173], strictly speaking it is not quite right. The BW baseline formula, when included the Z^2 form, states that even one proton, i.e., Z=1, is able to contribute as a corrected factor to the binding energy, even though there is nothing to repel it. In this case, the correction to the binding energy should not be quite as big. In such a way, a more appropriate expression for the coulomb term is given by the form $\frac{Z*(Z-1)}{A^{\frac{1}{3}}}$ which is now zero for Z =1 and indicates that the biggest binding energy corresponds to any mass number for Z=1. However, the Coulomb terms $\frac{Z^2}{A^{1/3}}$ and $\frac{Z*(Z-1)}{A^{\frac{1}{3}}}$ give similar results for large values of A as reported in Ref. [174].

5) There are several popular solutions across the literature which aim to deal with problems related to different magnitudes of experimental uncertainties when entered the regression analysis. A popular method, which is usually applied, is to consider an artificial lower limit on the measurement uncertainties, allowing only uncertainties of around 50 keV to less than 150 keV to be included in the weighted least squares fit [100,113,117,121,166,175]. This suggestion could be proven to be useful for the present investigation, if more experimental doubly magic data were available to incorporate the fit.
An additional solution, presented in Ref. [79], has been assumed a constant error for all the experimental observables which is equal to the median of the experimental uncertainties of the nuclei included in the list. However, by performing such a weighted least squares fit, the results are exactly the same as in the case of an unweighted least squares regression analysis or when one considers a constant weight equal to 1 among all the observations.

Chapter 5

Discussion and Conclusions

In this research work, valence-shell corrections have been modeled in order to describe the parabolic trend of atomic mass data between two DM closed shells.

Given the research analysis and the results section, it was observed the relevance of the suggested terms, Eqs. (18) and (19), in the explanation of the parabolic shape of the residuals between the DM shell closures. Particularly, the suggested terms are able to explain the parabolic behavior of the residuals in the calcium and tin isotopic chains as well as the isotonic chain (N=28) using as a baseline model the BW formula. In addition, un unweighted least squares fit of the LDM1 formula was able to reveal the parabolic-like character of the oxygen isotopic chain which is also very well described by the addition of NN and 3N terms. More theoretical mass formulae should be tested for their efficacy to reproduce the DM nuclei better. The inclusion of NN and 3N terms can then be further considered. In such a way, residuals of even-even nuclei between the diagonal chains maybe can also be explained by the current phenomenological approach.

It is also worth mentioning that shell correction which is linear and quadratic in the number of valence nucleons and presented in Ref. [4], was added in the BW baseline formula and the results are compared with those suggested from the present investigation. The findings show that the shell correction of Ref. [4] can also capture the parabolic behavior of the residuals between the DM nuclei describing the observed trend of atomic mass data, with a very similar manner as those introduced by the present research work.

In addition, special treatment should also be given in the incorporation of a larger sample size of nuclei in the linear regression analysis. The limited number of available doubly-magic nuclei compared to the number of the model's parameters, can clearly influence the fitting procedure. Such a model could possibly represent the noise rather than the genuine relationships in the population.

Moreover, the process can be enhanced if special care is given to a precise estimation of the already measured observables. With such a way, the phenomenological approach of the present investigation will be possible to enhance its efficacy in describing the observed parabolic character of the residuals, by considering the experimental uncertainties in the fit. Particularly, the doubly magic nucleus ^{100}Sn is a critical nucleus [165] whose the experimental measured value should concentrate the experimental and theoretical efforts for a more accurate estimation of its value [136] .

It is also recommended that experimental attempts are essential for more input doubly magic nuclei. Indeed, the present theoretical approach could be tested to more atomic mass

regions. Therefore, new measurements of drip lines and data on magic numbers are required, e.g., ^{78}Ni.

Furthermore, in the current investigation, the hypothesis that have been adapted is that the origin of these terms, given by the Eqs. (18) and (19), is due to the presence of NN and 3N body forces. However, it is important to be stressed that although the expressions of the proposed terms can capture the observed parabolic shape of the residuals, a straightforward claim that these terms are a manifestation of the NN and 3N body forces cannot be made in this stage of the investigation. Future work towards this justification is essential so as to identify their true origin

Reference has already been made in the inclusion of an updated version of shell correction to the liquid-drop mass formulas according to the suggestion of the paper [4, 99]. Following the latter, additional terms have been added to the liquid-drop formula which are expressed as a function of valence nucleons incorporating the degeneracy of the proton and neutron valence shell and also presenting two-, three- and four- body forces.

The last statement are included here as a suggestion point for further investigation and can be used as instructions on additional theoretical work that is needed to be done so as to accurately evaluate the origin of these terms. Therefore, it should be noted that the present findings should be interpreted with caution and based on the realization that other studies have provided evidence towards an explanation of the effects of two- and three- body forces in atomic masses.

APPENDIX A

Input data and Results from the Fitting Procedure

In this appendix, results obtained by individual fits throughout the present investigation are included. One can access the information provided on each of these Tables, in accordance with the corresponding section and based on the numbering associated with them. Although it does not provide an analytical description for each case fit, it presents the appropriate supporting material to the results' chapter without interrupting the narrative flow of the research analysis to the reader.

Weighted least squares Fitting of the BW formula to the DM nuclei for A ≥ 16					
1) Fitting on the total binding energy (BE(MeV)) **2) Using the BW baseline formula of Eq. (5)** **3) Including the experimental uncertainties: 'unT (MeV)'** **4) Without including the pairing term (a_p) in the fit**					
Minimization Method	**a_v (MeV)**	**a_s (MeV)**	**a_c (MeV)**	**a_a (MeV)**	**a_p (MeV)**
Exact Solution: Eq. (26)	14.17	13.51	0.60	17.30	-
Scipy.curve.fit library from Python (Numerical Solution)	14.17 ± 0.18	13.51 ± 0.37	0.60 ± 0.026	17.30 ± 0.84	-
Lmfit library from Python (Numerical Solution)	13.99 ± 0.39	13.15 ± 0.79	0.57 ± 0.06	16.41 ± 1.78	-
MINUIT (Numerical Solution	13.99 ± 6e-11	13.14 ± 10e12	0.57 ± 23e-11	16.41 ± 7e-9	-

Table A.1: *Comparison of the results of the estimated best values of parameters between an analytical (or exact) and three numerical solutions for the weighted least squares fit of the BW baseline formula to the DM nuclei for A≥16.*

Unweighted Least Squares Fitting of the BW formula to the entire AME2016 table				
1) Fitting the BE in MeV **2) Using the BW baseline formula of Eq. (5)** **3) Without including the experimental uncertainties in the fit** **4) Including the pairing term as free parameter** **5) Minimization Method: iminuit**				
a_v (MeV)	**a_s (MeV)**	**a_c (MeV)**	**a_a (MeV)**	**a_p (MeV)**
15.44 ± 0.01	16.75 ± 0.04	0.69 ± 0.7e-3	22.68 ± 0.02	12.0 ± 0.5

Table A.2: *An unweighted least squares fit of the BW formula was performed to the entire AME2016 mass table. The MINUIT automatic routine was used, and a value of 12 ± 0.5 MeV was assigned to the pairing coefficient. The latter was adapted as a fixed value associated with the pairing parameter in the present investigation.*

Test 1 : Weighted least squares Fitting of the BW formula to the DM nuclei for A ≥ 16				
1) Fitting the BE in MeV **2) Using the BW baseline formula of Eq. (5)** **3) Replacing the actual experimental uncertainties of the DM nuclei, ^{100}Sn and ^{132}Sn, with the values of the experimental uncertainties of Test 1** **4) Including a fixed value of pairing parameter a_p = 12 MeV** **5) Minimization Method: scipy.curve.fit**				
a_v (MeV)	**a_s (MeV)**	**a_c (MeV)**	**a_a (MeV)**	**a_p (MeV)**
14.24 ± 0.24	14.32 ± 0.53	0.55 ± 0.02	18.17 ± 0.84	12.0 fixed

Table A.3: *A weighted least squares fit of the BW formula was performed to the DM nuclei (A ≥ 16) and the best fit coefficients are shown. The uncertainties of the experimental binding energies, that included in the fitting procedure, followed the conditions of the Test 1.*

Test 3: Weighted least squares Fitting of the BW formula to the DM nuclei for A ≥ 16				
1) Fitting the BE in MeV **2) Using the BW baseline formula of Eq. (5)** **3) Replacing the actual experimental uncertainties of the DM nuclei, ^{16}O, ^{40}Ca and ^{48}Ca with the values of the experimental uncertainties of Test 3** **4) Including a fixed value of pairing parameter a_p = 12MeV** **5) Minimization Method: scipy.curve.fit**				
a_v (MeV)	**a_s (MeV)**	**a_c (MeV)**	**a_a (MeV)**	**a_p (MeV)**
16.69 ± 0.92	20.12 ± 2.65	0.79 ± 0.06	25.21 ± 2.80	12.0 fixed

Table A.4: *A weighted least squares fit of the BW formula was performed to the DM nuclei (A ≥ 16) and the best fit coefficients are shown. The uncertainties of the experimental binding energies that included in the fitting procedure followed the conditions of the Test 3.*

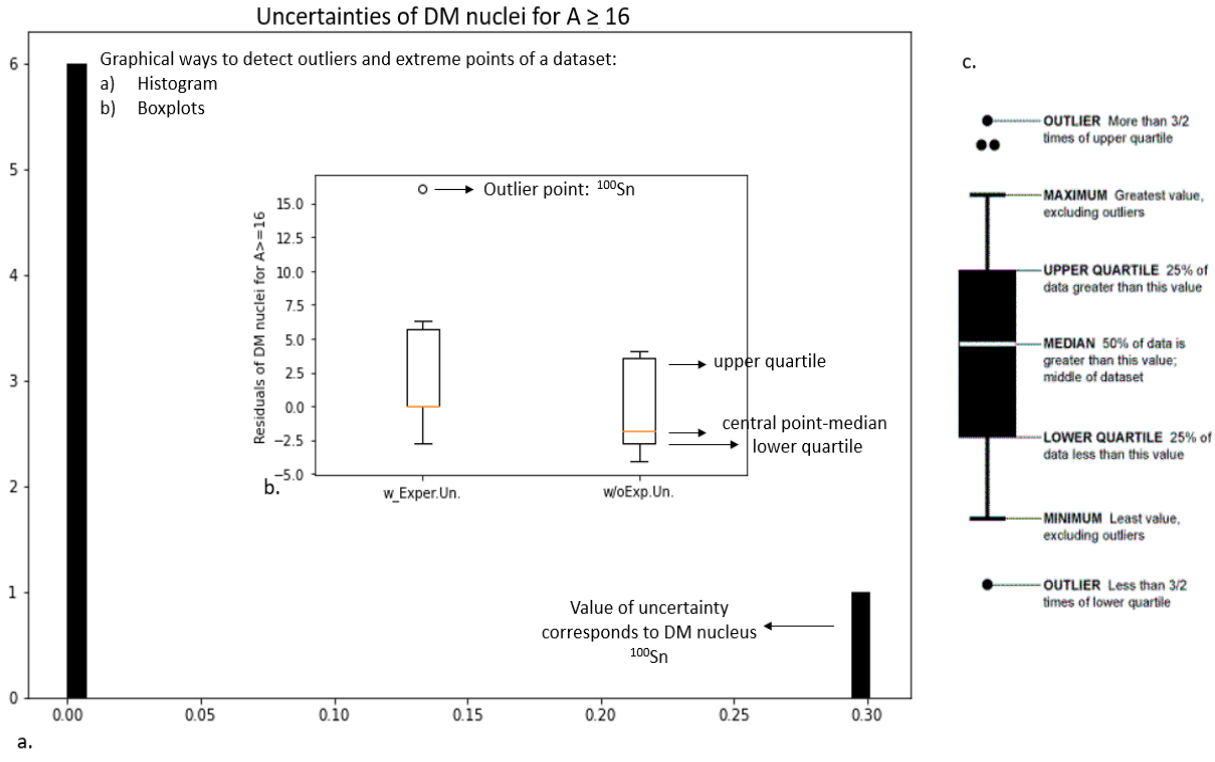

Figure A.1: *(a) Graphical representation of the uncertainties of the traditional DM nuclei for A ≥ 16 using a histogram. (b) Two boxplots are presented in the same plot. The LHS boxplot corresponds to the values of the residuals when a weighted least squares fit of the BW formula to the DM nuclei was performed (w_Exp.Un.) while the RHS boxplot corresponds to an unweighted least squares fitting procedure (w/oExp.Un.). (c) The box-and-whisker plot which is designed to present the distribution of a population, is shown. Available in Ref. [176].*

Unweighted least squares Fitting of the BW formula to the DM nuclei for A ≥ 16					
1) Fitting on the total binding energy (BE(MeV)) **2) Using the BW baseline formula of Eq. (5)** **3) Without including the uncertainties correspond to the BE(MeV) in the fit** **4) Without including the pairing contribution in the fitting procedure**					
Minimization Method	**a_v (MeV)**	**a_s (MeV)**	**a_c (MeV)**	**a_a (MeV)**	**a_p (MeV)**
Exact Solution: Eq. (26)	16.29	18.91	0.76	25.26	**-**
Scipy.curve.fit library from Python (Numerical Solution)	16.29 ± 1.39	18.90 ± 3.83	0.75 ± 0.10	25.26 ± 4.25	**-**
Lmfit library from Python (Numerical Solution)	16.29 ± 1.39	18.90 ± 3.83	0.75 ± 0.10	25.26 ± 4.25	**-**
MINUIT (Numerical Solution)	16.29 ± 0.27	18.9 ± 0.7	0.759 ± 0.020	25.3 ± 0.8	**-**
Results obtained by Ref. [117]: (Fit to AME2003)	15.36 (3)	16.42 (8)	0.691 (2)	22.53 (7)	**-**

Table A.5: *Comparison of the results of the estimated best values of parameters between an analytical (or exact) and three numerical solutions for the unweighted least squares fit of the BW baseline formula to the DM nuclei for A ≥ 16, without considering the contribution of pairing term.*

A) Unweighted Least Squares Fit of the BW baseline formula to binding energy data for DM nuclei (A ≥ 16) considering the pairing parameter as constant value of 12 MeV:

Input and Output Data related to the subsection (4.1.2) of the present thesis:

Parameters of Table 4.5 applied to the even-even nuclei of the following regions of interest:

The following Tables show input as well as a selection of output data for each of the examined regions of interest which were used for the evaluation of the current theoretical framework. The column names of the first row have been previously introduced in the main body of the thesis. However, a reference should be made to the notations: 'NNterm' and '3Nterm'. These terms describe the individual contributions of each of the NN and 3N expressions in the fitting procedure, following the estimation of B and D best fit coefficients obtained from the Eq. (39). In such a way, the physical representation of the 'NNterm' was easy to be distinguished from the column name 'NN' which here refers to a fit of Eq. (40) towards to the NN contribution only.

1) <u>Calcium isotopic chain (Z=20): from the DM nucleus ^{40}Ca to DM nucleus ^{48}Ca:</u>

Table A.6: *(I) Input data for the even-even nuclei lie between the DM nuclei: ^{40}Ca to ^{48}Ca*

N	Z	A	El	BE/A(keV)	un(keV)	BE/A(MeV)	un(MeV)	BE(MeV)	unT(MeV)	Valence Neutrons (n_n)	Valence Protons (n_p)	Valence Nucleons n
20	20	40	Ca	8551.303	0.001	8.551303	0.000001	342.05212	0.00004	0	0	0
22	20	42	Ca	8616.563	0.004	8.616563	0.000004	361.895646	0.000168	2	0	2
24	20	44	Ca	8658.175	0.007	8.658175	0.000007	380.9597	0.000308	4	0	4
26	20	46	Ca	8668.979	0.049	8.668979	0.000049	398.773034	0.002254	2	0	2
28	20	48	Ca	8666.686	0.002	8.666686	0.000002	416.000928	0.000096	0	0	0

Table A.7: *(II) Input and Output Data for the even-even nuclei lie between the two DM nuclei: ^{40}Ca to ^{48}Ca*

X	k	(NN+3N) MeV	(BW_Residuals-(NN+3N)) MeV	NNterm (MeV)	3Nterm (MeV)	NN (MeV)	(BW_Residuals-NN) MeV
0	0	0	0	0	0	0	0
10	24	-4.248	-0.474	-6.862	2.614	-4.430	-0.291
12	24	-5.620	0.000	-8.234	2.614	-5.316	-0.304
10	24	-4.248	0.474	-6.862	2.614	-4.430	0.656
0	0	0	0.977	0	0	0	0.977

2) Tin isotopic chain (Z=50): from the DM nucleus ^{100}Sn to DM nucleus ^{132}Sn:

Table A.8: *(I) Input data for the even-even nuclei lie between the two DM nuclei: ^{100}Sn and ^{132}Sn*

N	Z	A	El	BE/A(keV)	un(keV)	BE/A(MeV)	un(MeV)	BE(MeV)	unT(MeV)	Valence Neutrons (n_n)	Valence Protons (n_p)	Valence Nucleons (n)
50	50	100	Sn	8252.974	3.015	8.253	0.003	825.297	0.302	0	0	0
52	50	102	Sn	8324.43	0.981	8.324	0.001	849.092	0.100	2	0	2
54	50	104	Sn	8383.911	0.055	8.384	0.000	871.927	0.006	4	0	4
56	50	106	Sn	8432.038	0.048	8.432	0.000	893.796	0.005	6	0	6
58	50	108	Sn	8469.027	0.05	8.469	0.000	914.655	0.005	8	0	8
60	50	110	Sn	8496.087	0.125	8.496	0.000	934.570	0.014	10	0	10
62	50	112	Sn	8513.618	0.003	8.514	0.000	953.525	0.000	12	0	12
64	50	114	Sn	8522.566	0	8.523	0.000	971.573	0.000	14	0	14
66	50	116	Sn	8523.116	0.001	8.523	0.000	988.681	0.000	16	0	16
68	50	118	Sn	8516.533	0.004	8.517	0.000	1004.951	0.000	14	0	14
70	50	120	Sn	8504.492	0.007	8.504	0.000	1020.539	0.001	12	0	12
72	50	122	Sn	8487.907	0.02	8.488	0.000	1035.525	0.002	10	0	10
74	50	124	Sn	8467.421	0.008	8.467	0.000	1049.960	0.001	8	0	8
76	50	126	Sn	8443.523	0.083	8.444	0.000	1063.884	0.010	6	0	6
78	50	128	Sn	8416.979	0.138	8.417	0.000	1077.373	0.018	4	0	4
80	50	130	Sn	8386.816	0.014	8.387	0.000	1090.286	0.002	2	0	2
82	50	132	Sn	8354.872	0.015	8.355	0.000	1102.843	0.002	0	0	0

Table A.9: *(II) Input and Output data for the even-even nuclei lie between the two DM nuclei: ^{100}Sn to ^{132}Sn*

X	k	NN+3N (MeV)	(BW_Residuals-(NN+3N) MeV	NNterm (MeV)	3Nterm (MeV)	NN (MeV)	(BW_Residuals-NN) MeV
0	0	0	0	0	0	0	0
58	1176	-5.314	-0.406	-4.549	-0.766	-5.129	-0.591
108	2040	-9.798	-0.547	-8.470	-1.329	-9.550	-0.795
150	2640	-13.483	-0.514	-11.764	-1.719	-13.264	-0.733
184	3024	-16.399	-0.430	-14.430	-1.969	-16.271	-0.559
210	3240	-18.579	-0.297	-16.469	-2.110	-18.570	-0.307
228	3336	-20.053	-0.192	-17.881	-2.173	-20.162	-0.084
238	3360	-20.853	-0.119	-18.665	-2.188	-21.046	0.074
240	3360	-21.010	-0.157	-18.822	-2.188	-21.223	0.056
238	3360	-20.853	0.047	-18.665	-2.188	-21.046	0.240
228	3336	-20.053	0.252	-17.881	-2.173	-20.162	0.360
210	3240	-18.579	0.439	-16.469	-2.110	-18.570	0.429
184	3024	-16.399	0.568	-14.430	-1.969	-16.271	0.439
150	2640	-13.483	0.590	-11.764	-1.719	-13.264	0.371
108	2040	-9.798	0.496	-8.470	-1.329	-9.550	0.248

58	1176	-5.314	0.063	-4.549	-0.766	-5.129	-0.123
0	0	0	-0.567	0	0	0	-0.567

3) Isotonic chain (N=28) from the DM nucleus ^{48}Ca to DM nucleus ^{56}Ni:

Table A.10: *(I) Input data for the even-even nuclei lie between the two DM nuclei: ^{48}Ca to ^{56}Ni*

N	Z	A	El	BE/A(keV)	un(keV)	BE/A(MeV)	un(MeV)	BE(MeV)	unT(MeV)	Valence Neutrons (n_n)	Valence Protons (n_p)	Valence Nucleons (n)
28	20	48	Ca	8666.686	0.002	8.666686	0.000002	416.000928	0.000096	0	0	0
28	22	50	Ti	8755.718	0.002	8.755718	0.000002	437.7859	0.0001	0	2	2
28	24	52	Cr	8775.989	0.007	8.775989	0.000007	456.351428	0.000364	0	4	4
28	26	54	Fe	8736.382	0.007	8.736382	0.000007	471.764628	0.000378	0	2	2
28	28	56	Ni	8642.779	0.008	8.642779	0.000008	483.995624	0.000448	0	0	0

Table A.11: *(II) Input and Output data for the even-even nuclei between the two DM nuclei ^{40}Ca to ^{48}Ca*

X	k	(NN+3N) MeV	(BW_Residuals-(NN+3N)) MeV	NNterm (MeV)	3Nterm (MeV)	NN (MeV)	(BW_Residuals-NN) MeV
0	0	0	0	0	0	0	0
10	24	-3.6016	-0.5911	-7.0377	3.4361	-3.8413	-0.3514
12	24	-5.0091	0.0000	-8.4453	3.4361	-4.6096	-0.3996
10	24	-3.6016	0.5911	-7.0377	3.4361	-3.8413	0.8309
0	0	0	1.2331	0	0	0	1.2331

B) Unweighted Least Squares Fit of the LDM1 formula to binding energy data for DM nuclei (A ≥ 16) including the DM nucleus ^{24}O and considering the pairing parameter as constant value of 12 MeV :

Input and Output Data related to the section (4.2) of the present thesis.

Parameters of Table 4.10 applied to the even-even nuclei of the following regions of interest:

In a similar manner, the following Tables present a selection of output data for each of the regions of interest which were used for the evaluation of the current theoretical framework. The notation that have been given to the physical quantities of each of the columns is the same as before.

In addition, it should be noted that the experimental inputs correspond to the even-even nuclei of the examined regions of interest, remain the same and thus, there is no need to include such quantities here, as one can find them in the above Tables A.6 to A.11. However, both the input and output data correspond to the oxygen isotopic chain (Z=20) are included here.

1) <u>Calcium isotopic chain (Z=20): from the DM nucleus ^{40}Ca to DM nucleus ^{48}Ca:</u>

Table A.12: *(I) Output data for the even-even nuclei lie between the two DM nuclei: ^{40}Ca to ^{48}Ca*

Nucleus	LD (MeV)	BE(MeV)-LD(MeV)	BEexper(40Ca) (MeV)	(BE(^{A}Ca)-BE(^{40}Ca)) (MeV)	BEtheor(^{40}Ca) (MeV)	(BEtheor(^{A}Ca)-BEtheor(^{40}Ca)) (MeV)	LDM1_Residuals (MeV)
^{40}Ca	346.362	-4.310	342.052	0	346.362	0	0
^{42}Ca	370.405	-8.509	342.052	19.844	346.362	24.043	-4.200
^{44}Ca	390.584	-9.624	342.052	38.908	346.362	44.222	-5.315
^{46}Ca	407.323	-8.550	342.052	56.721	346.362	60.961	-4.240
^{48}Ca	420.991	-4.990	342.052	73.949	346.362	74.629	-0.680

Table A.13: *(II) Input and Output data for the even-even nuclei lie between the two DM nuclei: ^{40}Ca to ^{48}Ca*

X	k	NN+3N (MeV)	(LDM1_Residuals-(NN+3N)) MeV	NNterm (MeV)	3Nterm (MeV)	NN (MeV)	(LDM1_Residuals-NN) MeV
0	0	0	0	0	0	0	0
10	24	-4.220	0.020	-5.474	1.254	-4.307	0.108
12	24	-5.315	0.000	-6.569	1.254	-5.169	-0.146
10	24	-4.220	-0.020	-5.474	1.254	-4.307	0.067
0	0	0	-0.680	0	0	0	-0.680

2) Tin isotopic chain (Z=50): from the DM nucleus ^{100}Sn to DM nucleus ^{132}Sn:

Table A.14: *(I) Output data for the even-even nuclei lie between the two DM nuclei: ^{100}Sn and ^{132}Sn*

Nucleus	LD (MeV)	BE(MeV)-LD(MeV)	(BEexper(^{100}Sn)) MeV	(BE(^{A}Sn)-BE(^{100}Sn)) MeV	BEtheor(^{100}Sn) (MeV)	(BEtheor(^{A}Sn)-BEtheor(^{100}Sn)) (MeV)	LDM1_Residuals (MeV)
^{100}Sn	820.328	4.969	825.297	0	820.328	0	0
^{102}Sn	848.556	0.536	825.297	23.794	820.328	28.228	-4.433
^{104}Sn	874.950	-3.023	825.297	46.629	820.328	54.622	-7.993
^{106}Sn	899.614	-5.818	825.297	68.499	820.328	79.286	-10.787
^{108}Sn	922.643	-7.988	825.297	89.358	820.328	102.315	-12.957
^{110}Sn	944.125	-9.555	825.297	109.272	820.328	123.797	-14.525
^{112}Sn	964.144	-10.618	825.297	128.228	820.328	143.815	-15.588
^{114}Sn	982.775	-11.203	825.297	146.275	820.328	162.447	-16.172
^{116}Sn	1000.092	-11.410	825.297	163.384	820.328	179.764	-16.380
^{118}Sn	1016.160	-11.209	825.297	179.653	820.328	195.832	-16.179
^{120}Sn	1031.043	-10.504	825.297	195.242	820.328	210.715	-15.473
^{122}Sn	1044.799	-9.274	825.297	210.227	820.328	224.471	-14.244
^{124}Sn	1057.482	-7.522	825.297	224.663	820.328	237.154	-12.491
^{126}Sn	1069.145	-5.261	825.297	238.586	820.328	248.817	-10.230
^{128}Sn	1079.835	-2.461	825.297	252.076	820.328	259.507	-7.431
^{130}Sn	1089.597	0.689	825.297	264.989	820.328	269.269	-4.280
^{132}Sn	1098.474	4.369	825.297	277.546	820.328	278.146	-0.600

Table A.15: *(II) Input and Output data for the even-even nuclei lie between the two DM nuclei: ^{100}Sn and ^{132}Sn*

X	k	NN+3N (MeV)	(LDM1_Residuals-(NN+3N)) (MeV)	NNterm (MeV)	3Nterm (MeV)	NN (MeV)	(LDM1_Residuals-NN) (MeV)
0	0	0	0	0	0	0	0
58	1176	-4.191	-0.242	-3.345	-0.846	-3.986	-0.447
108	2040	-7.696	-0.297	-6.229	-1.467	-7.422	-0.571
150	2640	-10.549	-0.238	-8.651	-1.898	-10.308	-0.479
184	3024	-12.787	-0.170	-10.612	-2.174	-12.644	-0.313
210	3240	-14.441	-0.083	-12.112	-2.330	-14.431	-0.094
228	3336	-15.549	-0.039	-13.150	-2.399	-15.668	0.080
238	3360	-16.143	-0.029	-13.727	-2.416	-16.355	0.183
240	3360	-16.258	-0.122	-13.842	-2.416	-16.493	0.113
238	3360	-16.143	-0.036	-13.727	-2.416	-16.355	0.177
228	3336	-15.549	0.075	-13.150	-2.399	-15.668	0.195
210	3240	-14.441	0.198	-12.112	-2.330	-14.431	0.188
184	3024	-12.787	0.295	-10.612	-2.174	-12.644	0.153
150	2640	-10.549	0.319	-8.651	-1.898	-10.308	0.078
108	2040	-7.696	0.265	-6.229	-1.467	-7.422	-0.009

58	1176	-4.191	-0.089	-3.345	-0.846	-3.986	-0.294
0	0	0.000	-0.600	0	0	0	-0.600

4) Oxygen isotopic chain from the DM nucleus ^{16}O to DM nucleus ^{24}O:

***Table A.16**: (I) Input data for the even-even nuclei lie between the two DM nuclei from ^{16}O to ^{24}O*

N	Z	A	El	BE/A(keV)	un(keV)	BE/A(MeV)	un(MeV)	BE(MeV)	unT(MeV)	Valence Neutrons (n_n)	Valence Protons (n_p)	Valence Nucleons (n)
8	8	16	O	7976.206	0	7.976206	0.0000005	127.619296	0.000008	0	0	0
10	8	18	O	7767.097	0	7.767097	0.0000005	139.807746	0.000009	2	0	2
12	8	20	O	7568.57	0.044	7.56857	0.000044	151.3714	0.00088	4	0	4
14	8	22	O	7364.871	2.587	7.364871	0.002587	162.027162	0.056914	2	0	2
16	8	24	O	7039.685	6.87	7.039685	0.00687	168.95244	0.16488	0	0	0

***Table A.17:** (II) Output data for the even-even nuclei lie between the two DM nuclei from ^{16}O to ^{24}O*

Nucleus	LD (MeV)	BE(MeV)-LD(MeV)	BEexper(^{16}O) (MeV)	(BE(^{A}O)-BE(^{16}O)) MeV	BEtheor(^{16}O) (MeV)	(BEtheor(^{A}O)-BEtheor(^{16}O)) MeV	LDM1_Residuals (MeV)
^{16}O	125.317	2.303	127.619	0	125.317	0	0
^{18}O	144.497	-4.689	127.619	12.188	125.317	19.180	-6.992
^{20}O	157.186	-5.815	127.619	23.752	125.317	31.870	-8.118
^{22}O	164.679	-2.652	127.619	34.408	125.317	39.363	-4.955
^{24}O	167.897	1.055	127.619	41.333	125.317	42.581	-1.248

Table A.18: *Unweighted least squares fit of the BW formula to the BW formula to the DM nuclei for A ≥ 16:*

1) **Without including the experimental uncertainties**
2) **Including a fixed value of pairing parameter a_p=12MeV**
3) **Minimization method: scipy.curve.fit**

	Fit to the BE (MeV) (Eq. (5))	**Fit to the BE/A(MeV)**
DM Nuclei	**Residuals**	**Residuals**
^{100}Sn	4.0838094	0.0412005
^{132}Sn	3.5167529	0.0477544
^{40}Ca	-4.0628941	-0.0645543
^{48}Ca	-3.0861741	-0.0067985
^{16}O	3.7210328	0.0123641
^{56}Ni	-1.8530517	0.0285308
^{208}Pb	-2.4889696	-0.0584970

Residuals of (BE/A (MeV) x A)
0.0412005*100 = 4.1200520
0.0477544*132 =6.3035742
-0.0645543*40 =-2.5821704
-0.0067985*48 =-0.3263290
0.0123641*16 =0.1978250
0.0285308*56 =1.5977248
-0.0584970*208 =-12.1673677

Table A.19: *Weighted least squares fit of the BW formula to the DM nuclei for A ≥ 16:*

1) **Without including the experimental uncertainties**
2) **Including a fixed value of pairing parameter a_p =12 MeV**
3) **Minimization method: scipy.curve.fit**

	Fit to the BE (MeV) (Eq. (5))	**Fit to the BE/A (MeV)**
DM Nuclei	**Residuals**	**Residuals**
^{100}Sn	16.0473102	0.1604731
^{132}Sn	5.0808835	0.0384915
^{40}Ca	-0.0839196	-0.0020980
^{48}Ca	0.0420399	0.0008758
^{16}O	0.0011749	0.0000734
^{56}Ni	6.3608741	0.1135870
^{208}Pb	-2.7001316	-0.0129814

Residuals of (BE/A (MeV) x A)
0.1604731*100 =16.0473105
0.0384915*132 =5.0808837
-0.0020980*40 =-0.0839196
0.0008758*48 =0.0420399
0.0000734*16 =0.0011749
0.1135870*56=6.3608742
0.0129814*208 = -2.7001308

***Table A.20**: Best fit parameters for the unweighted least squares fit of the BW formula, Eq. (5), to the DM nuclei for A ≥16. (Fit BE/A (MeV))*

1) Fitting the BE/A in MeV
2) Using the BW baseline formula
3) Without including the experimental uncertainties
4) Including a fixed value of pairing parameter a_p = 12 MeV
5) Minimization method: scipy.curve.fit

a_v (MeV)	a_s (MeV)	a_c (MeV)	a_a (MeV)	a_p (MeV)
15.08 ± 0.53	16.15 ± 1.27	0.64 ± 0.05	21.45 ± 1.95	12.0 fixed

***Table A.21:** Best fit parameters for the unweighted least squares fit of the BW formula, Eq. (5), to the DM nuclei for A ≥ 16 (Fit BE(MeV)).*

1) Fitting the BE in MeV
2) Using the BW baseline formula
3) Without including the experimental uncertainties
4) Including a fixed value of pairing term a_p = 12 MeV
5) Minimization method: scipy.curve.fit

a_v (MeV)	a_s (MeV)	a_c (MeV)	a_a (MeV)	a_p (MeV)
16.86± 1.36	20.65± 3.75	0.79±0.10	26.81± 4.16	12.0 fixed

***Table A.22:** Best fit parameters for the weighted least squares fit of the BW formula to the DM nuclei for A ≥ 16 (Fit BE/A(MeV))*

1) Fitting the BE/A in MeV
2) Using the BW baseline formula
3) Including the experimental uncertainties (un(MeV))
4) Including a fixed value of pairing term a_p = 12 MeV
5) Minimization method: scipy.curve.fit

a_v (MeV)	a_s (MeV)	a_c (MeV)	a_a (MeV)	a_p (MeV)
14.81 ± 0.17	15.45 ± 0.35	0.64 ± 0.02	19.07 ± 0.78	12.0 fixed

Table A.23: *Best fit parameters for the weighted least squares fit of the BW formula, Eq.(5), to the DM nuclei for A ≥ 16.(Fit BE(MeV))*

1) **Fitting the BE in MeV**
2) **Using the BW baseline formula of Eq. (5)**
3) **Including the experimental uncertainties (unT(MeV))**
4) **Including a fixed value of pairing term a_p = 12 MeV**
5) **Minimization method: scipy.curve.fit**

a_v (MeV)	a_s (MeV)	a_c (MeV)	a_a (MeV)	a_p (MeV)
14.81 ± 0.17	15.45 ± 0.35	0.64 ± 0.02	19.07 ± 0.78	12.0 fixed

APPENDIX B

Python Codes to Compute the Number of Valence Neutrons/Protons of Nuclides

1st Code: Calculation of Valence Neutrons, Valence Protons and Valence Nucleons:

Calculations Functions taken from the Ref. [38]:

'J.Mendoza-Temis et al., 'Nuclear masses and the number of valence nucleons', Volume 799, Issues 1–4, 1 February 2008, Pages 84-93'

In the present analysis, these functions are described in the Eqs. (14),(15),(16),(17):

```
#Code starts:

choice_map = {1:'Neutrons', 2:'Protons', 3:'Nucleons'}

def calc(elements, entry='neutrons', elements_2=None):

    # Magic shell closures
    shell_closures = [2, 8, 20, 28, 50, 82]

    # Case where there are 0 valence elements
    if elements in shell_closures:
        valence_elements = 0

    else:
        # n_c1 and n_c2

        ## loop over closed shell values and compare with given N
        for i in range(len(shell_closures)-1):
            if shell_closures[i] < elements < shell_closures[i+1]:
                n_c1 = shell_closures[i]
                n_c2 = shell_closures[i+1]

                n_med = (n_c1+n_c2)//2
                break

        print('N: ',elements)
        print('n_c1: ', n_c1)
        print('n_c2: ', n_c2)
        print('N_med: ', n_med)


        if elements <= n_med:
            valence_elements = elements - n_c1
        else:
            valence_elements = n_c2 - elements
```

```
    if entity == 'nucleons':

        if elements_2 in shell_closures:
            valence_elements_2 = 0

        else:
            # n_c1 and n_c2

            ## loop over shell closures and compare with value of a
given N
            for i in range(len(shell_closures)-1):
                if shell_closures[i] < elements_2 <
shell_closures[i+1]:
                    n_c1 = shell_closures[i]
                    n_c2 = shell_closures[i+1]

                    n_med = (n_c1+n_c2)//2
                    break


            if elements_2 <= n_med:
                valence_elements_2 = elements_2 - n_c1
            else:
                valence_elements_2 = n_c2 - elements_2

            valence_elements = valence_elements + valence_elements_2

    if entry == 'nucleons':
        print('Valence {} for N={}, P={}: {}\n'.format(entry,
elements, elements_2,valence_elements))
    else:
        print('Valence {} for N={}: {}\n'.format(entry,
elements,valence_elements))


def main(choice=None, n=None):

    # Check if choice is given or not
    if not choice:

        # If not given, get choice from user
        while True:
            try:
                choice = int(input("""Please choose one of the below
options:
                1  :   Calculate Valence Neutrons
                2  :   Calculate Valence Protons
                3  :   Calculate Valence Nucleons
                              """))

                # Check for validity
                if choice not in [1, 2, 3]:
                    print('Enter correct choice.')
                    continue
                else:
                    break
            except:
                print('Enter correct choice.')
                continue
```

```
    # Check if N not given
    if not n and choice in [1,2]:

        # If not given, get from user
        while True:
            try:
                n = int(input('Enter {}:
'.format(choice_map[choice])))

                if n < 2 or n > 82:
                    print('Enter correct value of
{}'.format(choice_map[choice]))
                    continue
                else:
                    break
            except:
                print('Enter correct value of
{}'.format(choice_map[choice]))
                continue
    elif not n and choice == 3:
                # If not given, get from user
        while True:
            try:
                n = int(input('Enter Neutrons: '))

                if n < 2 or n > 82:
                    print('Enter correct value of Neutrons')
                    continue
                else:
                    break
            except:
                print('Enter correct value of Neutrons')
                continue

        while True:
            try:
                p = int(input('Enter Protons: '))

                if p< 2 or p> 82:
                    print('Enter correct value of Protons')
                    continue
                else:
                    break
            except:
                print('Enter correct value of Protons')
                continue


    #1) Call the function which is used to perform calculations
providing  an appropriate input.
    if choice == 1:
        calc(entry='neutrons', elements=n)
    elif choice == 2:
        calc(entry='protons', elements=n)
    elif choice == 3:
        calc(entry='nucleons', elements=n, elements_2=p)
    else:
        print('Enter correct choice 1, 2 or 3')

# 2)Test to verify if the code works and prints the correct values:
```

```
# Example: How many valence neutrons (entry = 'neutrons') have a
nucleus with 16 neutrons? (elements = 16)
# Similarly, instead of entry = 'neutrons' , it can change to entry
='protons' for a calculation of valence protons

calc(entry='neutrons', elements=16)
calc(entry='neutrons', elements=18)
calc(entry='neutrons', elements=20)
calc(entry='neutrons', elements=22)
calc(entry='neutrons', elements=24)
calc(entry='neutrons', elements=26)
calc(entry='neutrons', elements=28)
calc(entry='neutrons', elements=30)
calc(entry='neutrons', elements=32)
calc(entry='neutrons', elements=34)


# 3) In the next shell,  the code asks to make a choice:
#    1  :   Calculation of Valence Neutrons
#    2  :   Calculation of Valence Protons
#    3  :   Calculation of Valence Nucleons
# Type 1 or 2 or 3 based on the choice
# Then insert for which number of protons and/(or) neutrons want to
take the valences
# Calculations for single N :

main()

# 4) Calculations for list of N values of protons or neutrons
# Calculation of valence protons: Enter multiple of N in this list
and get the valence protons:
ls_N = [9, 56, 44, 33, 76]

# 1 : neutrons
# 2 : protons
choice = 2

for i in (ls_N):
    main(choice=choice, n=i)

# Calculation of valence neutrons: Enter multiple values of N in the
list and get the valence neutrons:

ls_N = [2,4,2,6,4,2,8,6,4,8,6,4,10,8,6,12,10]
choice = 1  #for neutrons

for i in (ls_N):
    main(choice=choice, n=i)
```

2nd Code: Calculation of Valence Nucleons:

Similarly, the Calculations Functions taken from the Ref. [38]:

'J.Mendoza-Temis et al., 'Nuclear masses and the number of valence nucleons', Volume 799, Issues 1–4, 1 February 2008, Pages 84-93'

In the present analysis, these functions are described in the Eqs.(14),(15),(16),(17).

```
# Code starts:

def valence(A,Z):
    N = A - Z
    cs = [2,8,20,28,50,82,126 ] #Closed shells of Neutrons or Protons
    ms = [5,14,24,39,66,104 ]   #Their corresponding mid shells
    val=0

# Calculation of Valence Neutrons (Nv)
    Nv=0
    for I in range( 6):
        if(N == cs[I] ):
            NV = 0
            break
        if ( N < cs[I] ):
            if ( N <= ms[I-1] ):
                Nv = N - cs[I-1]
            if ( N > ms[I-1] ):
                Nv =cs[I] - N
                break

# Calculation of Valence Protons (Pv)
    Pv=0
    for I in range(6):
        if ( Z == cs[I] ):
            Pv = 0
            break
        if ( Z < cs[I] ):
            if ( Z <= ms[I-1] ):
                Pv = Z - cs[I-1]
                break
            if ( Z > ms[I-1] ):
                Pv =cs[I] - Z
                break
# Calculation of Valence Nucleons
    val = Pv+Nv
    return val

# Insert Manually the Mass Number (A) and the Proton Number (Z)
# of the nucleus you want to calculate
# the valence nucleons

A=116 # 116Sn (I will test the magic nucleus 116Sn)
Z=66
ccc=valence(A,Z)
print(ccc)
```

References

1. K. Hebeler et al., Annu. Rev. Nucl. Part. Sci. 65, 457, (2015)
2. W.J. Huang et al., Chinese Phys. C 41 030002, (2017)
3. Meng Wang et al., Chinese Phys. C 41 030003, (2017)
4. Jorge G. Hirsch et al., J. Phys.: Conf. Ser. 322 012017, (2011)
5. Dezso Sarkadi, Journal of Theoretics, Vol. 5-6, Dec 2003/Jan 2004
6. D.S. Ahn et al., Physical Review Letters 123, 212501, (2019)
7. Heiko Hergert, Front. Phys. 8, 379, (2020)
8. J. D. Holt et al., Journal of Physics, G: Nuclear and Particle Physics, vol. 40, no. 7, p. 075105, (June 2013)
9. B. F. Gibson & B. H. McKellar, Few-Body Systems, 3(4), 143-170, (1988)
10. Krane, K. S., & Halliday, David., 'Introductory nuclear physics', Hoboken NJ: Wiley, (1987)
11. N. Kalantar-Nayestanaki, EPJ Web of Conferences 66, 01007, (2014)
12. Dean, David J., Physics Today, vol. 60, no. 11, pp. 48–53, Nov. (2007)
13. Arpad Horvath, Wikimedia Commons, 16 March 2006, Available from: https://commons.wikimedia.org/wiki/File:Quark_structure_proton.svg
14. Jacek Rybak, Wikimedia Commons, 15 January 2018 Available from: https://commons.wikimedia.org/wiki/File:Neutron_quark_structure.svg
15. Paul D. Cottle et al., Physics 5, 49, (2012)
16. Robert V. F. Janssens, Nature, vol. 459, no. 7250, pp. 1069–70, (June 2009)
17. Roger A Rydin, Annals of Nuclear Energy 38, 238-242, (2011)
18. S.R. Srtoberg et al., Physical Review Letters 126, 022501, (2021)
19. A. Bhagwat, Physical Review C 81, 044321, (2010)
20. H. Schatz, et al., Phys. Rev. Lett.; 86(16), 3471, (2001)
21. Greiner Maruhn et al., ''Nuclear Models'', Springer, (1996)
22. Sven Aberg, Nature volume 417, pages 499–501, (2002)
23. Jose-Luis Pinedo-Vega et al., Asian Journal of Physical and Chemical Sciences, 1(2): 1-10, Article no.AJOPACS.31266, (2016)
24. Vahid Mirzaei Mahmoud Abadi et al., Nuclear Science, Volume 2, Issue 1, pages 11-15, (March 2017)
25. B. Blank & P. H. Regan, Nuclear Physics News, 11:1, 15-22, (2001)
26. Kenjiro Takada, 2006, Internet Seminar, Microscopic World 3,The World of the Atomic Nucleus, Available from: https://ne.phys.kyushu-u.ac.jp/seminar/MicroWorld3_E/MicroWorld_3_E.html
27. R.F. Casten, 'Nuclear Structure from a Simple Perspective', Oxford University Press, (1990)
28. Ali Khalaf Hasan Al-Sened et al., International Journal of Current Research Vol. 8, Issue, 06, pp.33276-33280, June, (2016)
29. Christian Iliadis, 'Nuclear Physics of Stars', Wiley-Vch, Cop, (2015)

30. S. Adhikari and C. Samanta, International Journal of Modern Physics E, vol. 13, no. 05, pp. 987–97, Oct., (2004)
31. K. Langanke et al., Phys. Rev.C67 , 044314, (2003)
32. R. F Casten, 'Nuclear Structure from a Simple Perspective', Oxford University Press, (2005)
33. R. Sheline et al., Phys. Lett. B., 41,115, (1972)
34. J. S. Lilley, Nuclear Physics : Principles and Applications. J. Wiley, (2001)
35. T. Miyagi et al., Physical review C 102, 034320, (2020)
36. M. Mayer, & J. Jensen (1964). Elementary theory of nuclear shell structure by Maria Goeppert Mayer and J. Hans D. Jensen. New York: Wiley.
37. J. Barea et al., Revista Mexicana De Fisica S 54 (3) 5-10, (2008)
38. J.Mendoza-Temis et al., Nuclear Physics A, Elsevier, 799, pp. 84–93, (2008)
39. K. Heyde, 'Basic Ideas and Concepts in Nuclear Physics: An Introductory Approach, Third Edition (Fundamental & Applied Nuclear Physics)', (2004)
40. Yang, Fujia, and Joseph H. Hamilton, 'Modern Atomic and Nuclear Physics', World Scientific, (2010)
41. Dallin S. Durfee 2015, Brigham Young University
Available from: http://pms.iitk.ernet.in/ICT/physics_courses/akj/AKJain_IITR_Ch_2.html
42. A. Lépine-Szily and P. Descouvemont, International Journal of Astrobiology, vol. 11, no. 4, pp. 243–50, (May 2012)
43. Website: https://www.asc.ohio-state.edu/kagan.1/phy367/Lectures/P367_lec_14.html
44. Alessandro Pastore et al., J. Phys. G: Nucl. Part. Phys. (2021)
45. Ning Wang et al., Physics Letters B 734 , 215-219, (2014)
46. Haife Zharg et al., Nuclear Physics A 929, 38-53, (2014)
47. Min Liu et al., Physical Review C 84, 014333, (2011)
48. H. Zhang et al., Nuclear Physics A 929, 38-53, (2014)
49. A. Pastore et al., Phys. Rev. C 101, 035804, (2020)
50. S. Cht. Mavrodiev, and M. A. Deliyergiyev, International Journal of Modern Physics E, vol. 27, no. 02, p. 1850015, (Feb. 2018)
51. A. Bhagwat et al., AIP Conference Proceedings 1524, 20, (2013)
52. G. Audi, International Journal of Mass Spectrometry, 'A lecture on the evaluation of atomic masses', arXiv:nucl-ex/0302020
53. D. Lunney , J. M. Pearson and C. Thibault, Rev. Mod. Phys. 75 1021, (2003)
54. M. Wang et al., AIP Conference Proceedings 1484, 79, (2012)
55. W.J. Huang et al., Chinese Phys. C 45 030002, (2021)
56. Meng Wang et al., Chinese Phys. C 45 030003, (2021)
57. J. Toivanen et al., Physical Review C 78, 034306, (2008)
58. J.M. Pearson et al., Nuclear Physics A 777, 623-644, (2006)
59. Irving O. Morales et al., Physical Review C 83, 054309, (2011)
60. J.M. Pearson, Hyperfine Interactions, 132, 59-74, (2001)
61. Luigi Coraggio et al., Frontiers in Physics, Journal Volume: 8; Journal ID: ISSN 2296-424X, (2021)

62. P. Moller et al., Atomic Data and Nuclear Data Tables, vol. 59, no. 2, pp. 185–381, (Mar. 1995)
63. W. Myers and W. Swiatecki, Ann. Phys. 84 186, (1974)
64. P. Moller and J. R. Nix, At. Data Nucl. Data Tables, 39 213, (1988)
65. W. D. Myers and W. J. Swiateck, Nucl. Phys. A 601, 141 71, (1996)
66. S. Goriely, AIP. Conf. Proc. 529, 287, (2000)
67. J. D. Walecka, Ann. Phys. 83, 491, (1974)
68. S. K. Patra, R. K. Gupta and W. Greiner, World Scientific Publishing Company, pp. 994–1024, (2013), (doi:10.1142/97898128166340026)
69. S. G. Zhou et al., Phys. Rev. C 82, 011301, (2010)
70. Z. M. Niu et al., Phys. Rev. C 87, 037301, (2013)
71. S. Baohua and M. Jie, Chin. Phys. Lett. 25, 2429, (2008)
72. Z. M. Niu, S. Baohua and M. Jie, Phys. Rev. C 80, 065806, (2009)
73. Z. M. Niu and C. Y. Gao, Int. J. Mod. Phys. E 19, 2247, (2010)
74. Z. M. Niu et al., Sci. China Phys. Mech. Astron. 54, 119, (2011)
75. X. D. Xu et al., Phys. Rev. C 87 , 015805, (2013)
76. X. D. Xu et al., Phys. Lett. B 723, 172, (2013)
77. A. Bhagwat, X. Viñas, M. Centelles, P. Schuck and R.Wyss,Phys. Rev. C86, 044316, (2012)
78. K. Pomorski and J. Dudek, Phys. Rev. C67, 044316, (2003)
79. A. Bhagwat, Phys. Rev. C 90, 064306, (4 December 2014)
80. G. T. Garvey and I. Kelson, Phys. Rev. Lett. 16, 197, (1966), (doi:10.1103/PhysRev Lett.16.197)
81. G. T. Garvey et al., Rev. Mod. Phys. 41, S1, (1969), (doi:10.1103/RevModPhys.41.S1)
82. J. Janecke and P. J. Masson, At. Data Nucl. Data Tables 39, 265, (1988), (doi:10. 1016/0092-640X(88)90028-9)
83. Y. Y. Cheng, Y. M. Zhao and A. Arima, Phys. Rev. C 89, 061304, (2014)
84. S. Liran and N. Zeldes, At. Data Nucl. Data Tables 17, 431, (1976), (doi:10. 1016/0092-640X(76)90033-4)
85. H. Koura et al., Nucl. Phys. A 674, 47, (2000), (doi:10.1016/S0375-9474(00) 00155-X)
86. H. Koura, T. Tachibana, M. Uno, and M. Yamada, Prog. Theor. Phys. 113, 305 (2005)
87. Pomorski et al., Physical Review C 67, 044316, (2003)
88. K. Pomorski and B. Nerlo-Pomorska, Acta Physica Polonica B Proceedings Supplement, vol. 6, no. 4, p. 1129, (2003), (https://doi.org/10.5506/aphyspolbsupp.6.1129)
89. L. Satpathy and R.C.Nayak, At. Data Nucl. Data Tables, Vol. 39, No.2, (July 1988)
90. R. Nayak and L. Satpathy, At. Data Nucl. Data Tables 73, 213, (1999)
91. N. Wang and M. Liu, Phys. Rev. C 84, 051303(R), (2011)
92. N. Wang and M. Liu J., Phys.: Conf. Ser. 420 012057, (2013)
93. N. Wang, Z. Liang, M. Liu, and X. Wu, Phys. Rev. C 82, 044304, (2010)
94. N. Wang and M. Liu , Phys. Rev. C 81, 067302 , (2010)
95. N. Wang, M. Liu, and X. Wu, Phys. Rev. C 81, 044322, (2010)
96. J. Duflo and A. Zuker, Phys. Rev. C 52, R23, (1995)
97. J. Duflo and A. P. Zuker, Phys. Rev. C 59, R2347, (1999)
98. A. P. Zuker, Rev. Mexic. Fis. S 44, 129, (2008)
99. J. Mendoza-Temis, J. G. Hirsch, and A. P. Zuker, Nucl. Phys. A 843, 14-36, (2010)

100. M. W. Kirson, Nuclear Physics A 893 , 27-42 , (2012)
101. Min Liu et al., Nuclear Physics A 768 , 80–98, (2006)
102. S. Goriely, N. Chamel, and J. M. Pearson, Phys. Rev. C 82, 035804, (2010)
103. S. Goriely, S. Hilaire, M. Girod, and S. Peru, Phys. Rev. Lett. 102, 242501, (2009)
104. A. Pastore et al., Journal of Physics G: Nuclear and Particle Physics, vol. 48, no. 8, p. 084001, (Aug. 2021)
105. Z.M. Niu et al., Physics Letters B 778, 48-53, (2018)
106. A. Sobiczewski et al., Physical Review C 90, 017302, (2014)
107. L. S. Geng, H. Toki and J.Meng, Prog. Theor. Phys. 113, 7856, (2005)
108. Y. A. Litvinov et al., Int. J. Mod. Phys. E 21 , 1250038, (2012)
109. A. Sobiczewski and Y. A. Litvinov, Phys. Scri. T154, 014001, (2013)
110. S. Athanassopoulos et al., Nucl. Phys. A 743, 222, (2004)
111. A.E.L. Dieperink and P. Van Isacker, Eur. Phys. J. A 42 269, (2009)
112. C. Barbero et al., Nuclear Physics A 874, 81–97, (2012)
113. G. Royer, Nucl. Phys. A 807 105, (2008)
114. A. Ozawa et al., Phys. Rev. Lett. 84, 5493, (2000)
115. D. N. Basu, International Journal of Modern Physics E, vol. 13, no. 04, pp. 747–58, (Aug. 2004), (https://doi.org/10.1142/s0218301304002491)
116. P. Roy Chowdhury et al., Modern Physics Letters A, vol. 20, no. 21, pp. 1605–18, (July 2005), (https://doi.org/10.1142/s021773230501666x)
117. M. W. Kirson, Nuclear Physics A, vol. 798, no. 1-2, pp. 29–60, (Jan. 2008)
118. C.F. Von Weizsacker, Z. Phys. C96, 431, (1935)
119. A. Pastore et al 2021 Phys. Educ. 56 035012 (part 2)
120. N. Upadhyay et al., Journal of Interpolation and Approximation in Scientific Computing 2013,1-16,(2013), (doi:10.5899/2013/jiasc-00046)
121. G. Royer et al., Physical Review C 73, 067302, (2006)
122. A. Pastore, Lectures on the module 'Statistical Methods in Data Analysis MSc', Physics Department, University of York.
123. A. Pastore et al 2021 Phys. Educ. 56 035012 (part 1)
124. C. Samanta and S. Adhikari, Phys. Rev. C 65, 037301, (2002)
125. Atomic Mass Data Center (AMDC), The 2016 Atomic Mass Evaluation, Available from:
http://amdc.in2p3.fr/masstables/Ame2016/mass16.txt
126. Maria Piarulli et al., Front. Phys., 30 January (2020), (https://doi.org/10.3389/fphy.2019.00245)
127. Takaharu Otsuka et al., Phys. Rev. Lett. 105, 032501, (2010)
128. Subproject D1: Theoretical Nuclear structure physics, Technische Universität Darmstadt
129. H. Sakai, Few-Body Systems 41, 5-12, (2007)
130. J.L.Friar and B.F.Gibson, Ann. Rev. Nucl. Part. Sci. 34: 403-33, (1984)
131. B.F.Gibson and B.H.J. McKellar, Few-Body Systems 3, 143-170, (1988)
132. Kimiko Sekiguchi, SciPost Phys. Proc. 3, 029 (2020)
133. Jun-ichi Fujita and Hironari Miyazawa, Progress of Theoretical Physics, Volume 17, Issue 3, pages 360-365, (March 1957)

134. U. van Kolck, Physical Review C (Nuclear Physics), Volume 49, Issue 6, pp.2932-2941, (June 1994)
135. Evgeny Epelbaum et al., Rev.Mod.Phys.81:1773-1825, (2009)
136. K. Hebeler, Physics Reports 890, 1-116, (2021)
137. Luigi Coraggio et al., Front. Phys., (February 2021), (arXiv:2101.07915)
138. G. Hagen, Physical Review Letters 109, 032502, (2012)
139. A. P. Zuker, Phys. Rev. Lett. 90, 042502, (2003)
140. J. D. Holt and A. Schwenk, arxiv:1108:2680, (2011)
141. G. Hagen et al., Phys. Rev. Lett. 108, 242501, (2012), (arXiv:1202.2839)
142. J. D. Holt et al., J. Phys. G: Nucl. Part. Phys. 39 085111, (2012)
143. L. V. Grigorenko, I. G. Mukha, and M. V. Zhukov, Phys. Rev. Lett. 111, 042501, (2013)
144. K. Hagino and H. Sagawa, Phys. Rev. C 89, 014331, (2014)
145. A. Volya and V. Zelevinsky, Phys. At. Nucl. 77, 969, (2014)
146. K. Hebeler et al., Phys. Rev. C 83, 031301(R), (2011)
147. S.K. Bonger et al., Nuclear Physics A, 763, 59-79, (2005), (arXiv:nucl-th/0504043)
148. G. Mouze et al., Il Nuovo Cimento A (1965-1970) volume 103, pages 105–128, (1990)
149. I. Angeli , EPL 16 429, (1991)
150. M. Kaczmarczyk, Central European Journal of Physics volume 9, pages78–87, (2011)
151. National Nuclear Data Center, Brookhaven National Laboratory, Available from: https://www.nndc.bnl.gov/nudat2/
152. Bechtel Marine Propulsion Corporation (2010) and Fluor Marine Propulsion LLC (2019), Chart of Nuclides, 17th Edition, Revised 2009, Available from: https://nnlchartofthenuclides.com/nuclide
153. Leo H Kahane, 'Regression Basics', Sage Publications, Thousand Oaks, (2001)
154. H. Gavin, ' Fitting Models to Data, Generalized Linear Least Squares, and Error Analysis', (2019)
155. Supported material provided by : Machine Learning and Data Analysis for Nuclear Physics, a Nuclear TALENT Course at the ECT*, Trento, Italy, June 22 to July 3 (2020), MachineLearningECT/Day1.pdf at master · NuclearTalent/MachineLearningECT · GitHub
156. David C. Bailey, Royal Society Open Science, 4, 160600, (2017)
157. W. Mendenhall et al., 'A second course in statistics, Regression Analysis', (1996)
158. Matthew Newville, Till Stensitzki, Renee Otten, and others, (2021), (https://lmfit.github.io/lmfit-py/)
159. F. James, Minuit: Function Minimization and Error Analysis Reference Manual, Version 94.1, CERN, (1994)
160. Martin H. Petersen et al., s: J. Phys. Chem. C, 125, 15085−15093, (2021)
161. B. Cauchois et al., Physical Review C 98, 024305, (2018)
162. J. Dobaczewski et al., Journal of Physics G: Nucl. Part. Phys. 41 074001, (2014)
163. D. Benzaid et al., NUCL SCI TECH, 31:9, (2020)
164. A Pastore et al., J. Phys. G: Nucl. Part. Phys. 46 052001, (2019)
165. G.F. Bertsch et al., Physical Review C 71, 054311, (2005)
166. D. Neill et al., J. Phys.: Conf. Ser. 1643 012060, (2020)
167. A.E.L. Dieperink, P. Van Isacker, Eur. Phys. J. A 32, 11, (2007)
168. J. Mendoza-Temis, I. Morales, J. Barea, A. Frank, J.G. Hirsch, J.C. López-Vieyra, P. Van Isacker, V. Velázquez, Nucl. Phys. A 812, 28-43, (2008)

169. F. Iachello, A. Arima, The Interacting Boson Model (Cambridge University Press, Cambridge, England, (1987)
170. J.G. Hirsch et al., International Journal of Modern Physics E Vol. 17, No. supp01, pp. 398-411, (2008)
171. A.P. Zuker, Rev. Mex. Fis. S 54, 129, (2008), (http://rmf.fciencias.unam.mx/pdf/rmf-s/54/3/54 3 129.pdf)
172. J.Miles et al., 'Applying Regression and Correlation', SAGE Publications Ltd, November (2000)
173. G.F Bertsch et al., Phys. Rev. Lett. 119, 252501 (2017)
174. T. Potter, Nuclear and Particle Physics-Lecture 19, The semi-empirical mass formula, Lent/Easter Terms, (2021)
175. Na-Na Ma et al., Chinese Phys. C 43 044105, (2019)
176. Website: https://prepml.com/blog/matplotlib-1-data-visualization-using-python/